MESJTM

(ISSN 0976 3724)

MES JOURNAL OF TECHNOLOGY AND MANAGEMENT

VOL. 4, NO.1, 2020

DECEMBER 2020
INDIA

MES Journal of Technology and Management (MESJTM)

MESCE Kuttippuram

The **MES Journal of Technology and Management** was started by MES College of Engineering Kuttippuram to disseminate information about theory, practice, research and innovation in the field of Technology and Management. Also it will provide a forum for researchers to debate with the international community of researchers on these areas of concern with particular reference to India and other developing nations.

The journal connects the fields of science, engineering, and management disciplines. It addresses the issues involved in planning, designing, and integrating technical capabilities in order to shape and achieve an organization's strategic and organizational goals. In technology-based organizations, it encompasses not only R&D management, but also the full spectrum of management issues.

An interface between technology and other corporate functions, such as R&D, marketing, development and administration, is given by the journal. Its ultimate objective is to make a profound contribution to the advancement of theory, study and practice by serving as a leading forum for academic research to be published on all aspects of technology, innovation and engineering management.

MES College of Engineering
Kuttippuram, Thrikkanapuram South (P O)
Malappuram district, Kerala, India, PIN-679582
Ph: (+91) 494 3051108, (+91) 494 3051234
Fax: (+91) 494 2698081, Web: http://mesce.ac.in

ADVISORY COMMITTEE

Dr. Saeed Sepasi, University of Hawaii, Manoa, United States
Dr. Chanwit Boonchuay, Rajamangala University of Technology, Rattanakosin, Thailand
Dr. Tibin Joseph, Cardiff University, Cardiff, United Kingdom
Dr. Saly George, National Institute of Technology Calicut, India
Dr. Omar Farooq, Aligarh Muslim University, Uttar Pradesh, India
Dr. Nikhil Sasidharan, Asian Institute of Tech. Bangkok, Thailand
Dr. Praveenkumar K, LBS Engg. College Kasaragod, India
Dr. Paul Joseph K, National Institute of Technology Calicut, India
Dr. Vivek Mohan, Amrita Vishwa Vidyapeetham University, Coimbatore, India
Dr. Kittavit Buayai, Rajamungala Institute of Technology, Rattanakosin, Thailand
Dr. Nimal Madhu, Vidya Academy of Science and Technology, Thrissur, India
Dr. Sunanda C, College of Veterinary & Animal Science, Pookode, India.
Dr. Yusufuzzaman Khan, Aligarh Muslim Univ., Uttar Pradesh, India
Dr. Jayanandan B, National Institute of Technology Calicut, India

EDITORIAL BOARD

Patron

Prof. P O J Lebba, Secretary, MESCE

Chief Editor

Dr. A S Varadarajan A S, Principal, MESCE

Editor

Dr. Thasneem Fathima N K, Asso. Prof., EEE

Associate Editors

Dr. Syed Jalaludeen Shah, HOD, CE
Dr. Sasidharan Sreedharan, HOD, CSE
Dr. Rahmathunza I, HOD, ME
Dr. Gopakumar A, HOD, ECE
Dr. Nafeesa K, HOD, EEE
Dr. Bobby Mathews, HOD, AEI
Mr. Lino Abraham, HOD, IT
Dr. Prasanna T. K, HOD, Architecture
Dr. V A Sonny, HOD, MBA
Ms. Jameela Beevi U.S, HOD, Mathematics
Dr. Mini P P, HOD, Science and Humanities

TECHNICAL COMMITTEE

Dr. Shilpa Suresh, Asst. Prof., ECE
Dr. Abdul Jaleel E, Asst. Prof., AEI
Mr. S Gavudhama Karunanidhi, Asst. Prof, ME
Mr. Harikrishnan G R, Asst. Prof., CSE
Dr. Muneera C P, Asst. Prof., CE
Mr. Shijukumar P S, Asst. Prof., IT
Dr. Bindu Anto Ollukkaran, Asso. Prof., MBA
Dr. Suneesh P U, Asst. Prof., S&H
Ms. Priya Pradeep, Asst Professor, EEE
Dr. Geevar C Zacharias, Asst. Prof., MCA

MESSAGE

I am happy that MES College of Engineering Kuttippuram is bringing out 2020 edition of MES Journal of Technology and Management. This Journal is an attempt to encourage the research activities which provide an avenue to publish research outcomes. I wish the academic community will be greatly benefited by the research papers published in the Journal.

Prof. P O J Lebba

Patron

Message from Chief Editor

I am immensely happy to launch the fourth edition of MES Journal of Technology and Management (ISSN No.09763724), a multidisciplinary, peer-reviewed journal that publishes original research in various Engineering Sciences and Management.

Institutions of Engineering & Technology are to be viewed as incubation centres for Research and Development to bring about products and processes needed for the society and industry. An institution needs a wallet for storing and a hub for disseminating and sharing its research findings. The MESJTM serves both the purposes. It acts as an exposition platform for showcasing the research potentialities of the faculty and students of MESCE and other institutions.

The journal covers topics related to Electrical, Electronics, Civil, Mechanical, Computer Science and Management Practices. I am sure that the content of this journal will be of use to researchers working in the related areas.

Dr. A S Varadarajan

Chief Editor & Principal

Editor’s Note

Researchers spend long hours working on analysis and they want to show it to the public until they come to a clear conclusion. The focus of the MES Journal of Technology and Management is to introduce genuine research results to its readers and thus provide an unceasing cycle of technology and management research and exploration. This journal was established to assist academic scholars, scientists, professors and students seeking opportunities to publish their research work. It offers a platform for the sharing of research knowledge across different fields of engineering and management.

The journal's scope is established to include review articles, technical notes and case studies in all fields of engineering and management that will help to build a comprehensive understanding of society. In order to contribute to the improved understanding of technological and management problems, theories, analysis and practical work are encouraged. Emphasis is placed on contributions dealing with the practical, applications-led research on the use of technology.

Now, we are happy to publish the issue in December 2020 sharing the ideas and research findings, discussing contemporary issues and challenges in business and industry by academic researchers, practicing managers and students. I use this opportunity to thank the authors, reviewers, editorial committee members and all those who cooperated with this endeavor.

Dr. Thasneem Fathima N K

Editor

MES JOURNAL OF TECHNOLOGY AND MANAGEMENT

Vol. 4, No. 1, 2020

CONTENTS

MES JOURNAL OF TECHNOLOGY AND MANAGEMENT
Volume 4, No 1,1-4,2020

`Remote Sensing and 3D Analysis for Disaster Preparedness

Sindhuja Kasthala
Faculty of Architecture
Department of Architecture and Planning
NIT Calicut, India
sindhujakasthala@gmail.com

Binoy B. V.
Research Scholar
Department of Architecture and Planning
NIT Calicut, India
binoy9344@gmail.com

ABSTRACT

The importance and applications of Remote sensing and GIS in disaster preparedness is discussed with more emphasis on 3D visualization. This paper attempts to mark that the Visualization in the 3D domain can greatly improve the efficiency of disaster preparedness. View-shed analysis and Line of sight analysis are applied in GIS software, ArcGIS, to logically calculate the full visibility and partial visibility areas during ThrissurPooram, thereby providing a proactive calculation of maximum allowable crowd inside the venue complex and leading to crowd regulation strategies. Use of such three-dimensional visualization techniques in disaster preparedness stage will aid in calculating the critical limit of crowd above which stampedes, and other disastrous events can happen.

Keywords

Disaster preparedness; GIS; Remote Sensing; 3D Modelling; line of sight analysis

1. INTRODUCTION

Disaster preparedness, one of the important steps in disaster management cycle, refers to the measures taken to prepare and minimize loss from future disaster. Disaster preparedness helps to predict, plan and mitigate the impact on vulnerable populations. "Disaster preparedness activities embedded with risk reduction measures can prevent disaster situations and also result in saving maximum lives and livelihoods during any disaster situation."(IFRC, 2017). The continuous and integrated process of Disaster Preparedness involves many technologies such as Remote Sensing, Geographical Information Systems and Global Positioning System. This paper discusses about the role of Remote Sensing and 3D analysis in disaster preparedness. The role of Remote Sensing in the preparedness stage for various disasters vary from predicting spread/direction of Fire to measuring strain accumulation for Earthquakes (I. Z. Gitas, 2008)(Karen E. Joyce, 2009). 3D Modelling which is an amalgamation of GIS and remote sensing is very helpful in creating faster solutions for disaster preparedness. This paper focuses on Remote Sensing technology and its three-dimensional visualization capabilities for

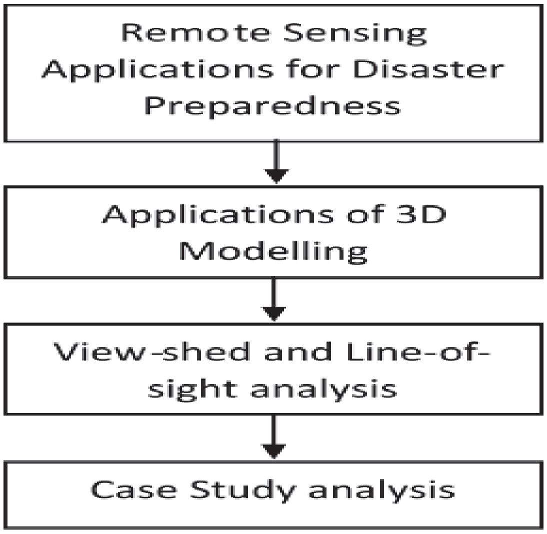

Figure 1 Flowchart shows the general Methodology followed

disaster preparedness in ThrissurPooram mass gathering. The case study emphasizes on application of 3D analysis technique and its usage for the better crowd management during ThrissurPooram.

2. 3D MODELLING APPLICATIONS IN DISASTER PREPAREDNESS

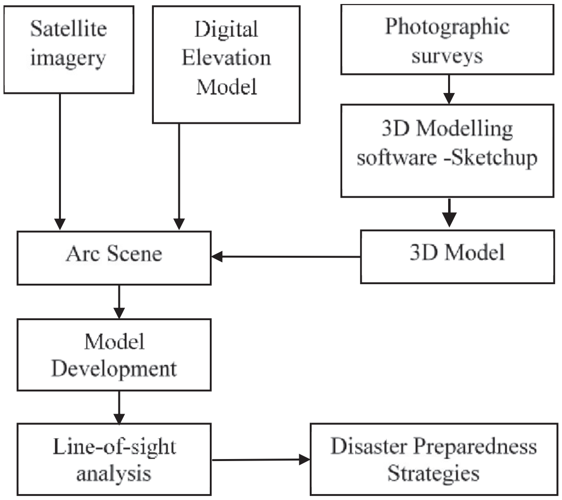

Figure 2 Methodology of the live case study

3D Modelling if used in an effective way will help to analyze volumetric data and provide solutions for Pre-disaster planning. 3D GIS can effectively be used in various disaster preparedness situations like analyzing floods, tsunamis and fire emergencies. In urban areas, the optimal location of ambulances, possible snipper locations, position of emergency response teams and many similar solutions can be found out by using three-dimensional analysis in GIS. 3D modelling techniques generally used in the domain of disaster management are raster based View-shed Analysis and vector based Line-of-sight analysis. View-shed analysis is done in the two-dimensional window and line-of-sight is done in three-dimensional window of GIS software.

View-shed analysis determines the visibility of surface locations from a set of point or polyline observers using geodesic methods. It transforms the elevation surface into a geocentric 3D coordinate system and runs 3D sightlines to each transformed cell center. The Line-of-sight analysis calculates visibility between the first and last vertex of each line feature given its position in 3D space relative to the obstructions provided by a surface or multipatch feature class (Esri, 2017). The first vertex defines the observation point, whereas the last is the observation target. Visibility is determined along the sight line between these two points. An optional obstruction point feature class can be produced to visualize the first location along the sight line that impedes the observer's visibility of the target. If the sight line is obstructed by any part of the surface before hitting a feature, then the obstruction point is on the surface.

3D visualization can give a volumetric perspective to analyze possible disastrous situations and provide inputs for effective management. The application of one of these 3D modelling techniques for a disaster preparedness situation is showcased in the live case study given below.

3. LINE-OF-SIGHT ANALYSIS FOR A CROWD GATHERING VENUE

The study encompasses a disaster preparedness approach for a crowd gathering in Thrissur, Pooram, which happens every year in the ThekkinkaduMaidan of Vadakunnathan temple in the center of Thrissur city. The gathering which attracts lakhs of people into a smaller area is vulnerable to crowd disasters such as stampedes. In such gatherings, even a minor mistake can cause unfortunate events. For deriving the disaster preparedness strategies for the event, a 3D modelling technique, line of sight analysis, is employed for the ThrissurPooram ground. Line of sight analysis was used for analyzing the full visible and partially visible zones at Pooram venue (ThekkinkaduMaidan). The procedure adopted for the line-of-sight analysis and preparedness strategies is discussed below and also shown in the flow chart (see Figure 2).

The pictures obtained from the initial field visits and photographic surveys are used in the generation of realistic 3D models. These photographs are given as input for a 3D modelling software Sketch-up and a three-dimensional model of the temple with its surroundings was created. The model is imported to arc scene software using the interchangeable collada format. Digital Elevation Model was generated using a two-stage procedure, initially spot heights are extracted for Thekkinkadumaidan and its premises using Google Earth followed by DEM generation in ArcGIS using interpolation techniques(S.K. & J.O., 1988). The DEM generated in ArcMap was imported to arc scene followed by the draping of satellite image and buildings over the DEM to get a virtual 3D look.

Line of sight analysis was done in Arc scene by setting the event as target and adjusting the observer points spatially (see Figure 3). By varying the observer points in the whole venue area, the full-visible areas and partial-visible areas are attained (see Figure 4). This helped in the calculation of the 'total available area' from where people can stand and view the event to be approximate 55,100 m^2. Crowd capacity analysis of the total available area was done to estimate the maximum allowable crowd for a safe crowd density of 5 persons per m^2(Oberhagemann, 2012). This analysis sets the safe limit as 3 lakh people who can view the event.

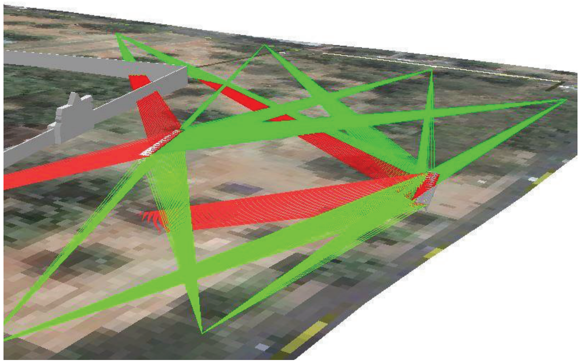

Figure 4 Line of sight analysis

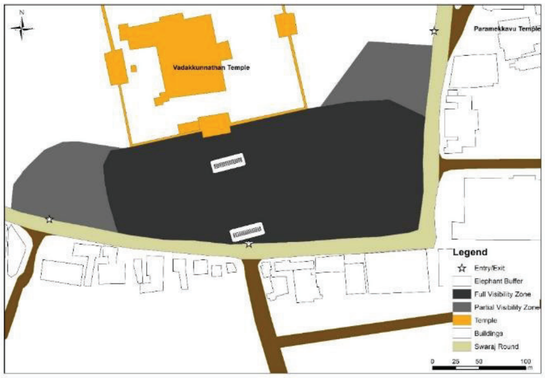

Figure 3 Visibility zones

This analysis will help to take adequate measures in controlling and curbing the number of people allowed in the ground to avoid disastrous events such as stampede.

CONCLUSIONS

The benefits of using 3D modelling in disaster preparedness stage of disaster management are highlighted in this paper. Even though the benefits of GIS and remote sensing are known to disaster managers, the knowledge of 3D modelling is yet (B V & B, 2014)(S.K. & J.O., 1988)to reach professionals. Remotes sensing is used in Disaster management domain but only for the applications like damage assessment and early warning. The use of GIS and 3D modelling for planning mass events are less frequently studied. Line of sight analysis and View shed analysis can solve issues by quickly analyzing situation in 3D, thereby proving solutions. By employing line-of-sight analysis technique, we found out the maximum number of allowable people for the safe management in Pooram mass gathering. This will help in providing effective measures for crowd management reducing the risk for stampedes. 3D visualization provided in an appropriate way should help the entire disaster management process.

REFERENCES

[1] B V, B., & B, S. (2014). Virtual 3d Mapping and Analysis Using Remote Sensing Data and Photographs.*International Journal of Remote Sensing & Geoscience (IJRSG)*, 42-46.

[2] *Esri*. (2017). Retrieved from esri website: http://www.esri.com/

[3] I. Z. Gitas, A. P. (2008). Contribution of remote sensing to disaster management activities: A case study of the large fires in the Peloponnese, Greece. *International Journal of Remote Sensing*, 1847-1853.

[4] *IFRC*. (2017, 08 07). Retrieved from International Federation of Red Cross and Red Crescent Society: http://www.ifrc.org/en/what-we-do/disaster-management/preparing-for-disaster/

[5] Karen E. Joyce, S. E. (2009). A review of the status of satellite remote sensing and image processing techniques for mapping natural hazards and disasters. *Progress in Physical Geography*, 183-207.

[6] Oberhagemann, D. D. (2012). *Static and Dynamic Crowd Densities at Major Public Events,* . Technical-scientific advisory board (TWD): German Fire Protection Association.

[7] S.K., J., & J.O., D. (1988). Extracting Topographic Structure from Digital Elevation Data for Geographic Information System Analysis. *PHOTOGRAMMETRIC ENGINEERING AND REMOTE SENSING*, 1593-1600.

[8] Still, G. K. (2014). *Introduction to Crowd Science.* CRC Press .

SindhujaKasthala received the B.Arch. Degree from School of Planning and Architecture Vijayawada, Andhra Pradesh and the M.Tech degree in Disaster Mitigation and Management from IIT Roorke.

Binoy B V received the B.Tech. Degree in electronics and communication engineering from Cochin University, Kerala and the M.Tech in Remote Sensing from Anna University, Chennai

.

MES JOURNAL OF TECHNOLOGY AND MANAGEMENT
Volume 4,No 1,5-11,2020

Optimization of Fluid Application Parameters during Hard Turning of OHNS Tool Steel Using Minimal Cutting Fluid Application

Anil Raj
Christ Faculty of Engineering,
Bangalore, Karnataka 560074.
anil.raj@christuniveristy.in

K. Leo Dev Wins
Karunya Institute of
Technology and sciences,
Coimbatore, Tamilnadu 641114
leo@karunya.edu

A. S. Varadarajan
MES college of Engineering
Kuttipuram, Kerala
varadarajan_as@yahoo.co.in

ABSTRACT.

Turning of hardened steel is characterized by high cutting temperatures and cutting force which makes is necessary to use large amounts of cutting fluid. The option of machining with minimal cutting fluid application (MCFA) seems a viable alternative to flood cooling since they counter the effects of using large amounts of cutting fluid such as significant operating cost and its negative impact on workshop environment and operator health due to the toxic nature of cutting fluids. MCFA aims at better overall cutting performance by reducing the cutting force which results in less power consumption and less heat generation while giving a better surface finish. The current paper aims to present optimized fluid application parameters during the hard turning of Oil hardened non shrinkable (OHNS) steel using MCFA. The cutting speed, feed and depth of cut are set constant at 115mm/min, 0.05mm/rev and 1mm respectively. Taguchi's DOE approach is used to select the L_9 orthogonal array. The fluid application parameters considered for MCFA are pressure at the injectors, frequency of pulsing, composition of cutting fluid and quantity of cutting fluid. The output parameters considered are cutting force and cutting temperature. Confirmation tests were performed to compare the predicted values with the experimental results and it was found that the predicted values matched well with the experimental results.

Keywords: OHNS steel, Hard turning, Minimal cutting fluid application, Taguchi DOE

1. INTRODUCTION

In modern machining industries, paramount importance is given to achieving increasingly efficient and eco friendly manufacturing systems that are capable of giving maximum levels of productivity at the highest quality while simultaneously machining costs at a minimum. To reach such levels of high productivity while using hardened steels, the usually high machining time taking process must be sped up (Hwang et al,2009). Conventionally, hardened steel components followed a three step process of rough machining followed by a heat treatment to bring up the hardness as required and a final round of finish machining for dimensional accuracy. The introduction of CBN and ceramic tools and other tools of high hot hardness was a solution to such time and labour intensive machining methods. This simplified process of machining the steel blank to its final dimension in the hardened state was a much profitable alternative. The process of hard turning is one such process that is quickly replacing traditional methods of machining in the automotive and tool and die industries.

However, the hard turning of steels is associated with severe cutting conditions characterized by high cutting forces and high cutting temperatures making it important to use a robust machine tool coupled with appropriate cooling systems to produce work of required surface integrity while avoiding thermal distortions in the metal. Although dry turning of hardened steels is practiced, it is usually not recommended due to the high cost of the ultra hard tool inserts that are capable of resisting such severe cutting conditions. Dry machining is not practical for high speed operations due to substantial decrease in tool life caused by sustained exposure to the resultant high cutting temperatures at the cutting zone. Elimination or reduction of cutting fluid may cause thermal distortions which are major concern due to excessive cutting zone temperatures (Klocke et al, 1997).

The logical alternative of flood cooling involves the direct bulk application of a cutting fluid at the cutting zone. This method relies mainly on the convective mode of heat transfer to dissipate the large amounts of heat generated. Friction at the tool chip interface is brought down due to the lubrication which further reduces the total power consumption. There has been some research on the effect of minimal cutting fluid application (MCFA) application during machining of hardened steels indicating overall improvement in cutting performance specifically in-terms of surface integrity and tool life (Vardarajan et al, 2002). The reason for the emergence of MQL application signifies a need to eliminate not only the machining costs but also the associated economic and ecological effects of storing, using and disposing the toxic cutting oils (Dhar et al, 2007). Cutting oils have known to cause adverse effects such as respiratory sickness, hyper pigmentation, oil acne, irritation of the skin etc on prolonged exposure (Sutherland et al, 2000).

Significant volumetric reduction of cutting fluids can be brought forward by MQL method in which small amounts of cutting fluid are atomized in a dispersion of pressurized air. This is then aimed precisely at the cutting zone for maximum penetration of chip tool interface allowing for maximum dissipation of heat which follows modes of convective and evaporative, unlike traditional flood cooling, where heat transfer is mainly in the convective mode making it less effective. This study made use of the Minimal cutting fluid application setup developed in-house at Karunya University. Proposing a set of cutting and fluid application parameters that give optimal cutting conditions for least cutting force and cutting temperature in the hard turning of OHNS steel is the intent of this study. Various studies were conducted on machining using MCFA but very few give optimized fluid application parameters.

2. EXPERIMENT

2.1 Selection of material

OHNS steel is selected as work material in the present investigation. This material is of good hardenablity, enjoys wide usage in applications such as pressure die casting tools, extrusion tools, forging dies, hot shear blades, stamping dies and plastic moulds. The material was hardened to 45 HRC. The OHNS steel is chemically composed of the following as shown in Table 1.

Table 1 Composition of work piece material

C	Mn	Cr	W	V	Si	Fe
0.95	1.15	0.5	0.5	0.2	0.28	balance

Hot punches and dies for blanking, bending, swaging and forging; hot extrusion dies for aluminium; cores, ejector pins, inserts and nozzles for aluminium, tin and lead die casting are some of the applications of OHNS steel. A cylindrical work piece of length 360 mm and diameter 70 mm was used in this investigation.

2.2 Selection of cutting tool

The cutting tool inserts and the tool holder were selected as per the recommendations of M/s TaeguTec India (P) Limited who extend their technical/material support for this research work. Accordingly, SNMG 120408 coated carbide inserts manufactured by TaeguTec Pvt. Ltd. were used in this study. The cutting tool has an orthogonal rake angle of 6° and a nose radius of 0.8 mm.

2.3 Selection of parameters and levels

The cutting speed, feed rate per revolution and depth of cut are the three main control parameters in turning operations. The selection of fluid application parameters was done based on the earlier work reported in the area of machining with minimal cutting fluid application. The cutting speed, feed and depth of cut are set constant at 115mm/min, 0.05mm/rev and 1mm respectively. As a result of an earlier study, these values were found to produce optimal cutting conditions during hard turning of H13 steel. Table 2 shows fluid application parameters pressure at the fluid injectors, frequency of pulsing, quantity of fluid application and composition of cutting fluid. The selected output parameters were cutting force and cutting temperature.

Table 2 Fluid application parameters

Levels	Pressure (bar)	Frequency (pulses/min)	Composition (%/vol)	Quantity (ml)
1	50	500	10	4
2	75	600	20	8
3	100	700	30	12

2.4 Experimental setup

The MCFA setup was developed in house at Karunya University (Varadarajan et al., 2001). It consists of a P-4 fuel pump (Bosch make) coupled to an infinitely variable electric drive. Injector nozzles of single hole type with a specification DN0SD151 with a spray angle of 0° were used in the investigation. The setup uses two nozzles to project the high velocity steam along the cutting edge ensuring maximum possible interpenetration of both chip-tool and the work-tool interfaces. Experimentation was conducted on a medium duty Kirloskar Turnmaster-35 lathe. Variable cutting speed and variable feed was achieved by the use of infinitely variable DC motors. A Kistler dynamometer (type 9257B) was used to detect the cutting forces. Cutting temperature was measured using optical pyrometer. The minimal cutting fluid setup facilitated the independent variation of pressure at fluid injector, frequency of pulsing and the quantity (rate) of fluid application.

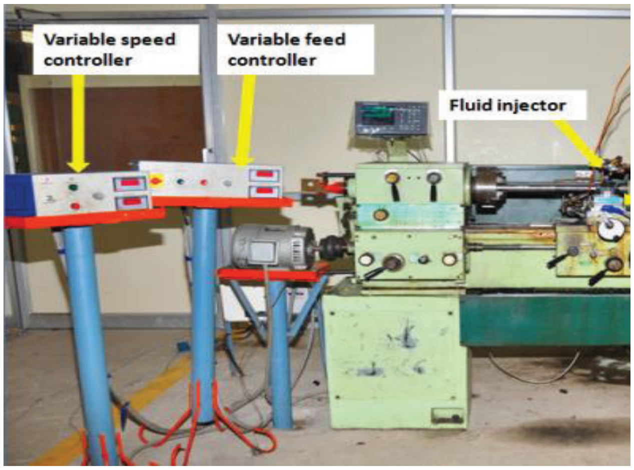

Figure 1 Experimental set up contains lathe and Minimal Fluid application set up.

2.5 Design of experiment

A nine run, three factor, three level orthogonal array was designed by following Taguchi's design of experiments to perform the experiments [11] which is shown in Table 3. The orthogonal array helped to greatly reduce the total number of runs [12] required to study the variation of the parameters affecting the quality characteristics.

Table 3 Design matrix for nine-run, three-level experiment with three factors

Standard order	**Factor columns**		
1	1	1	1
2	1	2	2
3	1	3	3
4	2	1	2
5	2	2	3
6	2	3	1
7	3	1	3
8	3	2	1
9	3	3	2

3. RESULTS AND DISCUSSION

In the experimental phase, preliminary experiments were conducted through trial runs. Trial runs helped in fixing the range of parameters. In the second phase, experiments were carried out using Taguchi L_9 orthogonal array with experimental values and the observed readings are presented in Table 4. Confirmatory runs were also conducted to verify the correctness of the readings.

Table 4 Response variables observed during the MCFA machining

S. No	Pressure	Frequency	Composition	Quantity	Cutting force	Cutting temperature
	(bar)	(pulses/ min)	(%)	(ml/min)	(N)	(˚C)
1	50	500	10	4	288.1	175.85
2	50	600	20	8	254	150.75
3	50	700	30	12	273.3	177.9
4	75	500	20	12	260.6	145.75
5	75	600	30	4	261.4	151.8
6	75	700	10	8	247.4	142.7
7	100	500	30	8	238.5	136.6
8	100	600	10	12	198.3	113.2
9	100	700	20	4	224	139.83

3.1 Analysis of cutting temperature

Fig. 2 shows the relative significance of cutting parameters on the cutting temperature.

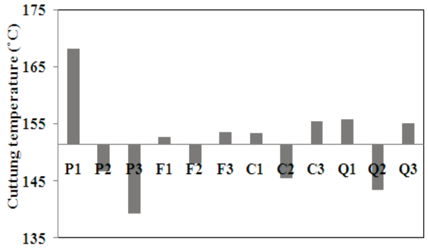

Fig. 2 Relative significance of fluid application parameters on cutting temperature
(p-Pressure at injector, f-Frequency, q-Quantity, c-Composition)

ANOVA was also carried out using Qualitek-4 software to find out the percentage influence of individual parameters on cutting temperature. It was found that the interaction effects were not significant.

From Fig.2, it is found that the highest pressure of 100 bar (P3), highest level of frequency of 600 pulses/min (F2), the highest level of percentage composition of oil by volume of 20% (C2) and quantity of 4ml/min (Q2) contributed most at attaining the reduction in cutting temperature. Analysis of variance was conducted and summarised as in table 5.

Table 5 ANOVA summary for cutting temperature.

Col#/ Factor	DOF (f)	Percent (%)
Pressure [bar]	2	71.429
Frequency [pulses/min]	2	2.541
Composition [%]	2	8.683
Quantity [ml]	2	15.44
Error	9	1.907
Total	17	100.00%

From Table 5, it is clear that the pressure of cutting fluid applied shows a significant effect on hard turning of OHNS steel. The quantity of cutting fluid applied, composition of cutting fluid and frequency of application also shows some effects on controlling machining parameters.

3.3 Analysis of cutting force

From Fig.3, it is found that the highest pressure of 100bar (P3), highest level of frequency of 600 pulses/min (F2), the highest level of percentage composition of oil by volume of 20% (C2) and quantity of 4ml/min (Q2) contributed most at attaining the reduction in cutting force.

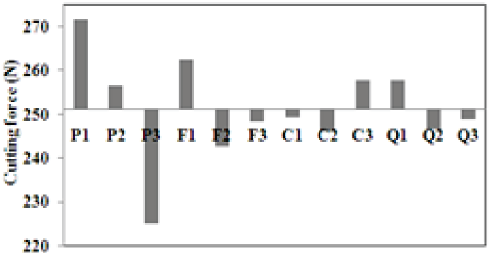

Fig. 3 Relative significance of parameters on cutting force (P-pressure at the inector, F- frequency of pulsing, C- % composition of cutting fluid and Q- quantity of application)

Table 6 ANOVA summary of the input parameters on cutting force

Col#/ Factor	DOF (f)	Percent (%)
Pressure [bar]	2	75.757
Frequency [pulses/min]	2	13.689
Composition [%]	2	4.562
Quantity [ml]	2	4.553
Error	9	1.439
Total	17	100.00%

From table 6, it is clear that the pressure of cutting fluid applied shows a significant effect on hard turning of OHNS steel. The quantity of cutting fluid applied, composition of cutting fluid and frequency of application also shows some effects on controlling machining parameters.

4. CONCLUSION

1. This study was conducted to find the effect of fluid application parameters on Hard turning of OHNS steel.
2. The cutting fluid under high pressure was found to be a very effective parameter in the reduction of cutting force and cutting temperature.
3. Quantity of cutting fluid found to be the second important factor the affect reduction in cutting temperature.
4. Frequency of pulsing seem to be very effective in case of reduction of cutting force. The pulsing fluid help to increase Rebinder effect which in turn reduce cutting force.
5. Since no cutting fluid was used in the investigation it promoted green environment in the shop floor, minimized the industrial hazard.

REFERENCES

[1] H.K. Tönshoff, C. Arendt, R. Ben Amor, Cutting of hardened steel., Annals CIRP 49(2), 2000 547–566.

[2] W. König, T. Hochschule, R. Komanduri, D. Schenectady and H. K. Tönshoff, Machining of hard materials, Annal CIRP, 33(2), 1984, 417– 427.

[3] NIOSH (2001) 'Metal Working Fluids - Recommendation for Chronic Inhalation Studies', National Institute for Occupational Safety and Health (NIOSH), Cincinnati, OH USA 45226.

[4] P. Leskover and J. Grun, The metallurgical aspect of machining, Annals of CIRP, 35(1), 1986 537-550.

[5] N. R. Dhar, S. Paul and A. B. Chattopadhyay, The influence of cryogenic cooling on tool wear, dimensional accuracy and surface finish in turning AISI 1040 and E4340C steels, Wear, 249, 2002, 932–942.

[6] F. Klocke and G. Eisenblatter, Dry cutting. Annals of CIRP, 46(2), 1997, 519-525.

[7] J. W. Sutherland, An experimental Investigation of air quality in wet and dry turning. Annals of CIRP, 35(2), 2000, 519-532.

[8] Mohammad Usman Ghani, Nuri A. Abukhshim and M. A. Sheikh, An investigation of heat partition and tool wear in hard turning of H13 tool steel with CBN cutting tools. Int J Adv Manuf Technol, 39, 2008, 874–888.

[9] A. Vernon and T. Özel, Factors affecting surface roughness in finish hard turning. In: Proceedings of the 17th International Conference on Production Research (ICPR-17), Blacksburg,Virginia, August 2003.

[10] J. Kopac, M. Bahor and C. M. Sokovi, Optimal machining parameters for achieving the desired surface roughness in fine turning of cold pre-formed steel workpieces. International Journal of Machine Tools Manufacture, 42(6), 2002, 707–716.

[11] W. H. Yang and Y. S. Tarng, Design optimization of cutting parameters for turning operations based on the Taguchi method, Journal of Materials Processing Technology, 84, 1998, 122–129.

[12] J. P. Davim, A note on the determination of optimal cutting conditions on the surface finish obtained in turning using design experiments. J Mater Process Technology, 116(2/3), 2001, 305–308.

Dr. Anil Raj received his PhD degree from Karunya Institute of Technology and Science'.

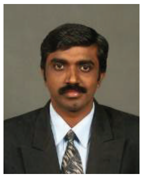

Dr. K. Leo Dev Wins is currently working as professor in the department of Mechanical Engineering at Karunya Institute of Technology and Sciences, Coimbatore.

Dr Varadharajan A S has obtained his M.Tech and PhD from IIT Madras. Currently he is the Principal in MES College of Engineering

MES JOURNAL OF TECHNOLOGY AND MANAGEMENT
Volume 4,No 1,12-23,2020

Adaptive Robust Controller for Vehicle Active Suspension System with Actuator Dynamics

Dynamics

Shyma Muhammed
Department Of Electrical Engineering
MES College of Engineering
Kuttipuram,
shymaanas@gmail.com

Shijila P T
Department Of Electrical Engineering
MES College of Engineering
Kuttipuram,
shijashilla@gmail.com

ABSTRACT

Vehicle suspension systems are of importance for contributing to the car's handling and keeping vehicle occupants comfortable and reasonably well isolated from road noise, bumps, vibrations, etc. In particular, active suspension systems have remained attractive for many years, since appropriate improvements of active suspensions have a potential to improve ride comfort and vehicle maneuverability. Suspension system keeps the tires in contact with the road and allows relative motion between two. This paper aims to design a controller for vehicle suspension system after mathematically modelling it as a linear system by using half car model. Modeling and analysis of the active suspension system considering the actuator dynamics are carried out. A new strategy named adaptive robust control (ARC) which is a combination of adaptive control and robust control methods is proposed here to account for uncertainties in systems. The efficacy of the proposed controller is shown through illustrative examples. It is evident from the simulation results that better performance is achieved using ARC controller with actuator dynamics.

Keywords

Adaptive robust controller; vehicle active suspension system; half car model.

1. INTRODUCTION

Traditionally automotive suspension designs have been compromising between the three conflicting criteria's namely road handling, load carrying, and passenger comfort. The suspension system must support the vehicle, provide directional control using handling maneuvers and provide effective isolation of passengers and load disturbance. Ability to store, dissipate and to introduce energy to the system are the main features of an active suspension system and depending upon operating conditions its parameters may vary. [2]

The car body from the car wheel can be physically separated using a mechanism known as Suspension system. This can minimize the vertical acceleration transmitted to the passenger which directly provides road comfort [2]. The main classification of Suspension are passive, semi-active, and active systems. Various types of springs and dampers or shock absorbers contained in passive suspension systems which help to isolate the vehicle from road noise, bumps and vibrations. However, when optimizing a passive suspension system, the physically possible limits will be reached and thus passive suspension wills always a compromise between comfort, handling and ride stability [3]. In order to provide significantly more efficient performance electronically controlled actuators are used in active suspension systems

Suspension system in automobiles is mainly to improve the ride comfort and road handling. Suspension systems are designed to maintain vehicle stability by reducing the effects of dynamic loads while providing a comfortable ride via the reduction of impulse forces from terrain features. Several performance characteristics have to be considered in order to achieve a good suspension system. These characteristics deal with regulation of body movement, regulation of suspension movement and force distribution. Ideally the suspension should isolate the body from road disturbances and inertial disturbances associated with cornering and braking or acceleration.

Anti-Lock Braking System (ABS) was the first assistance system appears in production vehicles [3-4]. A set of valves are used here to modulate pressure to the brakes at individual wheels. Different longitudinal forces on each side of the vehicle will be produced while it provide maximum braking on each wheel. This will apply yaw moment which may cause an undesirable rotation of the vehicle and is the main drawback of ABS system.

A quarter suspension car model is discussed in [5] .The sprung mass, acceleration, suspension deflection and tire deflection are considered as the optimization object. Linear matrix inequalities are solved to obtain the non-fragile state feedback H-infinity controller.

In [12] a new modeling technique to represent a half-car motion equation in the state space form is considered. The pitch and heave control scheme is proposed in [4] which is similar to the stability augmentation system (SAS) used in aircraft control, which is simply a feedback control designed to increase the relative damping of a particular mode of motion of the system. In [11,13] back stepping control is introduced for control of half car suspension system model to improve the inherent trade-off between ride quality and suspension travel. Nonlinear filters are fitted along front and rear wheel of tire. Bandwidth of two nonlinear filters depends on magnitude of front and rear suspension travel. Suspension travel is the space variation between the car body and the tires. If suspension travel is small, controller has softens the suspension for enhancing passenger comfort. If suspension travel approaches its limit, controller has shifts its attention to rattle space utilization by stiffening the suspension.

Adaptive robust controller is designed for Vibration control for Half-car suspension model in [10]. In response to uncertainties in systems and the possible actuator saturation, a saturated adaptive robust control (ARC) strategy is proposed. Especially anti-windup compensator is added to adjust control strategy in a manner conducive to stability and performance preservation in the presence of saturation. But actuator dynamics are not taken in to account here.

Ideally the suspension should isolate the body from road disturbances and inertial disturbances associated with concerning and braking or acceleration. There has been a widespread interest in using advanced control technique to improve the performance of vehicle suspension system. Improving the ride comfort in vehicles is an active research area due to developing technology. This paper proposes an Adaptive Robust Controller (ARC) method for a vehicle suspension system after mathematically modelling it as a linear system by using half car model to minimize the suspension deflection. Modeling and analysis of the active suspension system with the actuator dynamics are carried out here.

2. SYSTEM DESCRIPTION

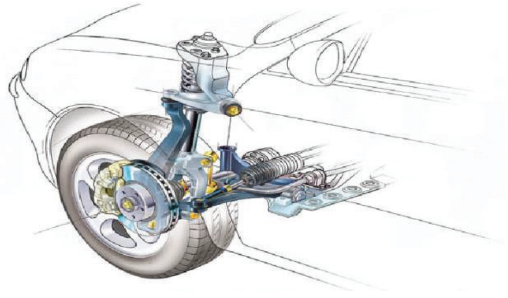

Figure 1: Suspension system

Figure 1 depicts a suspension system which provides road handling and isolation of vehicle bodies from the irregularities of road surfaces. Suspension systems are designed to maintain vehicle stability by reducing the effects of dynamic loads while providing a comfortable ride via the reduction of impulse forces from terrain features. Suspension is the term given to the system of springs, shock absorbers and linkages that connects a vehicle to its wheels. Main function is the minimization of the vertical acceleration transmitted to the passenger. Mechanism is that separates the car body from the car wheel. A typical vehicle suspension is made up of two components: a spring and a damper. The spring is chosen based solely on the weight of the vehicle, while the damper is the component that defines the suspension’s placement on the compromise curve.

Passive suspension system, semi-active suspension system and active suspension system are the major three types of suspension system.Traditional suspension consists springs and dampers are referred to as passive suspension, then if the suspension is externally controlled it is known as Semi-active or active suspension. Active suspension system has the ability to response to the vertical changes in the road input. The damper or spring is interceding by the force actuator. This force actuator has its own task which is to add or dissipate energy from the system. The force actuator is control by various types of controller determine by the designer.

3. MATHEMATICAL MODELING OF HALF- CAR SUSPENSION SYSTEM

The mathematical modelling of a two degree of freedom quarter car body for an active suspension system is being carried out by using basic laws of mechanics. Modelling of suspension system has been taking into account the following observations.

1. The suspension system modelled here is considered two degree of freedom system and

assumed to be a linear or approximately linear system for half car.

2. Some minor forces (including flex in the vehicle body, movement and backlash in various linkages, joints and gear system) are neglected for reducing the complexity of the system because effect of these forces is minimal due to low intensity. Hence these left out for the system model.

3. Tyre material is considered as having damping property as well as stiffness.

Mathematical modelling is the first and most crucial step in developing a control algorithm for a suspension system[1]. The dynamic model, which describes the relationship between the input and output, enables ones to understand the behaviour of the system better. Based on this mathematical equation in the modelling, control law can be designed with the objectives to minimize the vertical acceleration of the car body and good tire-road contact. In this paper the suspension system is modeled as a linear suspension system. The state variable can be represented as a vertical and pitch movement of the car body and wheels. In order to obtain linear model, roll angle is assume to be small.

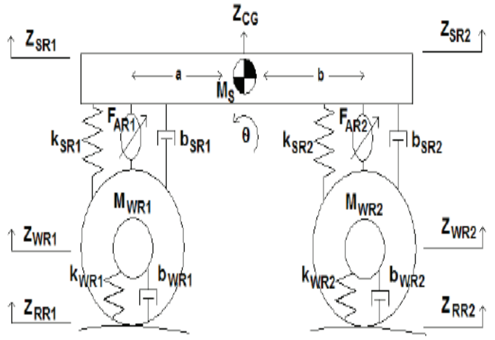

Figure 2: Half car model

Mathematical modeling for active suspension is derived from Fig 2. Suspension system can be modeled approximately by spring-mass-dashpot system of four degrees of freedom. It is called half car model, where the sprung mass m_S is attached by the suspension, modeled as spring and a damper to the unsprung masses m_{WR1}, m_{WR2}. m_{WR1} , m_{WR2}Both vertical motion and pitch motion of vehicles are considered in developing equations of motion for half-car suspension. For active suspension, the automatic actuator is connected and is modeled by control force.

For sprung mass, Forces in the vertical direction at the CG,

$$m_s\ddot{Z}_{CG} = F_{KSR1} + F_{BSR1} + F_{KSR2} + F_{BSR2} + F_{AR1} + F_{AR2} \quad (1)$$

Sum of the moments around the CG (pitch)

$$\dot{J}yy\ddot{\theta} = -a(F_{KSR1} + F_{BSR1}) + b(F_{KSR2} + F_{BSR2}) - aF_{AR1} + bF_{AR2}$$
(2)

Sum of the forces in the vertical direction at the right front wheel

$$m_{WR1}\ddot{Z}_{WR1} = -F_{KSR1} + F_{KWR1} - F_{BSR1} + F_{BWR1} - F_{AR1} \quad (3)$$

Sum of the forces in the vertical direction at the right rear wheel

$$m_{WR2}\ddot{Z}_{WR2} = -F_{KSR2} + F_{KWR2} - F_{BSR2} + F_{BWR2} - F_{AR2} \quad (4)$$

Here

$$F_{KSR1} = k_{SR1}(Z_{SR1} - Z_{WR1})$$
$$F_{BSR1} = b_{SR1}(\dot{Z}_{SR1} - \dot{Z}_{WR1})$$
$$F_{KSR2} = k_{SR2}(Z_{SR2} - Z_{WR2})$$
$$F_{BSR2} = b_{SR2}(\dot{Z}_{SR2} - \dot{Z}_{WR2})$$
$$F_{KWR1} = k_{WR1}(Z_{WR1} - Z_{RR1})$$
$$F_{BWR1} = b_{WR1}(\dot{Z}_{WR1} - \dot{Z}_{RR1})$$
$$F_{KWR2} = k_{WR2}(Z_{WR2} - Z_{RR2})$$
$$F_{BWR2} = b_{WR2}(\dot{Z}_{WR2} - \dot{Z}_{RR2})$$

Now use small angle approximation to simplify

$$Z_{SR1} = Z_{CG} - a\theta$$
$$\dot{Z}_{SR1} = Z_{CG} - a\dot{\theta}$$
$$Z_{SR2} = Z_{CG} + b\theta$$
$$\dot{Z}_{SR2} = Z_{CG} + b\dot{\theta} \quad (5)$$

Plug in for the corner positions and velocities

$$m_S = -k_{SR1}[Z_{CG} - a\theta] - b_{SR1}[\dot{Z}_{CG} - a\dot{\theta}]$$
$$+ k_{SR1}Z_{WR1} + b_{SR1}\dot{Z}_{WR1} - k_{SR2}[Z_{CG} - b\theta]$$
$$- b_{SR2}[\dot{Z}_{CG} - b\dot{\theta}] + k_{SR2}Z_{WR2} + b_{SR2}\dot{Z}_{WR2}$$
$$+ F_{AR1} + F_{AR2} \quad (6)$$

$$j_{yy}\ddot{\theta} = -ak_{SR1}[Z_{CG} - a\theta] - bb_{SR1}[\dot{Z}_{CG} - a\dot{\theta}] -$$
$$a[k_{SR1}Z_{WR1} - b_{SR1}\dot{Z}_{WR1}] - bk_{SR2}[Z_{CG} + b\theta] -$$

$$bb_{SR2}[\dot{Z}_{CG} + b\dot{\theta}] + b[k_{SR2}Z_{WR2} + b_{SR2}\dot{Z}_{WR2}] - aF_{AR1} +$$

$$\begin{aligned} j_{yy}\ddot{\theta} = &-ak_{SR1}[Z_{CG} - a\theta] - b_{SR1}[\dot{Z}_{CG} - a\dot{\theta}] \\ &- a[k_{SR1}Z_{WR1} - b_{SR1}\dot{Z}_{WR1}] - bk_{SR2}[Z_{CG} - b\theta] \\ &- b_{SR2}[\dot{Z}_{CG} - b\dot{\theta}] + b[k_{SR2}Z_{WR2} + b_{SR2}\dot{Z}_{WR2}] \end{aligned}$$

$$bF_{AR2} - aF_{AR1} + bF_{AR2} \tag{7}$$

$$m_{WR1}\ddot{Z}_{WR1} = -k_{SR1}[Z_{CG} - a\theta] - b_{SR1}[\dot{Z}_{CG} - a\dot{\theta}] - [k_{WR1} + k_{SR1}]Z_{WR1} - [b_{WR1} + b_{SR1}]\dot{Z}_{WR1} - F_{AR1})$$

$$\begin{aligned} m_{WR1}\ddot{Z}_{WR1} = &-k_{SR1}[Z_{CG} - a\theta] - b_{SR1}[\dot{Z}_{CG} - a\dot{\theta}] \\ &-[k_{WR1} + k_{SR1}]Z_{WR1} - [b_{WR1} + b_{SR1}]\dot{Z}_{WR1} - F_{AR1}) \end{aligned} \tag{8}$$

$$m_{WR2}\ddot{Z}_{WR2} = k_{SR12}[Z_{CG} + b\theta] \mp [\dot{Z}_{CG} + b\dot{\theta}] - [k_{WR2} + k_{SR2}]Z_{WR2} - [b_{WR2} + b_{SR2}]\dot{Z}_{WR2} - F_{AR2}$$

$$\begin{aligned} m_{WR1}\ddot{Z}_{WR2} = &k_{SR12}[Z_{CG} + b\theta] \mp [\dot{Z}_{CG} + b\dot{\theta}] \\ &-[k_{WR2} + k_{SR2}]Z_{WR2} - [b_{WR2} + b_{SR2}]\dot{Z}_{WR2} - F_{AR2}) \end{aligned} \tag{9}$$

By defining the state variables as

$$\begin{aligned} &X_1 = Z_{CG}, X_2 = Z_{CG}, X_3 = \theta \\ &X_4 = \dot{\theta}, X_5 = Z_{WR1}, X_6 = \dot{Z}_{WR1} \\ &X_7 = Z_{WR2}, X_8 = \dot{Z}_{WR2} \end{aligned} \tag{10}$$

State space equation can be written as

$$\begin{aligned} &\dot{\mathrm{X}}(\mathrm{t}) = \mathrm{AX}(\mathrm{t}) + \mathrm{BU}(\mathrm{t}) \\ &\mathrm{Y}(\mathrm{t}) = \mathrm{CX}(\mathrm{t}) + \mathrm{DU}(\mathrm{t}) \end{aligned} \tag{11}$$

Where

$$\begin{aligned} &\dot{X}_1 = \dot{Z}_{CG} = X_2, \dot{X}_2 = \ddot{Z}_{CG} \\ &\dot{X}_3 = \dot{\theta} = X_4, \dot{X}_4 = \ddot{\theta} \\ &\dot{X}_5 = \dot{Z}_{WR1} = X_6, \dot{X}_6 = \ddot{Z}_{WR1} \\ &\dot{X}_7 = \dot{Z}_{WR2} = X_8, \dot{X}_8 = \ddot{Z}_{WR2}\ \dot{X}_7 = \dot{Z}_{WR2} = X_8 \end{aligned} \tag{12}$$

$$A = \begin{bmatrix} 0 & 1 & 0 & 0 & 0 & 0 & 0 & 0 \\ \frac{-k_{SR1} - k_{SR2}}{m_S} & \frac{-b_{SR1} - b_{SR2}}{m_S} & \frac{-ak_{SR1} - bk_{SR2}}{m_S} & \frac{-ab_{SR1} - bb_{SR2}}{m_S} & \frac{k_{SR1}}{m_S} & \frac{b_{SR1}}{m_S} & \frac{k_{SR2}}{m_S} & \frac{b_{SR2}}{m_S} \\ 0 & 0 & 0 & 1 & 0 & 0 & 0 & 0 \\ \frac{ak_{SR1} - bk_{SR2}}{j_{yy}} & \frac{ab_{SR1} - bb_{SR2}}{j_{yy}} & \frac{-a^2k_{SR1} - b^2k_{SR2}}{j_{yy}} & \frac{-a^2b_{SR1} - b^2b_{SR2}}{j_{yy}} & \frac{-ak_{SR1}}{j_{yy}} & \frac{-ab_{SR1}}{j_{yy}} & \frac{bk_{SR2}}{j_{yy}} & \frac{bb_{SR2}}{j_{yy}} \\ 0 & 0 & 0 & 0 & 0 & 1 & 0 & 0 \\ \frac{k_{SR1}}{m_{WR1}} & \frac{b_{SR1}}{m_{WR1}} & \frac{-ak_{SR1}}{m_{WR1}} & \frac{-ab_{SR1}}{m_{WR1}} & \frac{-k_{WR1} - k_{SR1}}{m_{WR1}} & \frac{-b_{WR1} - b_{SR1}}{m_{WR1}} & 0 & 0 \\ 0 & 0 & 0 & 0 & 0 & 0 & 0 & 1 \\ \frac{k_{SR2}}{m_{WR2}} & \frac{b_{SR2}}{m_{WR2}} & \frac{bk_{SR2}}{m_{WR2}} & \frac{bb_{SR2}}{m_{WR2}} & 0 & 0 & \frac{-k_{WR2} - k_{SR2}}{m_{WR2}} & \frac{-b_{WR2} - b_{SR2}}{m_{WR2}} \end{bmatrix}$$

$$B = \begin{bmatrix} 0 & 0 \\ \frac{1}{m_s} & \frac{1}{m_s} \\ 0 & 0 \\ \frac{-a}{j_{yy}} & \frac{b}{j_{yy}} \\ 0 & 0 \\ \frac{-1}{m_{WR1}} & 0 \\ 0 & 0 \\ 0 & \frac{-1}{m_{WR2}} \end{bmatrix}$$

$$C = \begin{bmatrix} 1 & 0 & 0 & 0 & 0 & 0 & 0 & 0 \end{bmatrix}$$

$$D = \begin{bmatrix} 0 & 0 & 0 & 0 & 0 & 0 & 0 & 0 \end{bmatrix}$$

State space representation of half car active suspension system is given below

$$\begin{bmatrix} \dot{Z}_{CG} \\ \ddot{Z}_{CG} \\ \dot{\theta} \\ \ddot{\theta} \\ \dot{Z}_{WR1} \\ \ddot{Z}_{WR1} \\ \dot{Z}_{WR2} \\ \ddot{Z}_{WR2} \end{bmatrix} = A \begin{bmatrix} Z_{CG} \\ \dot{Z}_{CG} \\ \theta \\ \dot{\theta} \\ Z_{WR1} \\ \dot{Z}_{WR1} \\ Z_{WR2} \\ \dot{Z}_{WR2} \end{bmatrix} + B \begin{bmatrix} F_{AR1} \\ F_{AR2} \end{bmatrix} \tag{13}$$

$$Y = \begin{bmatrix} 1 & 0 & 0 & 0 & 0 & 0 & 0 & 0 \end{bmatrix} \begin{bmatrix} Z_{CG} \\ \dot{Z}_{CG} \\ \theta \\ \dot{\theta} \\ Z_{WR1} \\ \dot{Z}_{WR1} \\ Z_{WR2} \\ \dot{Z}_{WR2} \end{bmatrix} \quad (14)$$

Here

Z_{SR1} Z_{SR1}=Position of the front right body

Z_{SR2} Z_{SR2} =Position of the rear right body

Z_{WR1} Z_{WR1}=Position of the front right wheel

Z_{WR2} Z_{WR2}=Position of the rear right wheel

Z_{CG} Z_{CG} =Position of the body at CG

m_s m_S=Mass of the body at CG

a=Distance from CG to front axle.

b= Distance from CG to rear axle.

Table 1: Parameters of Half-car active suspension [9]

m_S	1 200 kg
j_{yy}	600 kgm^2
$m_{WR1} = m_{WR2}$	100 kg
a	1.2 m
b	1.5 m
$k_{SR1} = k_{SR2}$	15000 N/m
k_{WR1}	200000 N_s/m
k_{WR2}	150000 N_s/m
$b_{SR1} = b_{SR2}$	1500 N_s/m
b_{WR1}	1500 N_s/m
b_{WR2}	2000 N_s/m

4. MATHEMATICAL MODELING OF HALF-CAR SUSPENSION SYSTEM WITH ACTUATOR DYNAMICS

Hydraulic actuators are used for suspension systems to generate the pushing force between sprung and unsprung masses. Let the hydraulic actuator used for suspension model be a four-way valve-piston system, in which the force F_{AR1}, F_{AR2} F_{AR1}, F_{AR2} are

$$F_{AR1} = AP_{LF}$$

$$F_{AR1} = AP_{LF} F_{AR1} = AP_{LF} (15)$$

$$F_{AR2} = AP_{LR} \quad (16)$$

Where A is the area of piston and P_{LF} and P_{LR} are the pressure drop across the piston with respect to the front and rear suspensions [6]. The derivative of P_{LF} and P_{LR} are given in Equations (17) and (18).

$$\frac{V_t}{4\beta}\dot{P}_{LF} = Q_F - C_{tp}P_{LF} - A(\dot{Z}_{CG} + a\dot{\theta}) \; \frac{V_t}{4\beta}\dot{P}_{LF} = Q_F - C_{tp}P_{LF} - A\left(\dot{Z}_{CG} + a\dot{\theta}\right) \quad (17)$$

$$\frac{V_t}{4\beta}\dot{P}_{LF} = Q_R - C_{tp}P_{LR} - A(\dot{Z}_{CG} + a\dot{\theta}) \; \frac{V_t}{4\beta}\dot{P}_{Lr} = Q_R - C_{tp}P_{LR} - A(\dot{Z}_{CG} - b\dot{\theta}) \quad (18)$$

where V_t is the total actuator volume, β is the effective bulk modulus of system, Q_F,$Q_R$are the hydraulic load flow, and C_{tp} is the total leakage coefficient of piston. The relationship between the spool valve displacement and the hydraulic load flow is given as:

$$Q_F = \gamma\dot{x}_{VF} \; Q_F = \quad (19)$$

$$Q_R = \gamma\dot{x}_{VR} \; Q_R = \quad (20)$$

Here $\dot{x}_{VF}$, $\dot{x}_{VR}$ are controlled by the input to the servo-valve v_F, v_R. The valve dynamics are approximated by a linear filter with time constant τ:

$$\dot{x}_{VF} = \frac{1}{\tau}(-x_{VF} + v_F) \qquad (21)$$

$$\dot{x}_{VR} = \frac{1}{\tau}(-x_{VR} + v_R)\,\frac{1}{\tau}(-x_{VR} + v_R) \qquad (22)$$

The linear model of the hydraulic actuator is as follows:

$$\dot{P}_{LF} = \gamma \dot{x}_{VF} - \beta P_{LF} - \alpha A(\dot{Z}_{CG} + a\dot{\theta}) \qquad (23)$$

$$\dot{P}_{LR} = \gamma \dot{x}_{VR} - \beta P_{LR} - \alpha A(\dot{Z}_{CG} + b\dot{\theta}) \qquad (24)$$

Replace equations (1), (2), (3) and (4) with equations (16), (17), (23) and (24). Forces in the vertical direction at the CG,

$$\begin{aligned} m_s &= -k_{SR1}[Z_{CG} + a\theta] - b_{SR1}[\dot{Z}_{CG} - a\dot{\theta}] + k_{SR1}Z_{WR1} \\ &+ b_{SR1}\dot{Z}_{WR1} - k_{SR2}[Z_{CG} + b\theta] - b_{SR2}[\dot{Z}_{CG} - b\dot{\theta}] \\ &+ k_{SR2}Z_{WR2} + b_{SR2}\dot{Z}_{WR2} + AP_{LF} + AP_{LR} \end{aligned} \qquad (25)$$

Sum the moments around the CG (pitch),

$$\begin{aligned} j_{yy}\ddot{\theta} &= -ak_{SR1}[Z_{CG} - a\theta] - b_{SR1}[\dot{Z}_{CG} - a\dot{\theta}] - a[k_{SR1}Z_{WR1} \\ &- b_{SR1}\dot{Z}_{WR1}] - bk_{SR2}[Z_{CG} + b\theta] - bb_{SR2}[\dot{Z}_{CG} + b\dot{\theta}] \\ &+ b[k_{SR2}Z_{WR2} + b_{SR2}\dot{Z}_{WR2}] - aAP_{LF} + bAP_{LR} \end{aligned}$$

$$j_{yy}\ddot{\theta} = -ak_{SR1}[Z_{CG} - a\theta] - bb_{SR1}[\dot{Z}_{CG} - a\dot{\theta}] - a[k_{SR1}Z_{WR1} - b._{SR1}\,\dot{Z}_{WR1}] - bk_{SR2}[Z_{CG} + b\theta] - bb_{SR2}[\dot{Z}_{CG} + b\dot{\theta}] + b[k_{SR2}Z_{WR2} + b_{SR2}\dot{Z}_{WR2}] - aAP_{LF} + bAP_{LR} \qquad (26)$$

Sum of the forces in the vertical direction at the right front wheel

$$m_{WR1}\ddot{Z}_{WR1} = -k_{SR1}[Z_{CG} - a\theta] - b_{SR1}[\dot{Z}_{CG} - a\dot{\theta}] - [k_{WR1} + k_{SR1}]Z_{WR1} - [b_{WR1} + b_{SR1}]\dot{Z}_{WR1} -$$

$$m_{WR1}\ddot{Z}_{WR1} = -k_{SR1}[Z_{CG} - a\theta] - b_{SR1}[\dot{Z}_{CG} - a\dot{\theta}]$$

$$AP_{LF} - [k_{WR1} + k_{SR1}]Z_{WR1} - [b_{WR1} + b_{SR1}]\dot{Z}_{WR1} - AP_{LF}$$
(27)

Sum of the forces in the vertical direction at the right rear wheel

$$m_{WR2}\ddot{Z}_{WR2} = k_{SR12}[Z_{CG} + b\theta] \mp [\dot{Z}_{CG} + b\dot{\theta}] - [k_{WR2} + k_{SR2}]Z_{WR2} - [b_{WR2} + b_{SR2}]\dot{Z}_{WR2} - AP_{LR}$$

$$\begin{aligned} m_{WR2}\ddot{Z}_{WR2} &= -k_{SR12}[Z_{CG} + b\theta] \mp [\dot{Z}_{CG} + b\dot{\theta}] \\ &- [k_{WR2} + k_{SR2}]Z_{WR2} - [b_{WR2} + b_{SR2}]\dot{Z}_{WR2} - AP_{LR} \end{aligned} \qquad (28)$$

Let the state variables be

$$\begin{aligned} &X_1 = Z_{CG}, X_2 = \dot{Z}_{CG}, X_3 = \theta, X_4 = \dot{\theta} \\ &X_5 = Z_{WR1}, X_6 = \dot{Z}_{WR1}, X_7 = Z_{WR2} \\ &X_8 = \dot{Z}_{WR2}, X_9 = P_{LF}, X_{10} = x_{VF} \\ &X_{11} = P_{LR}, X_{12} = x_{VR} \end{aligned} \qquad (29)$$

State space equation can be written as

$$\begin{aligned} \dot{\mathrm{X}}(\mathrm{t}) &= \mathrm{AX(t)} + \mathrm{BU(t)} \\ \mathrm{Y(t)} &= \mathrm{CX(t)} + \mathrm{DU(t)} \end{aligned} \qquad (30)$$

Where

$$\begin{aligned} &\dot{X}_1 = \dot{Z}_{CG} = X_2, \dot{X}_2 = \ddot{Z}_{CG} \\ &\dot{X}_3 = \dot{\theta} = X_4, \dot{X}_4 = \ddot{\theta} \\ &\dot{X}_5 = \dot{Z}_{WR1} = X_6, \dot{X}_6 = \ddot{Z}_{WR1} \\ &\dot{X}_7 = \dot{Z}_{WR2} = X_8, \dot{X}_8 = \ddot{Z}_{WR2} \\ &\dot{X}_9 = \dot{P}_{LF}, \dot{X}_{10} = \dot{x}_{VF} \\ &\dot{X}_{11} = \dot{P}_{LR}, \dot{X}_{12} = \dot{x}_{VR} \end{aligned} \qquad (31)$$

$$A=\begin{bmatrix}
0 & 1 & 0 & 0 & 0 & 0 & 0 & 0 & 0 & 0 & 0 & 0\\
\frac{-k_{SR1}-k_{SR2}}{m_S} & \frac{-b_{SR1}-b_{SR2}}{m_S} & \frac{-ak_{SR1}-bk_{SR2}}{m_S} & \frac{-ab_{SR1}-bb_{SR2}}{m_S} & \frac{k_{SR1}}{m_S} & \frac{b_{SR1}}{m_S} & \frac{k_{SR2}}{m_S} & \frac{b_{SR2}}{m_S} & 0 & 0 & 0 & 0\\
0 & 0 & 0 & 1 & 0 & 0 & 0 & 0 & 0 & 0 & 0 & 0\\
\frac{ak_{SR1}-bk_{SR2}}{j_{yy}} & \frac{ab_{SR1}-bb_{SR2}}{j_{yy}} & \frac{-a^2k_{SR1}-b^2k_{SR2}}{j_{yy}} & \frac{-a^2b_{SR1}-b^2b_{SR2}}{j_{yy}} & \frac{-ak_{SR1}}{j_{yy}} & \frac{-ab_{SR1}}{j_{yy}} & \frac{bk_{SR2}}{j_{yy}} & \frac{bb_{SR2}}{j_{yy}} & 0 & 0 & 0 & 0\\
0 & 0 & 0 & 0 & 0 & 1 & 0 & 0 & 0 & 0 & 0 & 0\\
\frac{k_{SR1}}{m_{WR1}} & \frac{b_{SR1}}{m_{WR1}} & \frac{-ak_{SR1}}{m_{WR1}} & \frac{-ab_{SR1}}{m_{WR1}} & \frac{-k_{WR1}-k_{SR1}}{m_{WR1}} & \frac{-b_{WR1}-b_{SR1}}{m_{WR1}} & 0 & 0 & 0 & 0 & 0 & 0\\
0 & 0 & 0 & 0 & 0 & 0 & 0 & 1 & 0 & 0 & 0 & 0\\
\frac{k_{SR2}}{m_{WR2}} & \frac{b_{SR2}}{m_{WR2}} & \frac{bk_{SR2}}{m_{WR2}} & \frac{bb_{SR2}}{m_{WR2}} & 0 & 0 & \frac{-k_{WR2}-k_{SR2}}{m_{WR2}} & \frac{-b_{WR2}-b_{SR2}}{m_{WR2}} & 0 & 0 & 0 & 0\\
0 & -\alpha A & 0 & -\alpha Aa & 0 & 0 & 0 & 0 & -\beta & \gamma & 0 & 0\\
0 & 0 & 0 & 0 & 0 & 0 & 0 & 0 & 0 & \frac{-1}{\tau} & 0 & 0\\
0 & -\alpha A & 0 & \alpha Ab & 0 & 0 & 0 & 0 & 0 & 0 & -\beta & \gamma\\
0 & 0 & 0 & 0 & 0 & 0 & 0 & 0 & 0 & 0 & 0 & \frac{-1}{\tau}
\end{bmatrix}$$

$$B=\begin{bmatrix}
0 & 0\\
0 & 0\\
0 & 0\\
0 & 0\\
0 & 0\\
0 & 0\\
0 & 0\\
0 & 0\\
0 & 0\\
\frac{-1}{\tau} & 0\\
0 & 0\\
0 & \frac{-1}{\tau}
\end{bmatrix}$$

$$C=[1\quad 0\quad 0\quad 0\quad 0\quad 0\quad 0\quad 0\quad 0\quad 0\quad 0\quad 0]$$

$$D=[1] \tag{32}$$

State space representation of half car active suspension system is given below

$$\begin{bmatrix}\dot{Z}_{CG}\\ \ddot{Z}_{CG}\\ \dot{\theta}\\ \ddot{\theta}\\ \dot{Z}_{WR1}\\ \ddot{Z}_{WR1}\\ \dot{Z}_{WR2}\\ \ddot{Z}_{WR2}\\ \dot{P}_{LF}\\ \dot{x}_{VF}\\ \dot{P}_{LR}\\ \dot{x}_{VR}\end{bmatrix}=A\begin{bmatrix}Z_{CG}\\ \dot{Z}_{CG}\\ \theta\\ \dot{\theta}\\ Z_{WR1}\\ \dot{Z}_{WR1}\\ Z_{WR2}\\ \dot{Z}_{WR2}\\ P_{LF}\\ x_{VF}\\ P_{LR}\\ x_{VR}\end{bmatrix}+B\begin{bmatrix}v_F\\ v_R\end{bmatrix}$$

$$C=[1\quad 0\quad 0\quad 0\quad 0\quad 0\quad 0\quad 0\quad 0\quad 0\quad 0\quad 0]\begin{bmatrix}Z_{CG}\\ \dot{Z}_{CG}\\ \theta\\ \dot{\theta}\\ Z_{WR1}\\ \dot{Z}_{WR1}\\ Z_{WR2}\\ \dot{Z}_{WR2}\\ P_{LF}\\ x_{LF}\\ P_{LR}\\ x_{LR}\end{bmatrix} \tag{33}$$

5. ADAPTIVE ROBUST CONTROLLER (ARC)

Adaptive control is the control method used by a controller which must adapt to a controlled system with parameters which vary or are initially uncertain. It is differ from robust control in that it does not need a priori information about the bounds on these uncertain or time-varying parameters robust control guarantees that if the changes are within given bounds the control law need not be changed, while adaptive control is concerned with control law changing themselves. The foundation of adaptive control is parameter estimation Lyapunov stability is used to derive these update laws and shows convergence criterion. Projection and normalization are commonly used to improve the robustness of estimation algorithm. Adaptive controller is also called adjustable controller [6].

Robust control is a branch of control theory whose approach to controller design explicitly deals with uncertainty. Robust control method is designed to function properly provide that uncertain parameters or disturbances are found within some set. Robust control method aims to achieve robust performance and/or stability in the presence of bounded modelingerrors[7].

Adaptive Robust Controller (ARC) combines the benefits of deterministic robust control and adaptive control technique. Major advantage of ARC is that both transient and steady-state tracking accuracy can be guaranteed. Furthermore, asymptotic tracking can be achieved when no general uncertainty exists. ARC technique produce a continuous control law as opposed to switching laws commonly deployed in variable structure controller such as sliding mode control.

Adaptive Robust Controller design for half-car model with actuator dynamics

Consider the force dynamics for the active suspension system with actuator dynamics behavior are

$$\dot{P}_{LF} = \gamma \dot{x}_{VF} - \beta P_{LF} - \alpha A(\dot{Z}_{CG} + a\dot{\theta})$$

$$\dot{P}_{LF} = \gamma \dot{x}_{VF} - \beta P_{LF} - \alpha A(\dot{Z}_{CG} + a\dot{\theta}) \quad (34)$$

$$\dot{P}_{LR} = \gamma \dot{x}_{VR} - \beta P_{LR} - \alpha A(\dot{Z}_{CG} - b\dot{\theta})$$

$$\dot{P}_{LR} = \gamma \dot{x}_{VR} - \beta P_{LR} - \alpha A(\dot{Z}_{CG} - b\dot{\theta}) \quad (35)$$

Let P_{Ld} to denote the desired force and $e_1 = P_{LF} - P_{Ld}$ be the tracking error, a Lyapunov function is chosen to be:

$$V_1 = 1/2e_1^2 \; V_1 = 1/2e_1^2 \quad (36)$$

ARC control law consist of two parts, adaptive part and robust part.

$$u_A = u_{1a} + u_{1s} \; u_A = u_{1a} + u_{1s} \quad (37)$$

Bounds at $0<\theta_{1m}<\theta<\theta_{1M}$

Adaptive part is

$$u_{1a} = \frac{1}{k_3}(-k_1(\dot{Z}_{CG} + a\dot{\theta}) + k_2 P_{LF} + \frac{1}{\theta_{1M}}(\dot{P}_{Ld} + p_1 e_1)) \quad (38)$$

Robust part is

$$e_1 \frac{1}{4\theta_{1m}k_3}(-k_1(\dot{Z}_{CG} + a\dot{\theta}) + k_2 P_{LF} + \frac{1}{\theta_{1M}}(\dot{P}_{Ld} + p_1 e_1))$$

$$u_{1s} = e_1 \frac{1}{4\theta_{1m}k_3}(-k_1(\dot{Z}_{CG} + a\dot{\theta}) + k_2 P_{LF} + \frac{1}{\theta_{1M}}(\dot{P}_{Ld} + p_1 e_1)) \quad (39)$$

Using control law shown in above equations it is easy to show that

$$\dot{V}_1 \leq -p_1 e_1^2 + \varepsilon_{11} + \varepsilon_{12} \; \dot{V}_1 \leq -p_1 e_1^2 + \varepsilon_{11} + \varepsilon_{12} \quad (40)$$

Shows that the system is stable and the force tracking error is bounded. The transient and final tracking accuracy are adjustable by changing $p_1, \varepsilon_{11}, \varepsilon_{12}$

$$P_{Ld} = \dot{x}_{1r} - k_1 e_1$$

$$\dot{P}_{Ld} = \ddot{x}_{1r} - k_1 \dot{e}_1 \quad (41)$$

$$u_A = \frac{1}{K_3}\left[-K_1(\dot{Z}_{CG} + a\dot{\theta}) + K_2 P_{LF} + \frac{V}{\beta}(\ddot{x}_{5r} - d_3)\right]$$

$$u_B = \frac{1}{K_3}\left[-K_1(\dot{Z}_{CG} - b\dot{\theta}) + K_2 P_{LR} + \frac{V}{\beta}(\ddot{x}_{7r} - d_4)\right] \quad (42)$$

Then calculate real inputs by using above equations

$$u_3 = \frac{bu_A + u_B}{a+b}$$

$$u_4 = \frac{au_A + u_B}{a+b} \quad (43)$$

Solve u_3 and u_4 based on definition

$$u_3 = \frac{b}{K_3(a+b)}\left\{-K_1(X_2 + aX_4) + K_2X_9 + \frac{V}{\beta}(\ddot{X}_5 - d_3)\right\}$$
$$+\frac{1}{K_3(a+b)}\left\{-K_1(X_2 - bX_4) + K_2X_{11} + \frac{V}{\beta}(\ddot{X}_7 - d_3)\right\}$$
$$u_4 = \frac{a}{K_3(a+b)}\left\{-K_1(X_2 + aX_4) + K_2X_9 + \frac{V}{\beta}(\ddot{X}_5 - d_3)\right\}$$
$$+\frac{1}{K_3(a+b)}\left\{-K_1(X_2 - bX_4) + K_2X_{11} + \frac{V}{\beta}(\ddot{X}_7 - d_3)\right\} \qquad (44)$$

Substitute u₃ and u₄ into ẋ₁₀ and ẋ₁₂, obtain state space of controller

$$\begin{bmatrix}\dot{x}_5\\ \dot{x}_6\\ \dot{x}_7\\ \dot{x}_8\\ \dot{x}_9\\ \dot{x}_{10}\\ \dot{x}_{11}\\ \dot{x}_{12}\end{bmatrix} = \begin{bmatrix} 0 & 1 & 0 & 0 & 0 & 0 & 0 & 0\\ -\frac{k_{SR1}}{m_{WR1}} & -\frac{b_{SR1}}{m_{WR1}} & 0 & 0 & 0 & 0 & 0 & 0\\ 0 & 0 & 0 & 1 & 0 & 0 & 0 & 0\\ 0 & 0 & -\frac{k_{SR2}}{m_{WR2}} & -\frac{b_{SR2}}{m_{WR2}} & 0 & 0 & 0 & 0\\ 0 & 0 & 0 & 0 & 1 & 0 & 0 & 0\\ 0 & \frac{-K_1}{K_3\tau} & 0 & \frac{-K_1}{K_3\tau} & 0 & 0 & -\frac{K_2}{K_3\tau} & 0\\ 0 & 0 & 0 & 0 & 0 & 0 & 1 & 0\\ 0 & 0 & \frac{-K_1}{K_3} & \frac{-VK_1}{K_3\tau} & 0 & -\frac{K_2}{K_3\tau} & 0 & \frac{VK_1}{K_3\tau}\end{bmatrix}\begin{bmatrix}x_5\\ x_6\\ x_7\\ x_8\\ x_9\\ x_{10}\\ x_{11}\\ x_{12}\end{bmatrix}$$
$$+\begin{bmatrix} 0 & 0 & 0 & 0 & 0 & 0 & 0 & 0\\ -\frac{bm_S}{m_{WR}(a+b)\tau} & -\frac{j_{yy}}{m_{WR}(a+b)\tau} & \frac{bm_S}{m_{WR}(a+b)\tau} & \frac{j_{yy}}{m_{WR}(a+b)\tau} & 0 & 0 & 0 & 0\\ \frac{bm_S}{m_{WR}(a+b)\tau} & \frac{j_{yy}}{m_{WR}(a+b)\tau} & \frac{-bm_S}{m_{WR}(a+b)\tau} & \frac{j_{yy}}{m_{WR}(a+b)\tau} & 0 & 0 & 0 & 0\\ 0 & 0 & 0 & 0 & 0 & 0 & 0 & 0\\ 0 & 0 & 0 & 0 & 0 & 0 & 0 & 0\\ 0 & 0 & 0 & 0 & \frac{V}{K_3\beta\tau(a+b)} & \frac{V}{K_3\beta\tau(a+b)} & -\frac{V}{K_3\beta\tau(a+b)} & 0\\ 0 & 0 & 0 & 0 & 0 & 0 & 0 & 0\\ 0 & 0 & 0 & 0 & \frac{V}{K_3\beta\tau(a+b)} & \frac{V}{K_3\beta\tau(a+b)} & 0 & \frac{V}{K_3\beta\tau(a+b)}\end{bmatrix}\begin{bmatrix}\ddot{x}_{1r}\\ \ddot{x}_{3r}\\ \ddot{x}_{5r}\\ \ddot{x}_{7r}\\ d_1\\ d_2\\ d_3\\ d_4\end{bmatrix}$$

5. 5.1. Response of half-car model with actuator dynamics

Simulations are carried out in MATLAB with the modelled system dynamics. Figures 3 and 4 show the responses of the active suspension system with actuator dynamics for sprung mass and unsprung mass without controllers. For the sprungmass, the step response does not settled thus producing unstable performance. But in case of unsprungmass responses are settled down after 1 sec. To improve the performance of system by reducing the settling time, adaptive robust controllers are applied.

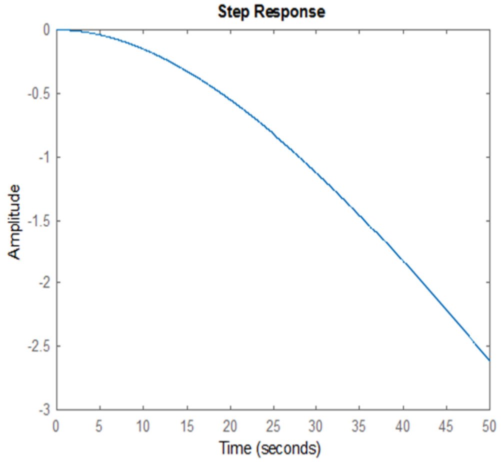

Figure. 3 Response of active suspension System without Controller for sprungmass with actuator dynamics

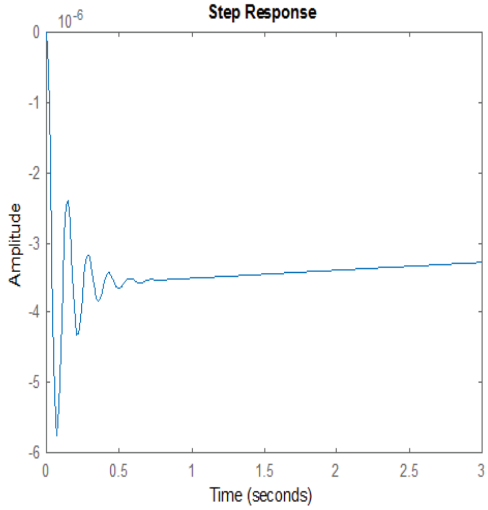

Figure 4 Response of active suspension System without Controller for unsprungmass with actuator dynamics

5.2 Adaptive Robust Controller response for half-car model with actuator dynamics

Adaptive robust controllers are designed for the half car model with actuator dynamics and the responses are obtained

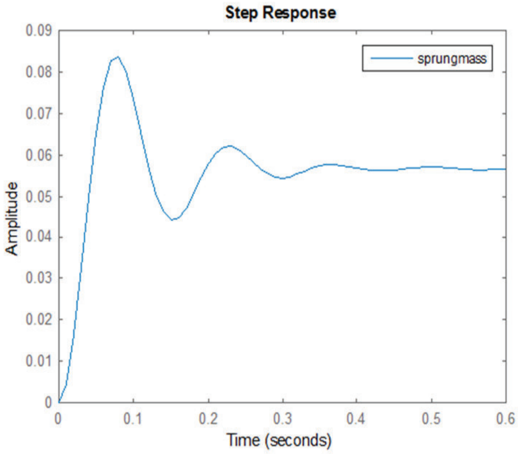

Figure 5 Response of active suspension System using ARC Controller for sprungmass with actuator dynamics

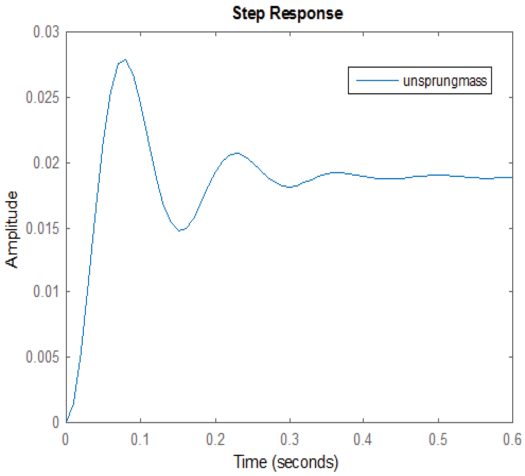

Figure 6 Response of active suspension System using ARC Controller for unsprungmass with actuator dynamics

Response of ARC controller with actuator dynamics for sprungmass and unsprungmass are shown in figures 5 and 6 respectively. The suspension system with actuator dynamics model produced better performance for ARC controller than without ARC controller. The suspension deflection is reduced and settling time for bothunsprungmass and sprungmass is 0.352s.

Comparison of performance of suspension system with actuator dynamics for different controllers are analyzed and shown in Table 1.

Table 1: Performance of suspension system with actuator dynamics for different controllers

Controller	Settling time	Controller effort
PID	NA(sprungmass) 0.612s(unsprungmass)	Good
ARC	0.352s (sprungmass And unsprungmass)	High

The analysis of Table 1 shows that the settling time is less for ARC controller suspension system with actuator dynamics than PID controllers. Result shows that ARC controller gives better performance compared to other controller.

CONCLUSION

Improving the ride comfort in vehicle is an active research area due to developing technology. Active suspension designs must resolve the inherent trade-offs between ride quality, handling, suspension travel and power consumption. The suspension must be able to minimize the vertical force transmitted to the passengers for passengers comfort. These objectives can be achieved by minimizing the vertical suspension deflection. In this paper, Adaptive Robust Controller and PID controller were designed and implemented on a car active suspension system in MATLAB platform. The implementation of PID controller reduces oscillation in the suspension system. But to provide more accurate performance, more advanced ARC controller is utilized. It can be seen that the magnitude of suspension deflection and settling time of the system are reduced by the ARC controller which is more important for the improvement in ride comfort. From the results, it can be concluded that for an active suspension system with actuator dynamics, ARC controller provided better performance than the conventional PID controller.

REFERENCES

[1] Abu Bakar Adham Bin Hell Mee, "Modeling and controller design for an active suspension system using half car model", *Thesis report*, May 2009.

[2] Ayman A. Aly, "Car Suspension Control Systems: Basic Principles", *International Journal Of Control, Automation And Systems* Vol.1, No.1, January 2012.

[3] Bosch Automotive Handbook, 6th Edition, *SAE Society of Automotive Engineers*,Inc,2004

[4] CamposJ 1, L. Davis, F. L Lewis, S. Ikenaga, S. Scully, and M. Evans, "Active Suspension Control of Ground Vehicle Heave and Pitch Motions", *Automation and Robotics Research Institute The University of Texas at Arlington 7300 Jack Newell Blvd. S, Fort Worth, Texas*76118-7115

[5] Du H , J. Lam, and K. Y. Sze, "Design of non-fragile H∞ controller for active vehicle suspensions," *J. Vib. Control*, vol. 11, no. 2, pp. 225–243,Feb. 2005.

[6] Fanping Bu and Bin Yao"Nonlinear adaptive robust control of hydraulic actuators regulated by proportional directional control valves with deadband and nonlinear flow gains" *Proceedings of the American Control Conference*, Chicago, Illinois June 2000.

[7] IrajHassanzadeh, Ghasem Alizadeh, Naser PourqorbanShirjoposht, Farzad Hashemzadeh, "A New Optimal Nonlinear Approach to Half Car Active Suspension Control", *IACSIT International Journal of Engineering and Technology* ,Vol. 2, No.1, February, 2010

[8] Robert L.W. & Kent L.L., "Modeling and Simulation of Dynamic System", Second Edition, Prentice-Hall,1997

[9] Samy Aly Hassan, The university of Leeds Department of Mechanical Engineering, Fundamental studies of passive, active and semi-active automotive suspension systems,July 1986

[10] Weichao Sun, Zhengli Zhao, and Huijun Gao, "Saturated Adaptive Robust Control for Active Suspension Systems" *IEEE Transactions on industrial electronics*, vol. 60, no. 9, september 2013

[11] Yagiz N and Y. Hacioglu, "Backstepping control of a vehicle with active suspensions," *Control Eng. Pract*., vol. 16, no. 12, pp. 1457–1467, Dec. 2008.

[12] Yahaya Md. Sam and Johari Halim Shah Bin Osman, "Modeling And Control Of The Active Suspension System Using Proportional Integral Sliding Mode Approach", *Asian Journal of Control*, Vol. 7, No. 2, pp. 91-98, June 2005

[13] Zhang H, Y. Shi, and A. S. Mehr, "Robust non-fragile dynamic vibration absorbers with uncertain factors*," J. Sound Vib*., vol. 330, no. 4, pp. 559–566, Feb. 2011.

Shyma Muhammed received the B.Tech degree in Electrical& Electronics Engineering from TKM College of Engineering ,Kollam,, Kerala in 1999 and the M.Tech degree in Instrumentation &Control from National Institute of Technology,Calicut in 2008. She acquired Phd in Control systems from NIT Calicut in 2016. She is currently working as an Associate Professor in MES College of Engineering,Kuttippuram

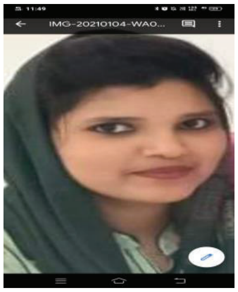

Mrs.Shijila P T acquired B Tech in Applied Electronics and Instrumentation Engineering from Royal College of Engineering ,Akkikavu in 2014 and M Tech in Instrumentation and Control Engineering from MES College of Engineering, Kuttipuram.

Preterm Birth Prediction Using Electrohysterogram Signals

Anju Madhavan
Department of Electrical and Electronics Engineering
MES College of Engineering, Kuttipuram
anjumadhavan92@gmail.com

Thazneem Fathima N.K
Department of Electrical and Electronics Engineering
MES College of Engineering, Kuttipuram
thasneemzaman1@gmail.com

Preetha R
Department of Electrical and Electronics Engineering
MES College of Engineering, Kuttipuram

ABSTRACT

Preterm birth is the largest cause of newborn sickness and mortality. Accurate prediction of preterm delivery improves the effectiveness of essential treatments. A better understanding of risk factors related to preterm birth has occurred in last few years and led to the introduction of several measures to reduce its occurrence. Conditions that can affect the respiratory, gastrointestinal, immune, central nervous, auditory and visual systems can seriously effect on preterm infants. This can also lead to long-term conditions, such as cerebral palsy, mental retardation, learning difficulties, including poor health and growth in some extreme cases. The analysis of uterine electrical signals could provide an easy path towards preterm birth detection. The work focuses on the electrohysterography (EHG) signal processing. Features based on wavelets and classifiers like linear, Support Vector Machine (SVM) classifier and KNN (K-Nearest Neighbor) classifier were used for analysis. An open dataset of Term-Preterm Electrohysterogram (TPEHG) database, containing 300 delivery records is used in this study. A simple, but efficient way for predicting premature deliveries, with six wavelet-based features and classified with linear classifier, SVM classifier and KNN classifier and performances were compared. K-NN Classifier provides a better accuracy of 93.75% compared to other two classifiers.

Keywords

Preterm birth; Electrohysterogram (EHG); Wavelet; Linear classifier; Support vector machine classifier; K-nearest neighbour classifier.

1. INTRODUCTION

Premature birth is found to be an important public health issue across the world because of its association with neonatal (first 28 days of life) mortality and short- and long-term morbidity and disability in later life. Preterm is explained by World Health Organization (WHO) as babies born alive before 37 completed weeks of gestation or fewer than 259 days of gestation since the first day of a woman's last menstrual period (LMP). Preterm birth prediction is very important because of its health and the economic consequences. Normally people are concentrating on reducing the effects caused by preterm birth. However, as this approach is costly, prevention is better. Effective preterm birth prediction can improve prevention by using appropriate medical and lifestyle interventions. One of the diagnostic tool used for preterm birth prediction is Electrohysterography (EHG). EHG is a specific form of electromyography (EMG), which measures electrical activity in muscular tissue near the uterus. Several studies have shown that the EHG record may vary for each woman, depending on whether she is in true labour or false labour and whether she will deliver term or preterm. EHG can be used for effective diagnosis of preterm birth.

According to WHO, every year about 15 million are born prematurely around the world and that is more than one in 10 of all babies born globally. Almost 1 million children die each year due to complications occurring in preterm birth [1]. In India, out of 26 million live births annually, 3.5 million are preterm and out of these 3.03 lakh babies die due to complications of preterm birth. Nowadays Preterm birth is the leading cause of neonatal death. Deaths of babies in the first month of life account for 40 percent of all deaths among children fewer than five years of age. The main cause of newborn deaths is preterm birth in the world. It is the second main cause of all child deaths under five, after pneumonia.

More than three-quarters of preterm can be saved with often inexpensive care such as essential care during child birth, antenatal steroid injections (given to pregnant women at risk of preterm labour under set criteria to strengthen the babies lungs) and postnatal care like kangaroo mother care (the baby is carried by the mother with skin-to-skin contact and frequent breastfeeding), and basic care for infections and breathing difficulties. Identification of risk factors in women with improved care before, between and during pregnancies; better access to contraceptives and increased empowerment/education can further decrease the preterm birth rate (the number of preterm births divided by the number of live births).

Preterm birth occurs for a variety of reasons. Preterm births can occur for three different reasons. According to roughly one-third are medically indicated or induced; delivery is brought forward for the best interest of the mother or baby. Another third occurs because the membranes rupture, prior to labour, called Preterm Premature Rupture of Membranes (PPROM). Lastly, spontaneous contractions (termed preterm labour or PTL) can develop. However, there is still a great deal of uncertainty about the level of risk each factor presents, and whether they are causes or effects. Nevertheless, in some of the causes of preterm labour, which may or may not end in preterm birth, these include infection, over-distension, burst blood vessels, surgical procedures, illnesses and congenital defects of the mother's uterus and cervical weakness. Further studies have also found other risk factors for PTL/PPROM [2, 3]. These include a previous preterm delivery (20%); last two births have been preterm (40%), and multiple births (twin pregnancy carries a 50% risk). Other health and lifestyle factors also include cervical and uterine abnormalities, recurrent antepartum hemorrhage, illnesses and infections, any invasive procedure or surgery, underweight or obese mothers, ethnicity, and social deprivation, long working hours/late nights, alcohol and drug use, and folic acid deficiency.

Predicting preterm birth and diagnosing preterm labour clearly have important consequences, for both health and the economy. However, most efforts have concentrated on mitigating the effects of preterm birth. Nevertheless, since this approach remains costly, it has been suggested that prevention could yield better results. Effective prediction of preterm births could contribute to improve prevention, through appropriate medical and lifestyle interventions. One promising method is the use of Electrohysterography (EHG). EHG measures electrical activity in the uterus, and is a specific form of electromyography (EMG), the measurement of such activity in muscular tissue. Several studies have shown that the EHG record may vary from woman to woman, depending on whether she is in true labour or false labour and whether she will deliver term or preterm. EHG provides a strong basis for objective predication and diagnosis of preterm birth.

In this, paper preterm birth is predicted by analyzing changes in EHG signals of a pregnant woman. EHG signal is acquired from the abdomen of pregnant woman. Several steps are to be followed for the further analysis and studies. EHG data processing mainly consists of three steps preprocessing, feature extraction and classification. These are depicted in the preprocessing includes the techniques done before processing EHG signals. Feature extraction includes the step of extracting features from preprocessed data. This feature vector inputs to the classifier and then classifies the data.

2. ELECREOHYSTEROGRAPHY

Electrohysterography (EHG) is the term given for the recording of electrical activity of the uterus, in the time domain. In order to retrieve EHG signals, bipolar electrodes are adhered to the abdominal surface. These are spaced at a horizontal, or vertical, distance of 2.5 cm to 7 cm apart. Most study, use four electrodes, although one study utilizes two [4]. In a series of other studies, sixteen electrodes also used, and a high density grid of 64 small electrodes were used. Results show that EHG may vary from woman to woman. This is dependent on whether she is in true or false labour, and whether she will deliver at term, or prematurely. The data was collected from a publicly available database called Term-Preterm Electrohysterogram Data Base (TPEHGDB) from Physionet. This includes uterine EMG obtained from 1997 to 2005 at the University Medical Centre Ljubljana, Department of Obstetrics and Gynecology.

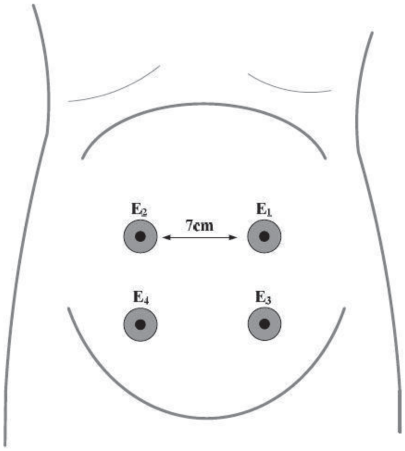

Figure 1: Electrode Placement

Each record is composed of three channels, recorded from 4 electrodes. The first electrode (E1) was placed 3.5 cm to the left and 3.5 cm above the navel. The second electrode (E2) is placed 3.5 cm to the right and 3.5 cm above the navel. The third electrode (E3) was placed 3.5 cm to the right and 3.5 cm below the navel and the fourth electrode (E4) was placed 3.5 cm to the left and 3.5cm below the navel as shown in Figure 1. The difference between potentials of electrode leads, were recorded and it gives 3 channels. Difference between first and second, second and third, third and fourth electrodes produce the first, second and third channel respectively.

3. METHODOLOGY

For term deliveries, true labour only starts within 24 hours. However, for preterm deliveries, it may start within 7 to 10 days. The change in EHG activity, from non-labour to labour, is dramatic; throughout the rest of pregnancy, any change in EHG is more gradual. The prescribed system is shown in the block diagram as in Figure 2.

3.1 Data Acquisition

The TPEHG dataset is used having 300 sample (262 terms, 38 preterm). Each signal is of 30 minutes duration and each signal was digitally filtered using 3 different digital Butterworth filters with a double-pass filtering scheme. The EHG data used for the study was shown in the Figure.3 and Fig. 4 and Fig. 3 shows the term data filtered at 0.3-3Hz,

recorded at 31.3 weeks of gestation and delivered at 40.29 weeks of gestation. Fig. 4 shows the preterm data filtered at 0.3-3Hz,

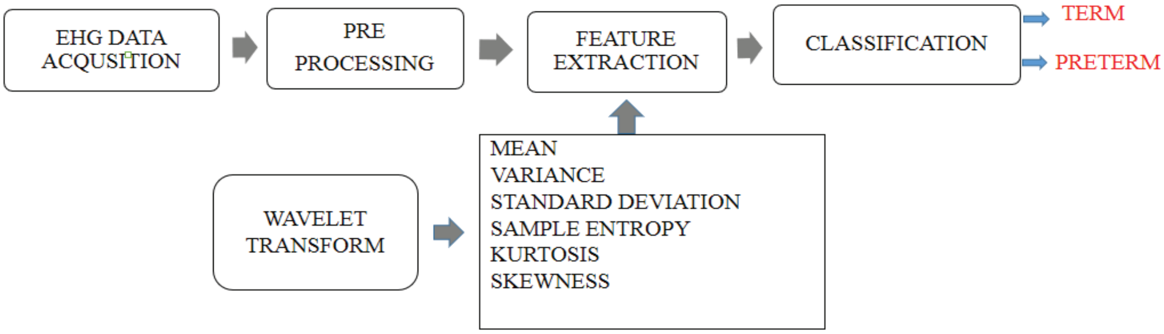

Figure SEQ Figure * ARABIC 2: System Description recorded at 31.3 weeks of gestation and delivered at 32.86 weeks of gestation. Term data samples are arranged in a random fashion. But a regular pattern of EHG bursts can be seen in the preterm EHG data and it gives a symptom of labour.

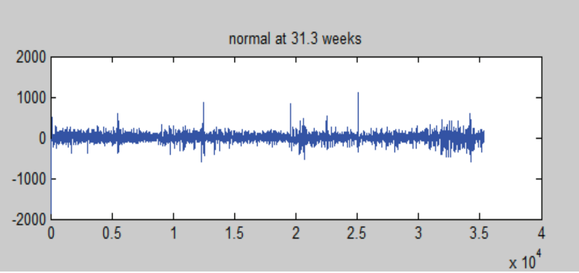

Figure 3: Normal EHG Signal-31.3 weeks

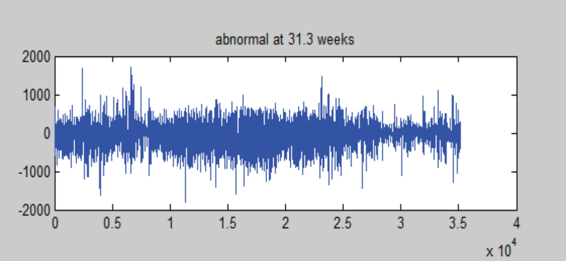

Figure 4: Abnormal EHG Signal-31.3 weeks

The individual records were 30 minutes in duration. Each signal has been sampled at 20 samples per second per channel with 16-bit resolution over a range of 2.5 mV. Each signal was digitally filtered using 3 different digital butterworth filters with a double-pass filtering scheme. The band-pass cutoff frequencies were from 0.08-4 Hz, 0.3-3 Hz and 0.3-4 Hz. Here 0.3-3 Hz filtered term and preterm EHG signals, recorded at 31.3 weeks of gestation were acquired for the study.

Table I: Term Pre-Term Dataset

Early/Later	Term	Pre-Term
Early	143	19
Later	119	19
Total (300)	142	38

3.2 Feature Extraction

In signal processing, there are many instances in which an input signal to a system contains extra unnecessary content or additional noise which can degrade the desired portion. Thus pre-processed data is used. The uterine is made up of hundreds millions of living cells whose responses are nonlinear. It may be called as a complex, nonlinear dynamic system. Figure 3, Figure 4 shows two examples of EHG signals from term and preterm. Due to the different physiological mechanism of these signals we may expect wavelet based six statistical features may separate EHG record delivering at term or pre-term.

Each event in signal processing has to be classified with respect to its specific features. In case of EHG analysis, these features are classically based on spectral characteristics. Unfortunately, up to now, it is not possible to know the real a priori classes. In addition, even though it is possible to identify some of them (Normal, pathological contractions), it is not realistic to attach them to ’universal’ features, due to the wide inter individual variety. Therefore, the classification process must be unsupervised, the class labeling being the ultimate step where each class is identified, comparing its features with those of the others classes [5].

In numerical analysis and functional analysis, a discrete wavelet transform (DWT) is any wavelet transform for which the wavelets are discretely sampled. As with other wavelet transforms, a key advantage it has over Fourier transforms is temporal resolution, it captures both frequency and location information (location in time). The Daubechies wavelets, based on the work of Ingrid Daubechies, are a family of orthogonal wavelets defining a discrete wavelet transform and characterized by a maximal number of vanishing moments for some given support. With each wavelet type of this class, there is a scaling function (called the father wavelet) which generates an orthogonal multi resolution analysis.

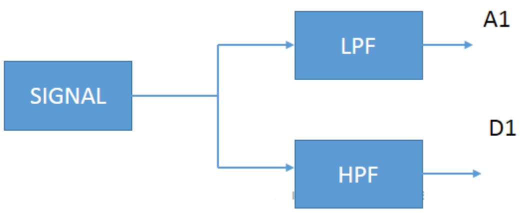

Figure 5: Wavelet Decomposition

In machine learning, pattern recognition and in image processing, feature extraction starts from an initial set of measured data and builds derived values (features) intended to be informative and non-redundant, facilitating the subsequent learning and generalization steps, and in some cases leading to better human interpretations. Feature extraction is related to dimensionality reduction. Feature extraction involves reducing the amount of resources required to describe a large set of data. Analysis with a large number of variables generally requires a large amount of memory and computation power, also it may cause a classification algorithm to over fit to training samples and generalize poorly to new samples. Feature extraction is a general term for methods of constructing combinations of the variables to get around these problems while still describing the data with sufficient accuracy. The features selected are mean, variance, standard deviation, entropy, skewness and kurtosis.

Entropy is a measure of disorder in physical systems and also a basic quantity with multiple field-specific interpretations. It has been associated with disorder, state-space volume, or lack of information. Skewness is a measure of the asymmetry of the probability distribution of a real-valued random variable about its mean. The skewness value can be positive or negative, or even undefined. Kurtosis is a descriptor of the shape of a probability distribution and, just as for skewness, there are different ways of quantifying it for a theoretical distribution and corresponding ways of estimating it from a sample from a population.

3.3 Classification

With the extracted features, classification is to be done. In the previous studies, complex classification methods are chosen for the term and preterm discrimination. Linear discriminant classifier (LDC), K-NN (Nearest-Neighbour) classifier and support vector machine classifier (SVMC) are used in this work. After the classification process, a comparison is done with the performance of the classifiers. Performance evaluation of classifier's are done using the metrics - Sensitivity, Specificity and Accuracy. This is based on the values of true negative (TN), true positive (TP), false negative (FN) and false positive (FP).

In the field of machine learning, the goal of statistical classification is to use an object's characteristics to identify which class (or group) it belongs to. A linear classifier achieves this by making a classification decision based on the value of a linear combination of the characteristics. An object's characteristics are also known as feature values and are typically presented to the machine in a vector called a feature vector. Such classifier's work well for practical problems such has document classification, and more generally for problems with many variables (features), reaching accuracy levels comparable to non-linear classifiers while taking less time to train and use. Support vector machines (SVM) are supervised learning models with associated learning algorithms that analyze data used for classification and regression analysis. Given a set of training examples, each marked as belonging to one or the other of two categories, an SVM training algorithm builds a model that assigns new examples to one category or the other, making it a non-probabilistic binary linear classifier. An SVM model is a representation of the examples as points in space, mapped so that the examples of the separate categories are divided by a clear gap that is as wide as possible. New examples are then mapped into that same space and predicted to belong to a category based on which side of the gap they fall.

In pattern recognition, the K-nearest neighbor's algorithm (K-NN) is a non-parametric method used for classification and regression. In both cases, the input consists of the K closest training examples in the feature space. The output depends on whether K-NN is used for classification or regression. In K-NN classification, the output is a class membership. An object is classified by a majority vote of its neighbors, with the object being assigned to the class most common among its K nearest neighbors (K is a positive integer, typically small). If K = 1, then the object is simply assigned to the class of that single nearest neighbor. In K-NN regression, the output is the property value for the object. This value is the average of the values of its k nearest neighbors. K-NN is a type of instance-based learning, or lazy learning, where the function is only approximated locally and all computation is deferred until classification. The K-NN algorithm is among the simplest of all machine learning algorithms.

4. RESULTS AND DISCUSSION

Feature extraction was done in the TPEHG database signal which is digitally filtered using 3 different digital Butterworth filters using a double-pass filtering scheme. The EHG signal frame of abnormal and normal is shown in Figure 6 and Figure 7 respectively.

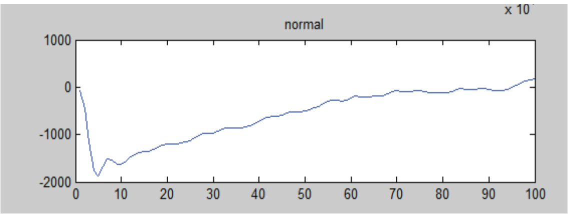

Figure 6: Abnormal EHG signal

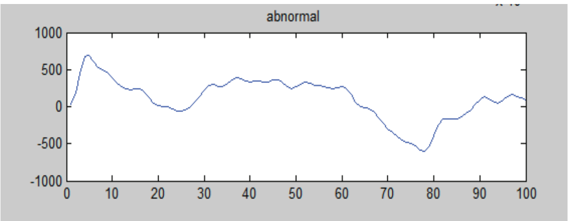

Figure 7: Normal EHG signal

The signal is framed to 5 second length and then the feature extraction is performed.

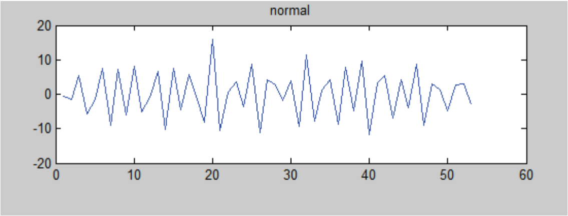

Figure 8: 1-Level detailed coefficient of Normal EHG

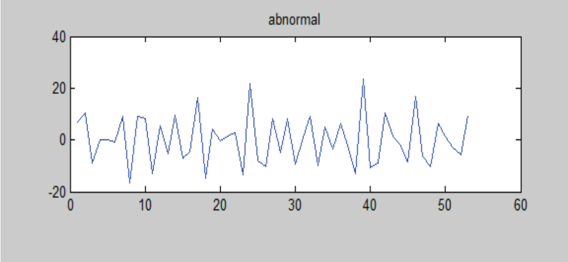

Figure 9: 1-Level detailed coefficient of Normal EHG

Wavelet decomposition is performed using 4-level Daubechies wavelet, the 1-level detailed coefficient of normal and abnormal EHG is shown in Fig. 8 and Fig. 9. The extraction performed using six statistical features. The statistical features considered in this work are mean, variance, standard deviation, sample entropy, kurtosis and skewness. Sample features are given in Table 2. The performances of three classifiers were evaluated using sensitivity, specificity and accuracy.

Table 2: .Feature Comparison

Feature	Term	Pre-term
Mean	0.001517	-0.0015079
Variance	9.623286	7.70444585
Standard deviation	92.60763	1.549465
Sample Entropy	-1.50054	59.35849
Kurtosis	3.210774	2.490331

Skewness	0.060242	-0.05793

4.1 Result of Linear Classifier

Seven wavelet based features were extracted for 20 term and 20 pre-term EHG data. The extracted features were submitted to linear classifier. 12 samples were used for training and the remaining 8 for testing. The specificity of classifier obtained is 87.5%, sensitivity is 75% and accuracy is 81.25%.The confusion matrix for linear classifier is given Table 3.

Table 3: Confusion Matrix of Linear Classifier

	Term	Pre- term
Term	7	1
Pre-term	2	6

4.2 Result of SVM Classifier

In the next stage, SVM classifier was used. Same as the linear classifier here also 20 samples taken (12-training, 8-testing). The specificity of classifier is 75%, sensitivity is 100% and accuracy is 87.5%. Compared to linear classifier the accuracy of SVM classifier is better and the confusion matrix of SVM classifier as shown in Table 4.

Table 4: Confusion Matrix of SVM Classifier

	Term	Pre- Term
Term	6	2
Pre-Term	0	8

4.3 Result of K-NN Classifier

In order to improve the results, K-NN classifier was used. Same as the linear classifier here also 20 samples were taken (12-training, 8-testing).The specificity of classifier is 100%, sensitivity is 88% and accuracy is 93.75%. Compared to linear classifier the accuracy of K-NN classifier is better and the confusion matrix of K-NN classifier is given in Table 5.

Table 5: Confusion Matrix of KNN Classifier

	Term	Pre- term
Term	8	0
Pre-term	1	7

The three classifiers performances are compared in Table 6, K-NN classifier shows a better accuracy compared to the other two classifiers.

Table 6: Classifier Performance Comparison

Classifier	Linear	SVM	KNN
Specificity	87.50	75.11	100
Sensitivity	75.00	100	80.00
Accuracy	81.25	87.5	93.75

Most of the uterine EHG signal studies have concentrated on predicting true labor, which is based on the last stage of the pregnancy duration. This work predict, term and preterm deliveries. It gives better results than those in [9], which reports a sensitivity of 47%, specificity of 90%. Furthermore, the results show improvement over reported in [7, 8]. Diab. et al. have used several alternative techniques, including artificial neural networks and autoregressive models [5, 6]. However, it should be noted that the sample size is much smaller than the sample size in this paper (20 preterm and 20 term). The comparison of results is shown in Table 8.

Table 8: Comparison with Previous Work

Sl. No	Author	Method	Accuracy
1	S. Bagha moradi	MLP neural and network	73%
2	Fergus. Cheung	TREEC Classification	90%

3	Proposed method	7-Wavelet based feature, KNN Classifier	93.75%

CONCLUSIONS

Medical information systems play a vital role in the biomedical domain. This has led to the various preprocessing algorithms and feature extraction techniques. Electrohysterography is a strong predictor to classify term and preterm records. The 0.3-3 Hz filtered TPEHG data is used for the classification between term and preterm records. After preprocessing the wavelet transform is applied and statistical features mean, variance, standard deviation, entropy, kurtosis and skewness as feature vector is taken. The classifiers used are linear, K-NN and SVM classifier. Performance of the classifiers is evaluated in terms of the metrics like accuracy, specificity and sensitivity. Accuracy of linear classifiers is 83.5% and that of K-NN classifier is 87.75% and the K-NN classifier provide a slightly better accuracy of 93.5%. With the help of simple algorithm, the obtained accuracy is found to be good compared with the previous reported results.

REFERENCES

[1] WHO Born too soon: ”The Global Action Report on Preterm Birth”,2012.

[2] Rattihalli R, Smith L, Field D, ”Prevention of preterm births: are we looking in the wrong place? Archives of disease in childhood”, *Fetal and neonatal* vol.97, no.3, pp.160-1, 2012.

[3] Goldenberg RL, Culhane JF, Iams JD, Romero R, “Epidemiology andcauses of preterm birth.”, *The Lancet* vol.371, no.9606, pp.75-84, 2008.

[4] Doret M, ”Uterine Electromyograpy Characteristics for early Diagnosis of Mifepristone-induced Preterm Labour.”, *Obstetrics and Gynecology*,vol.105, no.4, pp.822- 830, 2005.

[5] M.O.Diab,C.Marque and M.A.Khalil,”Classification for Uterine EMG Signals-Comparison between AR Model and Statistical Classification Method”, *International Journal of Computational Cognition*, vol.5, no.1, pp.8-14, 2007.

[6] B.Moslem, M.O.Diab, M.Khalil, C.Marque, ”Classification of uterine EMG signals by using supervised competitive learning”, *in IEEE Workshop on Signal Processing Systems*, pp.267-272, 2011.

[7] S.Baghamoradi, M.Naji, H.Aryadoost, ”Evaluation of cepstral analysis of EHG signals to prediction of preterm labor*”, in 18th Iranian Conference on Biomedical Engineering*, pp.81-83, 2011.

[8] Fergus.Cheung, A.Hussain, D. Al Jumeily and C.Dobbinand S.Iram,”Prediction of preterm deliveries from EHG signals using machine learning”,*PLosOne*, vol.8, no.10, pp.77-154, 2013.

[9] Verdenik I, Pajntar M, Leskosek B, ”Uterine electrical activity as predictor of preterm birth in women with preterm contractions”, *European journal of obstetrics, gynecology, and reproductive biology,* vol.95, no.2, pp.149-53, 2001.

[10] A. J. Hussain, P. Fergus, H. Al- Askar, D. Al- Jumeily, F. Jager, “Dynamic neural network architecture inspired by the immune algorithm to predict preterm deliveries in pregnant women”, *Neurocomputing Elseivier*, 151, 963–974, 2015.

[11] Idowu O, Fergus P, Hussain A, Dobbins C, and H. Al , “Advance artificial neural network classification techniques using ehg for detecting preterm births”, *Intelligent and Software Intensive Systems (CISIS), Eighth International Conference on IEEE*, 1, 95-100, 2014.

Anju Madhava did M.Tech in Instrumetation and Control from Kerala Technological University Kerala.
Received BTech in Applied Electronics and Instrumentation Engineering at Calicut University.

Dr. Thasneem Fathima did B Tech in Electrical and Electronics Engineering, M Tech in Instrumentation and Control from Aligarh Muslim University and Ph. D Biomedical Signal Processiong from NIT Calicut. Her research intersests include Biomedical Signal Processiong, Image processing and Artificial Intelligence.

Preetha R got her B.Tech and M.Tech degree from PSNA College of Engineering and Techno logy Dindigul.

MES JOURNAL OF TECHNOLOGY AND MANAGEMENT
Volume 4,No 1,33-37,2020

A Novel approach to Digital Predistortion Based Non Linearity Minimization in Power Amplifiers Using Adaptive Algorithms

Minu M
Department of Electronics and
Communication Engineering
MESCE Kuttippuram
Email: minumohammed.7@gmail.com

Nasarathul Nisha .P.K
Department of Electronics and
Communication Engineering
MESCE Kuttippuram
Email: nishanaisal@gmail.com

***Abstract*—This paper demonstrates the non linearityminimization in power amplifiers utilizing a method known as digital predistortion (DPD).The two principle elements of power amplifiers (PA) are linearity and efficiency. To accomplish high spectral efficiency and to satisfy increasing demand in transmission data rate, profoundly efficient and linear power amplifiers are required. So a trade off exist between both .Spectral regrowth and distortions are the main effects of the non linearities exhibited by the power amplifiers which further leads to the degradations in performance . For limiting these non linearities, numerous techniques are accessible. Among them Digital Pre distortion(DPD) strategy is the most widely recognized and successful technique.DPD can be realized in two architectures namely direct learning architecture (DLA) and indirect learning architecture (ILA) .Coefficients for linearizing the power amplifiers are estimated using adaptive algorithms such as least mean square error (LMS) algorithm and Recursive predictive error method (RPEM algorithm).The performance measures can be increased while we go for RPEM algorithm than LMS algorithm.**

***Key words :*Power amplifier(PA),Digital predistortion , Linearization,Intermodulation distortion (IMD),Direct learning architecture**

I. INTRODUCTION

Power ampliers are essential components in communication systems [1] and are inherently nonlinear. The nonlinearity creates spectral broadening beyond the signal bandwidth, which interferes with adjacent channels resulting adjascent channel power ratio. It also causes spectral regrowth,distortions like intermodulation distortion ,total harmonic distortions etc.Inband and sideband distortions [2], degrades not only the signal- to-distortion ratio of the channel and adjacent channels ,but also bit error rate performance. Newer transmission formats, such as wideband code division multiple access or orthogonal frequency division multiplexing , are especially vulnerable to the nonlinear distortions. So power amplifiers have to be linearized.Feedback ,feedforward, linear amplification of non linearcomponents,post distortion, predistortion [3] etc are some of the techniques available.But due to high efficiency and cost effectiveness predistortion is commonly used. The concept is to insert a nonlinear module between the input signal and the power amplifier.The nonlinear behavior exhibited by the power amplifier is compensated using digital predistortion applied to baseband signal.

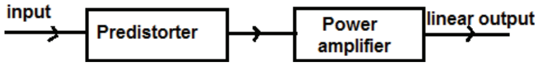

Fig. 1. Simple pre distortion technique

The predistortion in its simplest form is shown in Fig.1 given above. Predistortion technique results in cascading of a predistorter and a nonlinear power amplifier [4]. The inserted non linear element called pre distorter has inverse transfer characteristics of that of nonlinear power amplifier. Illustration of steps in predistortion is shown in Fig 2.

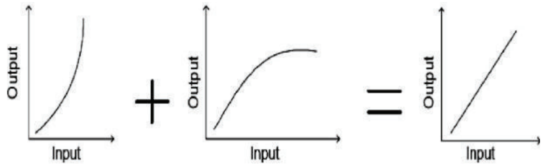

Predistorter Power Amplifier Predistorter + Power Amplifier

Fig. 2. Steps in Predistortion

Predistortion techniques can be classified into RF predistor- tion, IF predistortion, Baseband predistortion depending on position of predistorter.Predistorter operates at final carrier frequency in RF predistortion whereas in case of IF pre - distortion , it operates in intermediate frequency range. Adap- tive algorithms [5] can be applied to each of these tech- niques, but it is commonly applied to baseband predistortion. Therefore most commonly used technique is the adaptive digital predistortion. Since adaptive digital predistortion is basically applied to baseband signal, it is also known as baseband predistortion.DPD creates a correction signal using a set of nonlinear basis waveforms weighed by adjustable coefficients.Coefficients are optimized using adaptive algorithms such as least mean square ,recursive predictive error method etc. Amplitude modulation to amplitude modulation conversion (AM/AM) and amplitude modulation to phase modulation conversion (AM/PM) are the methods by which we can represent the nonlinear characteristics of power amplifier. Compensating these distortion [6] brought by power amplifier is the essence of the digital predistortion.

A. Architecture of digital predistortion

Learning architectures defines various structures for Predistortion .Learning architectures are of 2 types namely direct learning architecture (DLA) [7] and indirect learning architecture (ILA).Direct learning architecture shown in fig 3 is commonly used when compared to indirect learning architecture [8].Indirect learning architecture contains postdistorter whereas direct learning uses predistorter in the estimation loop. Predistorter finds the difference between output signal and reference signal which results in error signal .Adaptation algorithm takes the error signal to find the coefficients to minimize the non linearity.

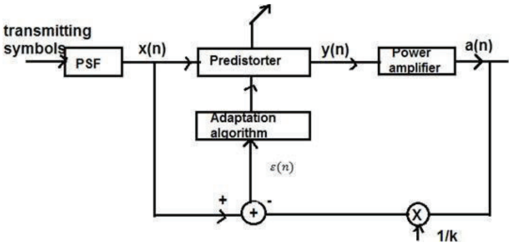

Fig. 3. Direct learning architecture

DLA shown in Fig.3 directly adjust the predistortion polynomial in feedforward path.x(n) is produced by band limiting the transmitted symbols .Pulse shaping filter (PSF) is used to bandlimit the signal. x(n) is predistorted to yield y(n) which is amplified by power amplifier with gain k. Error signal is thus generated and fed to adaptive algorithm which finds the predistortion parameters to make PSF output and feedback signal as close as possible.

II. NON LINEARITY MINIMIZATION TECHNIQUE

The inherently nonlinear power amplifiers are contained in each transmitter section of wireless base stations. Basically every transmitter section in communication systems ends with power amplifiers. The input signal provided to the system is the digital baseband signal which is converted to radio frequency (RF) output signal [9].Power amplifiers are designed to operate near saturation in order to achieve maximum efficiency, but as a result they become non linear. So many techniques are available to compensate for this. Such techniques are known as non linearity minimization techniques. Adaptive digital pre- distortion is the most prominent technique among them to compensate for the non linearity.Predistortion is applied to digitally baseband signal.

The digtal baseband transmitter shown in fig 4 consist of two paths namely transmit path and observation path [9] .The transmit path consisting of digital pre distorter, digital to analog converter, up converters , PA,converts input signal x(k) into RF output signal $y_{RF}(t)$.

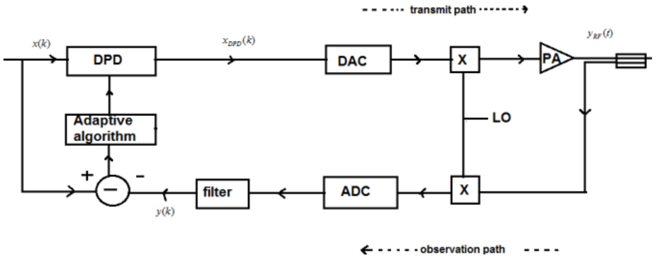

Fig. 4. Block diagram of Digital baseband transmitter section using DPD

The input signal which is pre distorted by means of DPD is converted to analog signal using DAC.Analog signal generated is unconverted and amplified using power amplifier to generate $y_{RF}(t)$. A portion of the output signal is coupled to the reverse path .The procedure [10]performed to generate input of power amplifier is reversed to get digital signal which is filtered ,and further provided to the subtractor.Subtractor finds the differnce between the input and output signal which results in error or the weighted non-linearity which is given to adaptation algorithm.It finds the coefficients which minimizes the error signal generated.The coefficient error vector generated is given to DPD to minimize the nonlinearity in power amplifier.Coefficients are calculated in existing system using least mean square algorithm (LMS).Since DPD [10] is cascaded with power amplifiers,it cancels the nonlinearity in power amplifiers because the properties exhibited by DPD is complement to that of power amplifier.Performance of digital predistortion in nonlinearity minimization is based on certain parameters such as total harmonic distortion(THD),intermodulation distor- tion(IMD) and adjascent channel power ratio.The input signal x(k) is predistorted to $x_{DPD}(k)$ as

$$x_{DPD}(k) = x(k) + \sum_{i=1}^{N} a_i.\gamma_i(k) \qquad (1)$$

where N is the number of waveforms in basis set ,i is the index and $\gamma_i(k)$ can be defined as the set of basis waveforms.Memory polynomial and gain polynomial are the 2 basis waveform set.The memory polynomial is defined in (2) where p denote polynomial order and m denote memory offset.

$$\gamma_{i,MP}(k) = |x(k-m)|^{p-1}.x(k-m) \qquad (2)$$

The gain polynomial basis waveform set is defined as

$$\gamma_{i,GP}(k) = |x(k-m)|^{p-1}.x(k) \qquad (3)$$

Predistorted signal in (1) can be defined in vector form:

$$x_{DPD}(k) = x(k) + \psi(k).\underline{a} \quad (4)$$

where

$\underline{a} = [a_1......a_N]^T$

$\psi(k) = [\gamma_i(k)......\gamma_N(k)]$ is the row vector.

The measured error in (5) is the difference between observed output signal and input signal

$$s(k) = tt_0^{-1}y(k) - x(k) \quad (5)$$

where tt_0 is the nominal gain given by

$$tt_0 = \frac{E[y(k)(x^*(k)]}{E[|x(k)|^2]}$$

The error signal is in (6) where $\underline{\Delta a}$ is the coefficient error vector and $s_0(k)$ is the error component orthogonal to basis waveform set.

$$s(k) = s_0(k) + \psi(k).\underline{\Delta a} \quad (6)$$

where

$\underline{\Delta a} = [\underline{\Delta a}_1....\underline{\Delta a}_N]^T$

Now rearrange (6) to get $s_0(k)$

$$s_0(k) = s(k) - \psi(k).\underline{\Delta a} \quad (7)$$

After applying superposition to (7) new basis waveform set is created as

$$L\{\psi(k)\} = \psi_L(k) \quad (8)$$

Least squared cost function referred as J_{DPD} is

$$J_{DPD} = E[|\{s(k)\} - \psi(k).\underline{\Delta a}|^2] \quad (9)$$

The autocorrelation of basis waveform set and cross corelation of error signal with basis waveform set are used to minimize (9) for the estimation of coefficient error vector.This coefficient estimate allows DPD to cancel the IMD 's generated to a great extent.

A. Algorithm

Adaptive algorithms [10] are the algorithms used to calculate the coefficients generated to minimize the error .Error is the weighted non linearity i.e difference between output signal and input signal. Two adaptive algorithms developed for direct learning architecture and indirect learning architecture are namely: the Least Mean Square (LMS) and the Recursive Prediction Error Method (RPEM) algorithms. The adaptive algorithms can be used for both architectures.In Existing system co efficients are calculated using least mean square method.Steps of calculating coefficents using LMS algorithm [10] is as given below.

1) LMS Algorithm:

(a) Two inputs to the algorithm are error signal generated and estimated non linearity.Let the estimated non linearity be z_p.
(b) Convert z_p which are 1D signals to 2D.
(c) Find conjugate of 2D signals i.ez.
(d) Estimate the product of the z with error signal.
(e) Add result of step (d) with that of delayed output of adder to get coefficients.

Inorder to increase the performance of various parameters ,proposed algorithm namely RPEM algorithm is used instead of existing algorithm (LMS).Steps of calculating coefficents using RPEM algorithm is as given below.

2) RPEM Algorithm:

(a) Consider error signal and data generated (Z_p) as 2 input signals.
(b) Convert Z_p to 2D signals.
(c) Take conjugate of Z_p as Z.
(d) Find transpose of Z_p as Z^T.
(e) Perform matrix multiplication as in (9).

$$Z^T * Z * P \quad (10)$$

(f) Add output matrix to a self generated feedback value L.

$$S = (Z^T * Z * P) + L \quad (11)$$

where S is the output of adder in (10).

(g) Consider inverse of S such as S^{-1}.
(h) Calculate the products of P with Z, S^{-1}, Z^T,and P itself.

$$P * Z * S^{-1} * Z^T * P \quad (12)$$

(i) Subtract result in (11) from P and divide by L to get

$$(P - (P * Z * S^{-1} * Z^T * P))/L \quad (13)$$

(j) Delay is provided to above result to generate P
(k) Apply matrix multiplication such as to get

$$P * Z * error \quad (14)$$

(l) Add above to delayed output of adder to generate coefficients

III. SIMULATION RESULTS

The proposed system has been implemented in MATLAB software.The learning architecture used in the proposed system is the polynomial based predistortion based direct learning architecture(DLA) which directly compares the input signal and output signal which results in error signal.Coefficients to minimize the error signal is generated by using simple and easy adaptation algorithms namely LMS algorithm and RPEM algorithm.LMS algorithm is used for the non linearity minimization in existing system whereas RPEM algorithm is the proposed algorithm to increase the efficiency of the existing system.A spectrum with actual power amplifier input (PA in),non linear PA output named as PA out and non linearity minimized spectrum while DPD is cascaded with PA out(PA+DPD) using LMS algorithm is plotted in Fig:5 .It shows that spectral regrowth produced in spectrum of PA output with non linearity is removed in linearized spectrum of power amplifier with cascaded DPD.

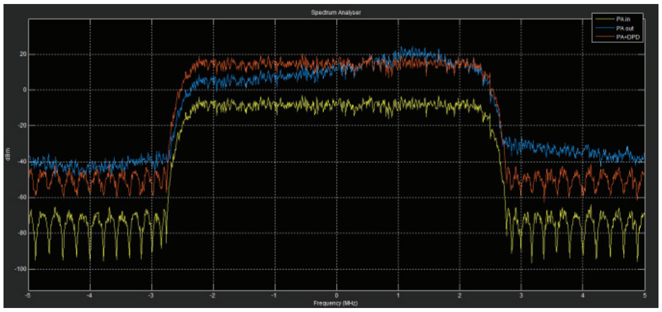

Fig. 5. Comparison of power spectral density of PA in,PAout,PA+DPD

A spectrum with the same three cases is again simulated using RPEM algorithm instead of LMS algorithm and plotted in Fig:6.It shows that spectral regrowth produced in spectrum of PA output with non linearity is removed in linearized spectrum of power amplifier with cascaded DPD to a great extent when compared with that of LMS algorithm.

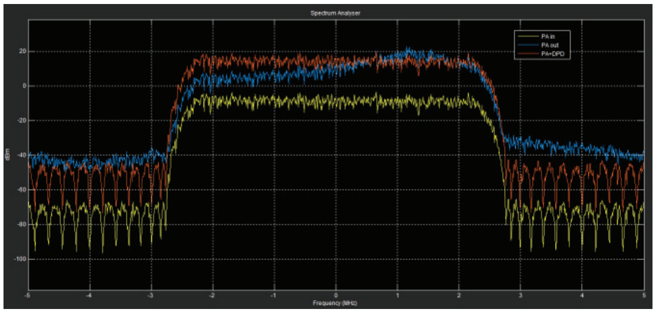

Fig. 6. Comparison of power spectral density of PA in,PAout,PA+DPD using RPEM algorithm

Various nonlinearity measurement parameters are Adjascentchannel power ratio(ACPR) ,Frequency error measurement ,Intermodulation distortion(IMD) and Total harmonic distortion.Table I shows a comparison of various ACPR values of PA output with non linearity , non linearity minimized ACPR values denoted as PA +DPD using LMS algorithms and RPEM algorithm.From Table I ,it is clear that in case of LMS algorithm ACPR lower has been reduced to -63.29 from -57.25 whereas it gets reduced to -67.20 in case of RPEM algorithm.Asimiliar reduction in upper ACPR is observed in RPEM algorithm while compared to that of LMS.So a better nonlinearity reduction in terms of ACPR occurs while we go for RPEM algorithm.A graph which shows the comparison of ACPR values of two algorithms is shown in Fig:7.

The comparison of Frequency error measurement values are shown in Table II which clearly shows that an error of 24

TABLE I
ACPR MEASUREMENT VALUES

Case	ACPR (dBc)	
	Lower	**Upper**
PA out	**-57.25**	**-48.83**
PA+DPD(LMS)	**-63.29**	**-63.04**
PA+DPD(RPEM)	**-67.20**	**-66.28**

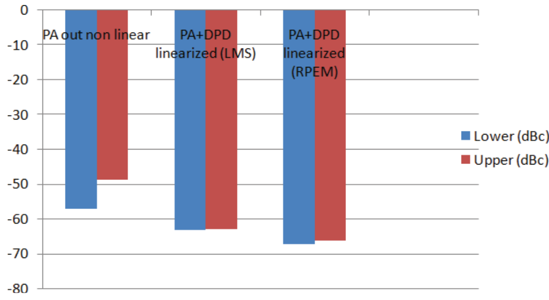

Fig. 7. Comparison of ACPR measurement values generated in LMS and RPEM algorithm

kHz which is occured due to nonlinearity has been reduced to -1.303 KHz using LMS algorithm and to -2.001 KHz in other case which is the where the error shown by the actual power amplifier input signal is -2.0280 KHz.So in terms of frequency measurement it is clear that nonlinearity is minimized to a great extent.

A graph which shows the comparison of Frequency error measurement values using two algorithms is shown in Fig:8.

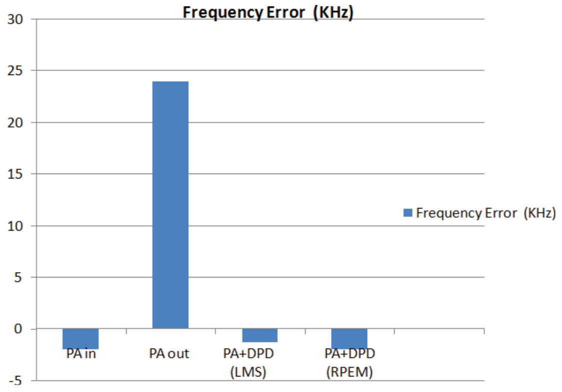

Fig. 8. Comparison of Frequency error values generated in LMS and RPEM algorithm

The other performance measurement comparisons using

TABLE II
FREQUENCY ERROR MEASUREMENT VALUES

Case	Frequency error (KHz)
PA in	**-2.0280**
PA out	**24**
PA+DPD (LMS)	**-1.303**
PA+DPD (RPEM)	**-2.001**

TABLE III
PERFORMANCE MEASUREMENT PARAMETERS

Parameters	LMS	RPEM
IMD (dBc)	-34.15	-36.03
THD (dBc)	-63.72	-68.15

both the algorithms are shown in Table III.System using LMS algorithm exhibits the intermodulation distortion of -34.15 dBc whereas total harmonic distortion (THD) of -63.72 dBc.While we simulate the system using RPEM algorithm IMD gets further reduced to -36.03 dBc and THD to -68.15 dBc .A graph which shows the comparison of Performance measurement Parameters using two algorithms is shown in Fig:9.

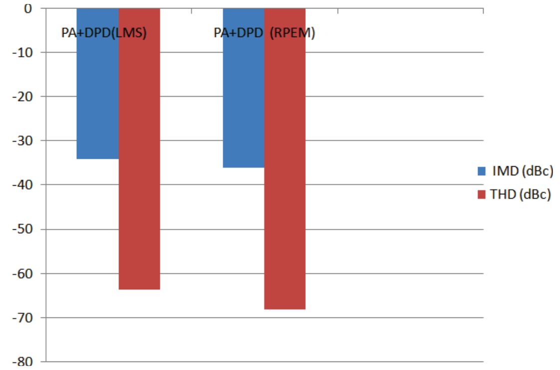

Fig. 9. Comparison of IMD and THD generated in LMS and RPEM algorithm

IV. CONCLUSION

Non linearity exhibited by the power amplifiers which are indispensible components in communication system can be minimized using polynomial method based digital predistortion. In order to minimize the error generated, coefficients are estimated using adaptive algorithms. The proposed RPEM algorithm used in DPD improves the performance of the parametersACPR,IMD,THD etc compared to existing algorithm namely LMS in digital pre distortion to a great extent.

REFERENCES

[1] Sonam Goyal and Jyoti Gupta," Review Of Power Amplifier Linearization Techniques in Communication ", International Journal of Engineering Research and Technology Vol .2, Issue 6 ,June 2013

[2] Cheng-Po Liang, Je-hong Jong, Wayne E. Stark and Jack R. East," Nonlinear Amplifier Effects in Communications Systems", ieee transactions on microwave theory and techniques, vol. 47, no.8.

[3] Rajbir Kaur and M.S. Patterh ," overview of the Linearization Techniques to mitigate the nonlinear effects of Power Amplifier ", An International Journal of Engineering Sciences, Vol.17,Jan 2016.

[4] P. M. Lavrador, T. R. Cunha, P. M. Cabral and J. C. Pedro, "The Linearity- Efficiency Compromise," IEEE Microwave Magazine, vol. 11, no. 5, pp. 44-58, Aug. 2010.

[5] Sweety Badhwar et al, "Design of Digital Predistortion Technique for RF Power Amplifier using Memory Polynomial ", Int. Journal of Engineering Research and Applications, Vol. 4, Issue 9, pp.01-03,September 2014.

[6] Harjinder Singh, Amandeep Singh Sappal, "Comparative Study of Power Amplifier Linearization Techniques ", International Journal of Engineering Research and Development, Volume 12, Issue 3, PP.45-48, March 2016.

[7] S. Choi, E. R. Jeong and Y. H. Lee, "A Direct Learning Structure for Adaptive Polynomial- Based Predistortion for Power Amplifier Lineariza- tion ",2007 IEEE 65th Vehicular Technology Conference - VTC2007- Spring, Dublin, 2007, pp. 1791-1795.

[8] R. N. Braithwaite, "A comparison of indirect learning and closed loop estimators used in digital predistortion of power amplifiers", 2015 IEEE MTT-S International Microwave Symposium, Phoenix, 2015, pp 1-4.

[9] H. Paaso and A. Mammela, "Comparison of direct learning and indirect learning predistortion architectures ", 2008 IEEE International Symposium on Wireless Communication Systems, Reykjavik, 2008, pp. 309-313.

[10] R. N. Braithwaite, "Closed-Loop Digital Predistortion (DPD) Using an Observation Path With Limited Bandwidth", in IEEE Transactions on Microwave Theory and Techniques, vol. 63, no. 2, pp. 726-736, Feb. 2015.

Nasarathul Nisha P.K is currently working as Assistant Professor in MES College of Engineering,Kuttippuram.She received the B.E degree in Telecommunication Engineering from PACE,Mangalore,India,in 2005,and the M.Tech degree in Telecommunication Engineering from the NIT,Calicut,India in 2012.

Minu M is currently working as Lecturer in SSM Polytechnic Tirur. She received the B.Tech degree in Electronics & Communication Engineering from MESCE,Kuttippuram,India,and the M.Tech degree in communication and signal processing from MESCE,India in 2017.

MES JOURNAL OF TECHNOLOGY AND MANAGEMENT
Volume 4,No 1,38-44,2020

INTEGRATION OF A CAMPUS MICROGRID WITH UTILITY GRID – A CASE STUDY

Saritha.K.S
Research Scholar, Electrical Dept., School of Engineering, CUSAT,
Cochin,Kerala,INDIA
sarithasngc@gmail.com

SasidharanSreedharan
Professor &Head,CSE Dept.,
M.E.S College of Engg.,
Kuttippuram, Kerala, INDIA
sasidharan@mesce.ac.in

Usha Nair,
Professor, Electrical Dept.,
School of Engineering, CUSAT,
Cochin,Kerala,INDIA
ushanair4@gmail.com

ABSTRACT

In this paper, integration of a campus micro-grid with a practical utility grid is proposed. The objective is to optimize the wind penetration so that generation from the conventional generators can be minimized and hence the generation cost. The power flow is carried out using PSAT software which is a globally accepted power system simulation tool. In the static analysis, the voltage limit, active –reactive power flow, eigen value stability also considered for the stable and reliable operation of the proposed network. In the proposed network, maximum wind penetration is achieved keeping the system constraints within the limit.

Keywords

Micro grid; Renewable Energy Resources; Eigen value; Distributed generation.

1. INTRODUCTION

The rapid increase in fuel price, scarcity of fossil fuel and at the same time the ever-growing power demand leads a new dynamism in the existing power system. As a result, Renewable Energy Resources (RESs) plays a vital role in the present power system scenario. This paper presents an optimal generation of wind energy thereby minimizing the fuel cost. This system consists of renewable energy sources such as solar, wind, biomass. Most of the power systems are interconnected which consists of conventional sources. So modifications are required for incorporating all the RESs and storage. The researchers are more interested in this field and their findings revealed that, for the smooth and efficient operation of modern power system require an integrated RESs with storage.

For the sustainable development of energy sector for any nation integrated energy sources are becoming essential. Generally, the Distributed Generators (DGs) are connected to the medium/low voltage line. These DG systems offer clean, efficient reliable, economical and flexible power source. The RES technologies are suitable for large scale as well as rural and remote area application. Globally, the electric Power generation from RESs has been progressively escalating in nature. During the last two decades, a significant growth in installed capacity of RESs has been achieved by the Indian power sector and now India is having the 5th largest wind power production capacity in the world. Moreover, government policy and regulatory framework are also encouraging RESs.

The main factors which lead to a revolution in a distribution network with micro-grid are lack of energy production in par with the increase in power demand and the environmental issues due to ample use of fossil fuel for energy production. A micro-grid is a localized power grid that contains both power supply and the technology to manage it. More than that, micro-grid's electricity is generated and distributed locally and the owners can sell excess power if it is in on-grid mode. Micro-grid will offer higher reliability, especially in emergencies or disasters and less dependent on a larger power grid, which may depend on energy sources that are polluting or inefficient. In this way, a micro-grid can support renewable energy use and energy storage at a lower cost.

One of the principal functions of an energy management system is to provide power and voltage for the distribution system devices. Control of power resources along with optimal power scheduling of the DGs and the other power resources interacting with distribution system is necessary, in order to meet the objective of smart grid and reduce the total energy losses. The key issues related to a power system network are voltage stability, optimal storage requirement, optimal placement of DGs, optimal power scheduling, maximum renewable penetration etc. The presence of DGs in the power system provides performance improvement such as voltage profile, power flow, reliability, protection and power quality stability [1].

The paper [2] introduces an effective method for the daily schedule of BESS in the power system with a large penetration of PV generation thereby minimize the fuel cost of generators. This paper [3] evaluate the coordination of electric vehicle as the distributed storage device and variable renewable sources for mitigating energy imbalance & offering significant potential for energy sustainability in an electricity infrastructure. Moreover, it is possible to considerably reduce Co_2 emission in electrical power system through large-scale integration of RESs.

In paper [4], the author discuss the idea of adding energy storage devices to the grid and its effect on the efficiency of distribution grids is investigated. Paper [5] aims to design a scheduling framework for optimal operation of the micro-grid from the perspective of security & economy. An efficient management and operation of a smart network of micro-grids is proposed in paper [6]. The objective function of this paper is to minimize the power exchanges among micro-grids, and to make each local energy storage system in a micro-grid works around a proper optimal value.

Paper [7] presents some methods for estimating the lifetime & operation hours of different sources and integrating this estimation in the energy management system will make it possible to control the lifetime of each energy source & reduce the total net present cost of the system. The case studies point up the importance of considering the estimations of the life span and generation costs in the energy management system when deciding which energy source to use.

In the paper [8], the impact of micro-grid (MG)on power system voltage stability is investigated. Here the authors examined the dynamic stability with and without micro-grid integrated to IEEE 14bus and proved that dynamic response time of the system with MG is faster than the basic system and also the bus voltages of the power system with MG shows better value.

Integrating the micro-grid with main grid/utility grid, there are many advantages such as voltage improvement, power reduction in conventional sources by increasing RES penetration. ie. generation cost is reduced. Reliability and flexibility increased. Reduction in power loss, loadability can be improved without the need for new addition of power sources or capital cost.

Here the main grid is selected as the practical system which is the Central Travancore grid of Kerala power system. It consists of 2 hydel stations Idukki and Sabarigiri and 2 thermal stations at BDPP and Kayamkulam (due to the high production cost of thermal stations these are not considered in the practical system). The proposed micro-grid is coupled to the practical grid and power flow using Newton Raphson method is carried out using PSAT software.

2. PROBLEM FORMULATION

This proposal is for investigating optimal energy management of an integrated micro-grid with the utility grid. An engineering college campus network is taken as the model by incorporating renewable source such as solar PV panel, wind turbine, biomass, etc. into the existing power system and the same is coupled to the main grid. The proposed micro-grid is self-sustainable in the stand-alone mode and also can exchange power from the renewable sources to the main grid through the inter connection. By this, the generation of the conventional sources can be reduced, resulting from economical and eco-friendly energy transaction. Considering the intermittency of the wind fluctuations and the solar irradiance, storage is also included for reliable and efficient power service. The main objective of this proposal is optimal energy management of DG units to minimize the power losses of the distribution considering the system constraints. In this work, the main stability factors such as voltage stability, small signal stability, and eigen value analysis are examined for the stable and reliable operation of the proposed network.

The objective function to be minimized in the distributed generation problem is the distribution systems active power losses formulated as:

$F = \text{Min}\,(P_L)$

$P_L = \sum_{k=1}^{nl} P_{LK}$

Subjected to the following equality constraints.

$$\left.\begin{aligned} P_{Gi} &= \sum_{j=1}^{n} |V_i||V_j||Y_{ij}|\cos(\delta_i - \delta_j - \theta_{ij}) + P_{Di} \quad (1) \\ Q_{Gi} &= \sum_{j=1}^{n} |V_i||V_j||Y_{ij}|\sin(\delta_i - \delta_j - \theta_{ij}) + Q_{Di} \end{aligned}\right\}$$

Inequality constraints are:

$$\left.\begin{aligned} &P_{Gi\,min} \le P_{Gi} \le P_{Gi\,max} \\ &Q_{Gi\,min} \le Q_{Gi} \le Q_{Gi\,max} \\ &Q_{Gi\,min} \le Q_{Gi} \le Q_{Gi\,max} \quad (2) \\ &|V_{i\,min}| \le |V_i| \le |V_{i\,max}| \\ &|V_{i\,min}| \le |V_i| \le |V_{i\,max}| \end{aligned}\right\}$$

$$\delta_{i\,min} \le \delta_i \le \delta_{i\,max}$$

Thermal constraint of distribution lines :

$$\left.\begin{aligned} &|MVA_{line}| \le |MVA_{line\,max}| \\ &|MVA_{line}| \le |MVA_{line\,max}| \\ &|P_{ij}| \le |P_{ij\,max}| \quad i,j = 1,2,\ldots.N_l \end{aligned}\right\}$$

$$|P_{ij}| \le |P_{ij\,max}| \quad i,j = 1,2,\ldots.N_l \qquad (3)$$

where ,

F = Objective function.

P_{LK} = Active power loss in the K^{th} line.

nl = the number of lines in the system.

Y_{ij}, θ_{ij} = Magnitude and phase angle of admittance.

P_{Gi},Q_{Gi} = active and reactive power of generator connected in i^{th} bus.

P_{Di} ,Q_{Di} = active and reactive load

P_{Li} ,Q_{Li} = active and reactive load connected in i^{th} bus.

V_i ,V_j = magnitude at i^{th}&j^{th} bus voltage.

δ_i , δ_j = phase angle of i^{th}&j^{th} bus voltage n = number of buses in the system.

MVA_{line} = apparent power flow through the transmission line.

P_{ij} = active power flow from i^{th} bus to j^{th} bus.

3. SIMULATION RESULTS & DISCUSSION

The simulation is carried out in 3 steps. The static analysis of the proposed micro-grid , main grid(Central Travancore grid) carried out and after that the micro-grid is integrated with the main grid and the power flow is carried out using Newton-Raphson's method by PSAT software which is a globally accepted power system simulation software[9].

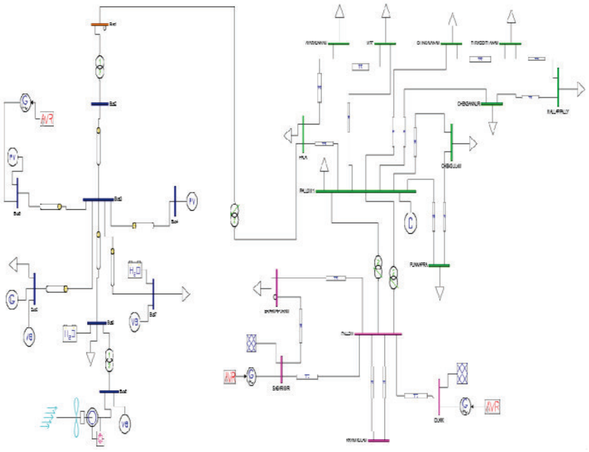

Figure 1: Microgrid- Main grid integration

In Fig.1 the PSAT simulation model is furnished. The proposed micro-grid consists renewable sources such as solar PV, wind, biomass, and considering the intermittency and fluctuation in the wind generation, storage system also included . Moreover 2 nos.of diesel generator sets and utility grid are linked to the micro-grid. The voltage stability, power flow, small signal stability, eigen value stability are considered for the analysis.

The power flow result of the proposed micro-grid before and after integration with the utility grid is furnished in Table 1.

Table 1: Power flow result

Parameters	Before Integration		After Integration
	Micro-grid	Central grid	
	(p.u)	(p.u)	(p.u)
Active Power generation	0.01225	2.6734	2.6854
Reactive Power generation	0.00968	0.89484	0.90341
Active load	0.01176	2.6257	2.6375
Reactive load	0.0086	0.95281	0.96141
Active power loss	0.00049	0.04768	0.04795
Reactive power loss	0.00108	-0.05797	-0.058

Fig.2 shows the voltage profile for the integrated microgrid - main grid , here it can be seen that all the buses keeps the voltage within the permissible limit and also the micro-grid bus voltage gets improved by the integration with main grid. Eventhough there is improvement in bus voltages in the main grid it is not evident as the micro-grid parameters are very low compared to main grid.

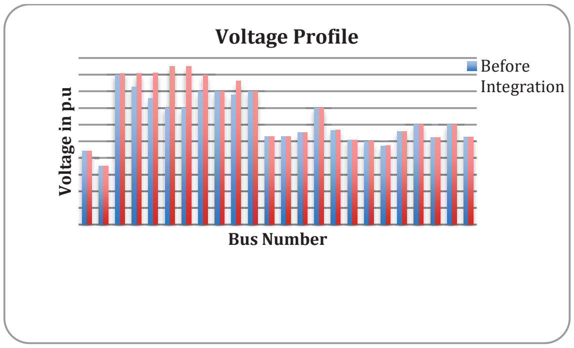

Figure 2: Microgrid- Main grid integration

A comparison of active power generation in micro-grid before and after integration with main grid (Central Travancore grid) is plotted in Fig.3&4. During the integration with main grid, maximum renewable power penetration from bus 9 (wind power) is achieved thereby, in main grid there is reduction in the power generation in the conventional generators.

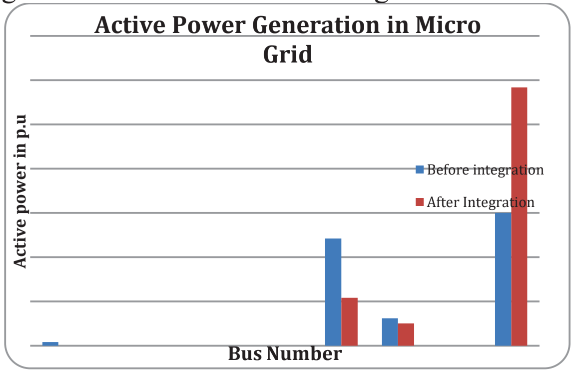

Figure 3: Active Power Generation in Micro-grid

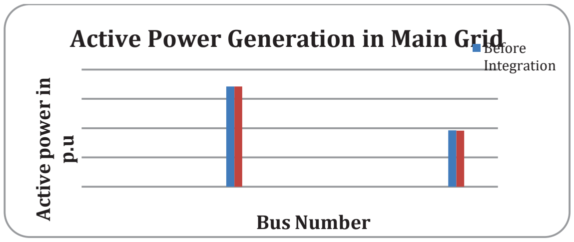

Figure 4: Active Power Generation in Main grid

The active power flow in central grid and micro-grid is separately shown in Fig.5&6. From these, it can be observed that power flow in micro-grid is more fluctuated than main grid.

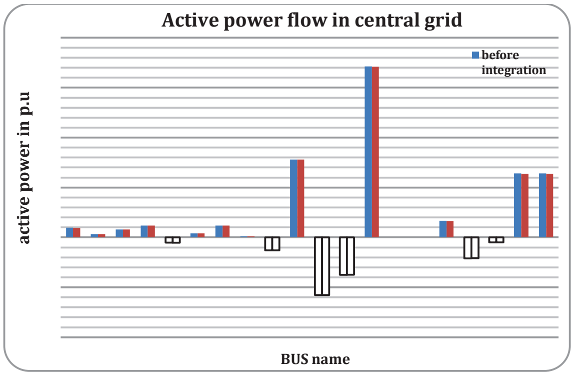

Figure 5: Active power flow Main grid

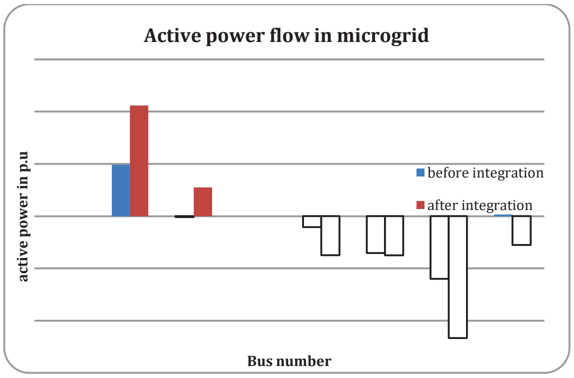

Figure 6: Active power flow in Micro-grid

In Fig.7, the integrated grid active power-flow is plotted.

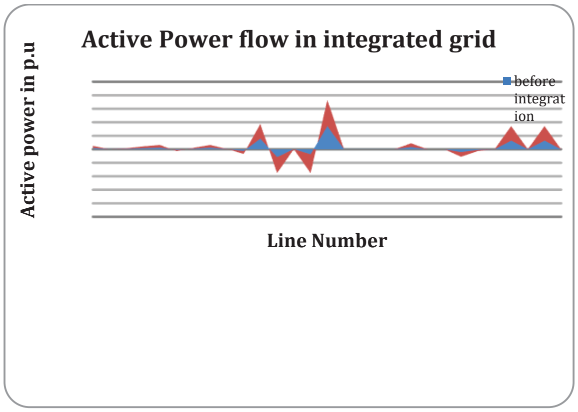

Figure 7: active power flow in microgrid-maingrid integration.

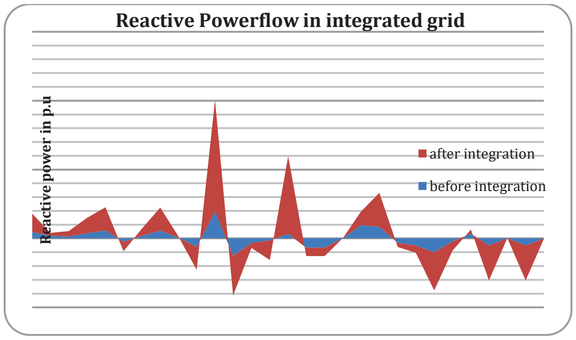

Figure 8: Reactive powerflow in integrated grid

Fig.8&9 shows the reactive power flow in micro grid and main grid. When the micro-grid is integrated with main grid there is significant change in the reactive power flow than in main grid. As a result the bus voltages in micro-grid is improved by the integration.

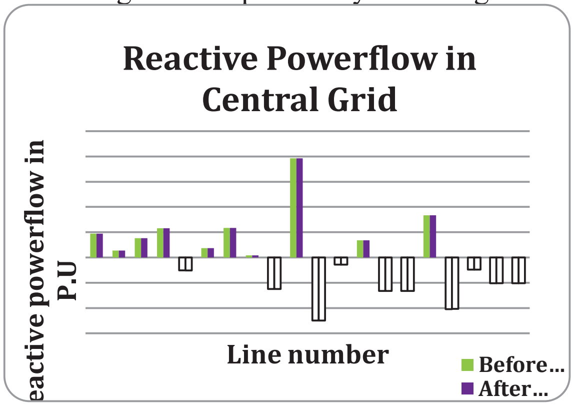

Figure 9: Reactive powerflow in main grid(Central Travancore Grid)

Fig.10 shows the reactive power flow in combined micro-grid –main grid network.

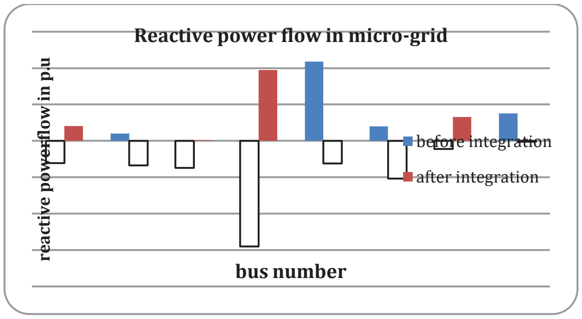

Figure 10: Reactive powerflow in microgrid

The stability in terms of eigen value analysis also carried out and furnished as below (Fig.11-13). It can be observed that in each case the all the roots are in the left half of s plane and in the case of Z domain map all the roots are inside the circle which shows the eigen value stability of the system.

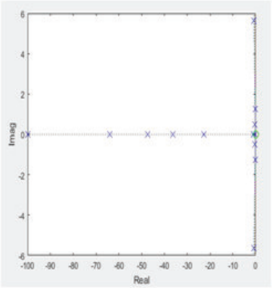

Fig.11(a) Central Travancore grid S domain map

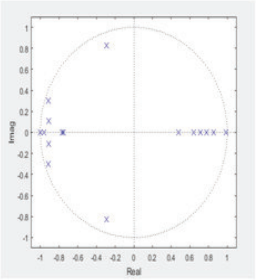

Fig.11(b) Z domain map

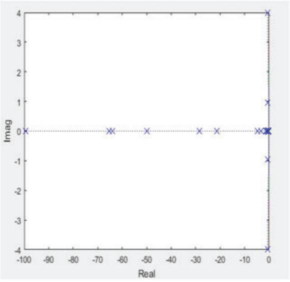

Fig.12(a) Microgrid S domain map

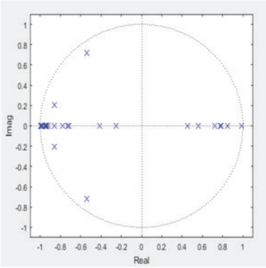

(b) Z domain map

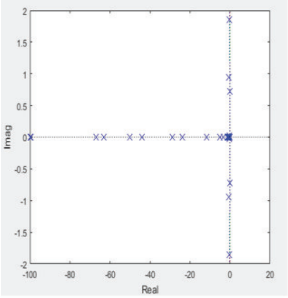

Fig.13(a)Integrated microgrid-maingrid S domain map

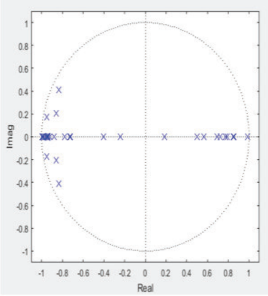

(b) Z domain map

4. CONCLUSIONS

In this paper, the proposed micro-grid is integrated with Central Travancore grid (utility) and the static analysis is carried out using PSAT software which is a globally accepted power system simulation software. The power flow using Newton-Raphson method is carried out for micro grid & central Travancore grid separately and then the combined system is simulated. The simulation results shows that by the integration the bus voltages in the micro-grid as well as main grid is improved and is more evident in the case of micro-grid. After integration, the variation in reactive power flow in micro-grid seems to be more than that of main grid. Considering the active power exchange between the microgrid-main grid network, more power is generated from bus 9 (wind power generation) and as a result the electric power generation from the costly conventional generators can be reduced. It can be concluded that by the integration of micro-grid with main grid, there is voltage improvement in the system as well as maximum penetration from renewable sources is achieved and by integrating more number of micro-grids into the main grid, the impact will be more appreciable.

ACKNOWLEDGMENTS

The authors are grateful to Dr Federico Milano,for his excellent simulation software PSAT.

REFERENCES

[1] A. Sobieh, M. Mandour, E. M. Saied, and M. M. Salama, “Optimal Number Size and Location of Distributed Generation Units in Radial Distribution Systems Using Grey Wolf Optimizer,” Int. Electr. Eng. J., vol. 7, no. 9, pp. 2367–2376, 2017.

[2] Y. Oka and A. Yokoyama, “Optimal operation scheduling and economical evaluation method of battery energy storage system in power system with a large penetration of photovoltaic

generation," 2013 IEEE Grenoble Conf. PowerTech, POWERTECH 2013, 2013.

[3] G. Haddadian, N. Khalili, M. Khodayar, and M. Shahidehpour, "Optimal coordination of variable renewable resources and electric vehicles as distributed storage for energy sustainability," Sustain. Energy, Grids Networks, vol. 6, pp. 14–24, 2016.

[4] M. Farrokhifar, "Electrical Power and Energy Systems Optimal operation of energy storage devices with RESs to improve efficiency of distribution grids ; technical and economical assessment," Int. J. Electr. Power Energy Syst., vol. 74, pp. 153–161, 2016.

[5] X. Wu, X. Wang, S. Member, C. Qu, S. Member, and A. Sets, "A Hierarchical Framework for Generation Scheduling of Microgrids," IEEE Trans. Power Delivary., vol. 29, no. 6, pp. 2448–2457, 2014.

[6] A. Ouammi, H. Dagdougui, and R. Sacile, "Optimal control of power flows and energy local storages in a network of microgrids modeled as a system of systems," IEEE Trans. Control Syst. Technol., vol. 23, no. 1, pp. 128–138, 2015

[7] P. García, J. P. Torreglosa, L. M. Fernández, F. Jurado, R. Langella, and A. Testa, "Energy management system based on techno-economic optimization for microgrids," Electr. Power Syst. Res., vol. 131, pp. 49–59, 2016.

[8] Burak YILDIRIM1, Muhsin Tunay GENÇOĞLU, "Impact of Microgrid on Power System Voltage Stability," 2nd International Conference on Advances in Engineering and Technology (RTET-2017),pp.158-162, 2017.

[9] Federico Milano, "Power System Analysis Toolbox documentation for PSAT" version 2.1.8, January 6, 2013.

Saritha.K.S received her M.Tech in Power Electronics and Power systems from Mahatma Gandhi University, Kerala, India in 2012. She is working as Associate Professor in the Department of Electrical & Electronics Engineering, Sree Narayana Gurukulam College of Engineering, Kadayiruppu, Kolenchery , Kerala, India. Presently she is pursuing Ph. D (Part Time) at School of Engineering, Electrical Dept., Cochin University of science and Technology ,Cochin, Kerala, India.

Dr. SasidharanSreedharan received his M.Tech in Electrical Power System from Govt. Engineering College, Thrissur, Kerala, India in 1998 and Ph.D from Asian Institute of Technology, Bangkok, in 2010 respectively. He was post-doctoral research fellow in RED Lab, Renewable Energy Design Laboratory, University of Hawaii, United Stated from 2014-2015. He is currently working as professor and Head of Computer and science Engineering, M.E.S College of Engineering, Kuttippuram, Kerala, India. His Research interests are in grid integration of Renewable, AI applications to power systems and grid stability

Dr. Usha Nair is a graduate and post graduate in Electrical Engineering. She has completed her Ph.D in 2009 from Cochin University of Science and Technology and presently working as Professor in the Department of Electrical Engineering in the same University. Her areas of interest are nonlinear dynamical analysis, renewable energy, control system design and time series analysis.

MES JOURNAL OF TECHNOLOGY AND MANAGEMENT
Volume 4, No 1,45-60,2020

Efficiency Improvement of Solar-Wind Hybrid Energy Conversion System

Nafeesa K, Anagha A P, Sajina M K, Nesihath M K
Dept.of Electrtical and Electronics Engineering,
MES College of Engineering Kuttippuram,
Kerala, India
nafeesakm@gmail.com

ABSTRACT

With increasing awareness of global warming and depletion of fossil fuel reserve, dependence on sustainable energy sources to preserve the earth for the future generations is a prioritized area of research. In addition to the hydro power, wind and photovoltaic energy are the two important sustainable energy sources to meet our energy demands. Non-predictive and intermittent nature of wind energy and varying solar irradiance levels due to sun intensity and unpredictable shadows cast by clouds, birds, trees etc. makes these sources unreliable. In the proposed system, wind and solar energy sources are combined by incorporating maximum power point tracking (MPPT) algorithms to improve the system power transfer efficiency and reliability and is interfaced to the grid through inverter. High Performance Adaptive Perturb and Observe MPPT is used in solar energy conversion system and Tip Speed Ratio (TSR) combined Hysteresis control method is used in wind energy conversion system

Keywords

DC-DC Converter, Irradiance, Maximum Power Point Tracking (MPPT), Tip Speed Ratio (TSR).

I. INTRODUCTION

Renewable sources of energy are gaining worldwide importance due to the depletion of non-renewable sources like fossil fuels together with the ever increasing demand of electrical energy. Alternative energy technologies like wind and solar based energy generation systems are receiving worldwide attention due to the rising rate of consumption of nuclear and fossil fuels. Even though hydroelectric production is dominant, the wind and solar energy sector are also growing fast in the present scenario. The common inherent drawback of wind and photovoltaic systems are their non-predictive intermittent natures that make them unreliable. However by combining these two intermittent sources the system reliability can be improved significantly. Also an adequate Maximum Power Point Tracking (MPPT) method would be adopted to maximize the power transfer efficiency. The power generated from these renewable sources needs power conditioning before connecting on DC link. Generally voltage source inverter is used to interface the Renewable Energy Source with the distribution system. The complete block diagram of the proposed system is shown in the Fig.1.

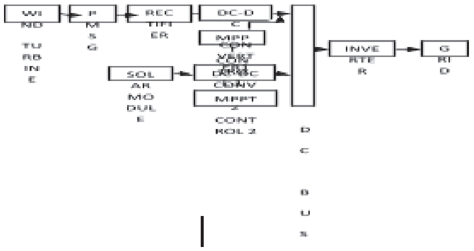

Figure.1 Block diagram of the proposed system

An effective MPPT techniques namely adaptive P&O method for solar part and Combined Hysteresis TSR control method for wind part which eliminates the drawback of traditional methods, is used in this work. The proposed P&O technique attempts to achieve improved performance with moderate cost, simple implementation, and does not depend on predefined constant values. The proposed control method for wind energy conversion system has fast dynamic characteristics, regardless of changes in wind speed. The power extracted from the proposed system is finally transferred to the grid through a three phase inverter synchronized at grid frequency.

II. SOLAR ENERGY CONVERSION SYSTEM

A solar module directly converts the solar energy into electrical energy by the use of photovoltaic effect. Solar PV panel is a nonlinear power source, where the panel output power varies with temperature and insolation. The nonlinear characteristic of a PV panel is a function of irradiance and temperature. Out of the various MPPT techniques studied, perturbation and observation (P&O) technique and incremental conductance method are the efficient methods to track the MPP by updating repeatedly the operating voltage of the PV array varying the duty cycle of the power converter with a fixed step size. This technique continuously observe the output voltage and current of a solar module and according to the variation of voltage and power a certain value called perturb value is either added or subtracted with the previous parameter. This technique suffers many disadvantages which include constant perturb value, slow performance, high computational burden and oscillations at operating point. Large perturb values cause higher oscillation at MPP and smaller perturb values result in slower response. Hence tradeoff problem between faster response and steady-state oscillations is inherent. Moreover, the perturb value is not generic; therefore, MPPT using a fixed perturb is system dependent.

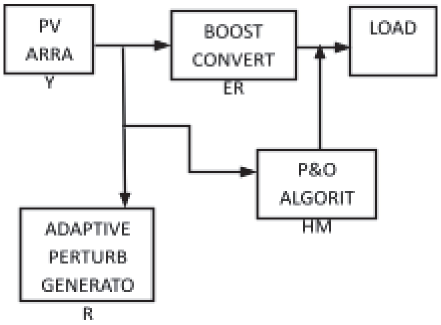

Figure 2: Block diagram of adaptive P&O method

The demerits of P&O technique can be eliminated by using high performance adaptive P&O technique. The proposed technique utilizes the slope of the P-V curve to generate an adaptive perturb. This method uses an algorithm that varies the perturb value automatically according to the changes in the system. The block diagram for adaptive perturb and observe method is shown in the Fig. 2. The flowchart of P&O algorithm used in this method is shown in Fig. 3

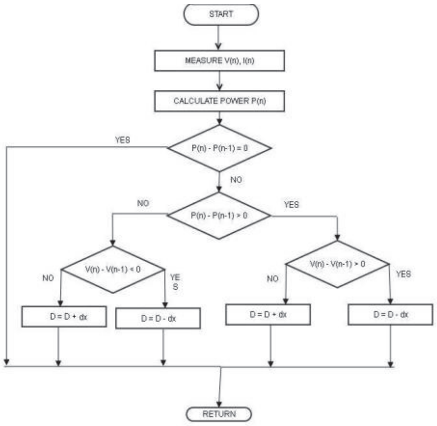

Figure 3: Flowchart of P&O technique

The main idea behind the proposed technique is that at the start of any P&O technique, large perturb steps are needed to quickly reach the MPP, and as the MPP is approached, the perturb value needs to be decreased to avoid large oscillations around this maximum output power operating point. The proposed adaptive technique utilizes the error between two successive array power signals calculated from the measured array voltage and current signals to create an adaptive perturb. Basically, at the start of the hill climbing process, this error is large and decreases as the maximum power operating point is approached at steady state.

Therefore, this error can be treated like an error signal in a closed-loop system that needs to be minimized at steady state. One of the main advantages of this method is that it gives relatively small oscillations during tracking and steady-state condition compared to traditional P&O method. The adaptive perturb value is obtained as,

$$a = M\frac{dp}{dv} \qquad (1)$$

where M gives the direction of perturbation (1 or -1) and $\frac{dp}{dv}$ gives the slope of the P-V curve. The value of $\frac{dp}{dv}$is such a way that the value is high at the starting of the MPP tracking and it approaches to zero as the MPP is reached.

III.WIND ENERGY CONVERSION SYSTEM

Wind energy conversion system (WECS) involves wind turbine, generator, rectifier and power electronic converter. Over the last four decades the evolution of wind power conversion technology has led to the development of different configurations of wind turbines, which utilize a wide variety of electric generators. PMSG has a simple structure and high efficiency due to its gearless arrangement. Hence it is selected as the generator for energy conversion in this work. A diode bridge rectifier is used to convert AC output from generator to DC. The DC system is set at a constant DC voltage and comprised of a battery bank, a controller to avoid the overcharging of batteries and a load. The load may be DC or may include an inverter to an AC system. Connecting a wind generator to a constant dc voltage has significant problems due to poor impedance matching between the generator and the constant dc voltage (battery), which will limit power transfer to the dc system. In response to these problems, a dc–dc converter is incorporated in the dc link.

Amount of power output from a WECS depends upon the accuracy with which the peak power points are tracked by the MPPT controller of the WECS control system irrespective of the type of generator used. An effective and low implementation cost MPPT algorithm is essential to enhance the efficiency and economics of wind energy conversion systems (WECS). An effective MPPT technique namely Combined Hysteresis-TSR control is used for wind side in this work. In the proposed MPPT method, the TSR control provides fast dynamic characteristics, and the added hysteresis controller corrects the MPP error at the steady state. An MPPT method using TSR control can rapidly track the MPP. However this MPPT method cannot guarantee the operation of the controller at the MPP when the errors occurring in the Cp-curve are caused by a variance in the blade characteristics. In this method, the hysteresis controller is combined with TSR control to solve this problem. The hysteresis control is similar to that used in the typical P&O control. This controller monitors the power output in order to have a band of maximum power when the wind turbine operates at the MPP of the modeled Cp-curve using TSR control. If the output of the wind turbine is unable to reach maximum power, the hysteresis controller varies the duty ratio within the hysteresis band to correct for the operating point. The hysteresis control is similar to that used in the typical P&O control. This controller monitors the power output in order to have a band of maximum power when the wind turbine operates at the MPP of the modeled Cp-curve using TSR control. If the output of the wind turbine is unable to reach maximum power, the hysteresis controller varies the duty ratio within the hysteresis band to correct for the operating point. Fig.4. shows a flowchart for the proposed MPPT method.

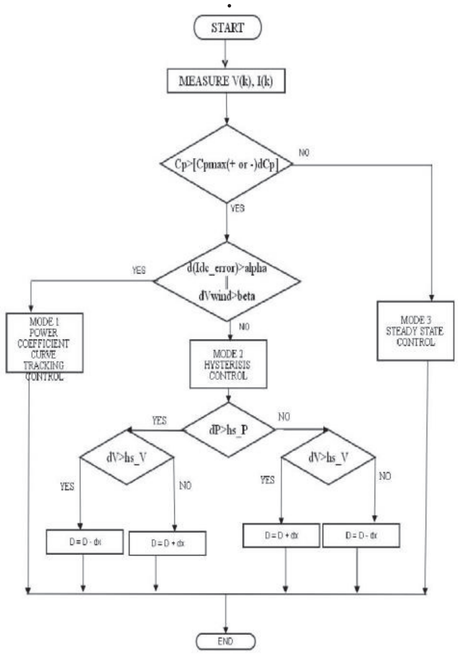

Figure 4: Flowchart of combined hysteresis TSR control

IV.GRID SIDE CIRCUIT

In order to supply electricity into a mains electricity system, the dc output from the module must be converted to ac at the correct voltage and frequency. An electronic inverter is used to do this. Modern inverters are very efficient (typically 97%), and use PID control systems to ensure that the PV array keeps working at its optimum voltage. Three-phase grid-connected voltage-source inverters (VSI) are employed to interface hybrid wind-solar electric systems with electric power grids as shown in Fig.5.

The inverter circuit plays a role of an intermediate circuit for synchronizing the output current with the grid voltage, which means the power factor is equal to unity which flows into the utility. Inverters receives a DC input and produce a constant amplitude sinusoidal output. Initially, most inverter technology used silicon controlled rectifier (SCR) devices and a transformer coupling to approximate a sine wave via line commutation. As power transistors became more feasible, most low to medium power inverter systems replaced the SCR with the MOSFET or the IGBT.

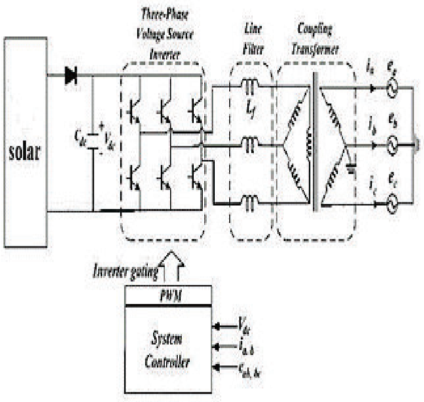

Figure 5: Block diagram of Grid side connections

The connection to the utility grid is made by means of a step-up Y-Y transformer, and a second-order low pass filters to reduce the perturbation on the distribution system from high-frequency switching harmonics generated by the PWM control of the VSI. To achieve these two goals, the three-phase line current is transformed from ABC reference frame to a dq rotating reference frame. The abc to dq0 transformation block computes the direct axis, quadratic axis, and zero sequence quantities in a two-axis rotating reference frame for a three-phase sinusoidal signal. The following transformation is used:

$$V_d = \frac{2}{3}\left(V_a \sin\sin(\square t) + V_b \ \square\square\square \sin\left(\omega t - \frac{2\pi}{3}\right) + V_c \sin\sin\left(\omega t + \frac{2\pi}{3}\right)\right) \qquad (2)$$

$$V_q = \frac{2}{3}\left(V_a \cos\cos(\square t) + V_b \square\square\square \cos\left(\omega t - \frac{2\pi}{3}\right) + V_c \cos\cos\left(\omega t + \frac{2\pi}{3}\right)\right) \quad (3)$$

$$V_0 = \frac{1}{3}(V_a + V_b + V_c) \quad (4)$$

where ω = rotation speed (rad/s) of the rotating frame.The transformation is the same for the case of a three-phase current, replace the V_a, V_b, V_c, V_d, V_q, andV_0 variables with the I_a, I_b, I_c, I_d, I_q, and I_0 variables.it is also known as a Park transformation. The q-axis current is used to control the power flow from the PV to the grid. On the other hand, the d-axis current is used to control the output power factor to unity.

For the requirement of stable grid voltage, two type of control processes are used, one is power control and the other one is current control. Both these control strategies are basically PID controllers. Power controller senses the grid voltage, grid current and gives the corresponding grid active and reactive power. The power controller also senses the inverter output voltage, current and gives the corresponding active, reactive power. The direct axis reference current (Idref) is obtained through PI controller. Idref is the one input of the current controller. The load voltage, load current are also sensed and the RMS value of the load is determined. The other input to the current controller is the quadrature axis reference current which is also obtained by using PI controller. In current controller inverter output current is converted into direct axis and quadrature axis currents. These two currents are compared with the current given by power controller outputs. Actual current is compared with the reference current and an error signal is fed to the PI controller. The PLL block models a Phase Lock Loop (PLL) closed-loop control system, which tracks the frequency and phase of a sinusoidal signal by using an internal frequency oscillator. The control system adjusts the internal oscillator frequency to keep the phase's difference to 0. The pulses obtained from the PI controller are given as gate signals to the inverter.

V. MODELLING AND SIMULATIONS

The complete system is modelled and simulated using Matlab/Simulink platform.

A.SOLAR ENERGY CONVERSION SYSTEM

The typical model of a solar cell is shown in Fig.6.An ideal solar cell is modelled by a current source in parallel with a diode. In practical, no solar cell is ideal, and hence a shunt resistance and a series resistance component are added to the model. From the equivalent circuit, basic equation for the output current is obtained as,

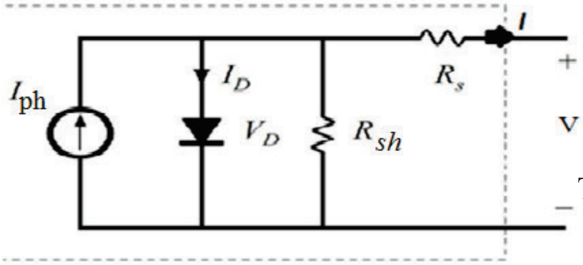

Figure 6: Equivalent circuit model of PV cell

$$I = I_{ph} - I_D - V_D/R_{sh} \quad (5)$$

where the photocurrent (I_{ph}) is obtained as the product of irradiance (G) and short circuit current (I_{sc}) given by,

$$Iph = G \times Isc \quad (6)$$

From the Shockley diode equation, the current through an ideal diode is obtained as,

$$I_D = I_0\left(exp\, exp\left(\frac{VD}{V_T}\right) - 1\right) \quad (7)$$

where $V_D$is the voltage across the diode, $I_o$is the reverse bias saturation current and $V_T$is the thermal voltage which are given in equations (8), (9), (10) respectively.

$$V_D = V + I\, R_S \quad (8)$$

$$V_T = (n \times K \times Tak)/q \quad (9)$$

$$I_o = Isc / (\exp(Voc / Vt) - 1) \quad (10)$$

Then the equation (5) becomes,

$$I = Iph - I_o \times (\exp((V + IRs) / V_T) - 1) \quad (11)$$

This can be written as a function of output current as,

$$f(I) = Iph - I - I_o \times (\exp((V + IRs) / V_T) - 1) = 0 \quad (12)$$

This function can be solved using Newton raphson method and the final output current from the solar cell, after a number of itration is obtained as,

$$I_2 = I_1 - f(I_1)/f'(I_1) \quad (13)$$

where I_2obtained is treated as the next value for further itration.

By using the above equations, a solar module containing 72 solar cells was modelled using matlab function block in Matlab/Simulink. About five itrations were done using newton raphson method and almost an exact output cureent was obtained.The parameters used for modelling solar module in this work is considered as, Open circuit voltage, V_{oc}= 43.5 V, Short circuit voltage, I_{sc}= 4.75 A, Rated voltage, V_{mpp} = 38V, Rated current, I_{mpp} =4 A.

As the irradiance and temperature is kept constant, the output voltage, current and power is constant. As constant irradiance and temperature are not practically possible due to natural changes in weather, a PV model with varying irradiance and temperature were also designed. The irradiance change affects the photon generated current and has very little effect on the open circuit voltage. The temperature variation affects the open circuit voltage and the short circuit current varies marginally. The dc-dc boost converter is used to enhance the output voltage and is also modelled using Matlab/Simulink. The P&O algorithm was implemented using Embedded Matlab. An adaptive perturb value is developed using the calculated value of dp/dv from the measured value of voltage and current of the solar module.

B. WIND ENERGY CONVERSION SYSTEM

The wind turbine is used for the conversion of wind kinetic energy to mechanical work. Its description comes from laws of conservation of energy and momentum that can be applied in a space, which is limited by flow surfaces. On the basis of relationships for the calculations of these two quantities, it is possible to express the value of the axial performance acting on the shaft by equation (14).

$$P_{tur} = \frac{1}{2}.\rho.\pi.R^2.w^3.C_p \quad ......14$$

where ρ is the air density, R is the radius of the turbine, w is the wind speed and C_p is the performance coefficient, which expresses the relationship between performances of the air flow and of the wind turbine, i.e. the efficiency of the wind turbine, in dependence on the wind speed or on the tip speed ratio of the turbine. From the value of the rotational motion performance, it is possible to determine the value of the torque acting on the shaft by the following equation.

$$M_{tur} = \frac{P_{tur}}{\omega_{tur}} = \frac{1}{2}.\rho.\pi.R^3.w^2.C_{M,} \qquad \text{.......15}$$

Where ω_{tur} is the turbine angular speed, and C_M is the torque coefficient. From these equations it is evident that the instantaneous values of the performance dependents on the wind speed. On the basis of these equations, it is possible to build the model of the wind turbine in Simulink platform. The parameters used in this wind turbine model are:

Parameter	Symbol	Value and Units
Air density	P	1.205 kg/m^3
Rotor radius	R	38 m

Inputs of the model are the wind speed and the turbine angular speed. Output quantity is the axial torque, which is transmitted by the drive train to the generator. Since the turbine should not operate when the wind speed is too high and too low, using switching action, the turbine is made to operate only for wind speed between 4m/s and 12m/s.

C_p value is calculated using the following equations:

$$C_p = C_1\left[\frac{C_2}{\lambda_i} - C_3\square - C_4\right]e^{-\frac{C_5}{\lambda_i}} + C_6\lambda \qquad \text{..16}$$

$$\frac{1}{\lambda_i} = \frac{1}{\lambda + 0.08\beta} - \frac{0.35}{\beta^3 + 1} \qquad \text{........17}$$

where C_1=0.5176, C_2=116, C_3=0.4, C_4=5, C_5=21 and C_6=0.0068. Pitch angle control is not performing in this method. Therefore β=0. Hence the equations (17) and (18) will become:

$$C_p = C_1\left[\frac{C_2}{\lambda_i} - C_4\right]e^{-\frac{C_5}{\lambda_i}} + C_6\lambda \qquad \text{.......18}$$

$$\frac{1}{\lambda_i} = \frac{1}{\lambda} - \frac{0.35}{1}$$ 19

A maximum Cp is achieved when the tip speed ratio is at the optimal value (λopt).

Two mass drive train model is utilized in this system. One mass is used to represent the turbine inertia; the other mass is equivalent to the generator inertia. The two-mass representation is described by the following equations:

$$\frac{d\omega_m}{dt} = \frac{T_m - T_e}{J_m}$$ 20

$$\frac{d\omega_{turb}}{dt} = \frac{T_{turb} - K_s\gamma}{J_{turb}}$$ 21

$$\frac{d\gamma}{dt} = (\omega_{turb} - {}^{\gamma}{}_{m})$$ 22

$$T_m = K_s{}^{\gamma} - D_{turb}(\omega_{turb} - {}^{\gamma}{}_{m})$$ ....(23)

where T is the torque; □ is the angular displacement between the two ends of the shaft; J is the inertia; and K_s is the shaft stiffness. The subscripts r, m and e stands for wind turbine rotor, generator mechanical and generator electrical, respectively. The characteristics of the simulated shaft are:Turbine Damping, D_{turb}= 14*(10^6) nms/rad, Rotor Inertia, J_{turb}= 6.1 * (10^6) kg mm, Shaft Stiffness, K_s= 83 * (10^6) Nm/rad, Generator Inertia, J_{gen}= 8.5 * (10^6) Nm/rad.

The generator parameters are:Number of Pole pairs, p = 40, Stator resistance, R_s = 1.7850 Ω, d-axis inductance, L_d = 8.5mH, q-axis inductance, L_q = 8.5mH, Magnetic flux linkage, λ_{fd} = 0.57 Vs.

The Simulink model is developed by integrating PMSG with wind turbine. The wind turbine converts the wind energy to the mechanical torque. It is fed to the one side of the gearbox. Then the mechanical energy is converted to the measurement of rotational motion angular speeds at both ends of the shaft. One of them is fed back to the turbine and determines the value of the performance coefficient and the second is fed into the generator and determines the value of the electromagnetic torque, which in turn fed into this drive train. For the variable speed operation of the WECS, a repeating sequence is used, with a time value of 0 to 1 second and the corresponding output values are 3 to 26 m/s.

The output of the PMSG is given to a rectifier to convert the AC input to DC. The converter that consists of up to six power switches connected in a bridge configuration. Connecting a wind generator to a constant dc voltage has significant problems due to the mismatching the poor impedance matching between the generator and the constant dc voltage, which will limit power transfer to the dc system. In response to these problems, researchers have investigated incorporating a DC-DC converter in the dc link. The block diagram showing the PMSG, the rectifier and the boost converter is shown in the Fig.7.

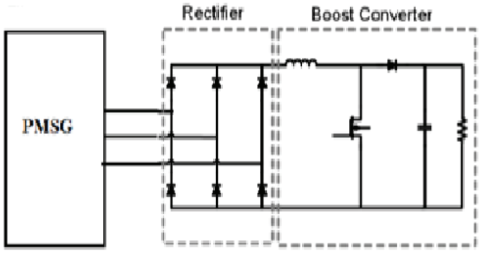

Figure 7: Block diagram containing PMSG, rectifier, boost converter

The algorithm of Combined Hysteresis TSR control was implemented using Embedded Matlab.Initially the system operates using TSR control by the current controller circuit. The current through the inductor of the boost converter is controlled to obtain the desired duty ratio. Once the change in wind speed stabilizes, the system continues to be in TSR mode only until the inductor current error minimizes. After that the system checks the value of power coefficient, $C_{p.}$ The system continues its previous state if the C_p is inside the set bandwidth. It is known as steady state control. Once the power coefficient exceeds the set bandwidth, the hysteresis control is performed. Hysteresis control is similar to the normal P&O method. The duty ratio is incremented or decremented based on the change in voltage and power with respect to the set voltage and set power. These preset terms are also known as hysteresis voltage and power.

The magnitude of the preset values is found by the trial and error method. And the set conditions are:ΔC_p = 0.1, Minimum current error = 10 units, Minimum wind speed change = 1.1 units, Hysteresis power = 16 * (10^{-17}) units, Hysteresis voltage = 2.5 * (10^{-6}), Increment/decrement in duty ratio = 0.1. The system to generate the reference inductor current and the complete MPPT system developed in Matlab Simulink based on the set conditions.

VI.RESULTS AND DISCUSSIONS

The variation in the inputs to solar module such as irradiance and temperature areapplied using repeating sequence stair. On the basis of this model, the output characteristics of PV module are simulated without MPPT control and with MPPT control as shown in Fig.8 and Fig.9 respectively. The boosted output voltage is also shown in Fig.10

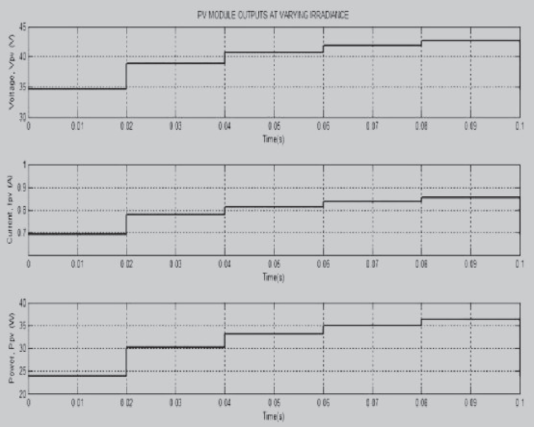

Figure 7: Output characteristics without MPPT

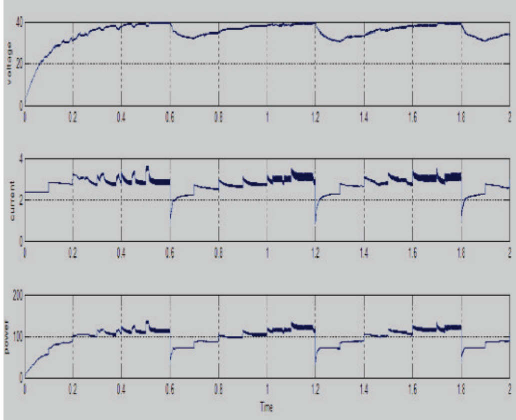

Figure 8: Output characteristics with MPPT

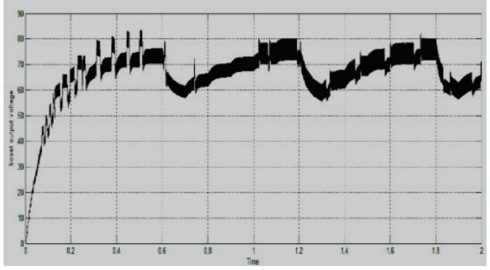

Figure 9: Boosted output voltage

In theWECS, without MPPT control, the output voltage of the wind generator is fixed, while in the system with MPPT control, the voltage is adjusted by the MPPT controller. Fig.10 and Fig.11 show the simulation results for the systems without and with MPPT control, respectively.

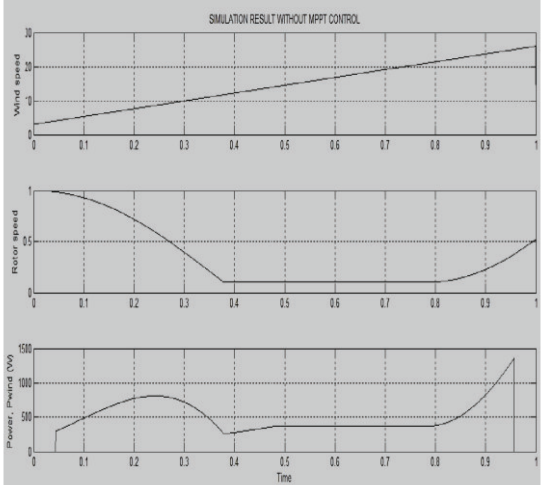

Figure 10: Simulation results without MPPT

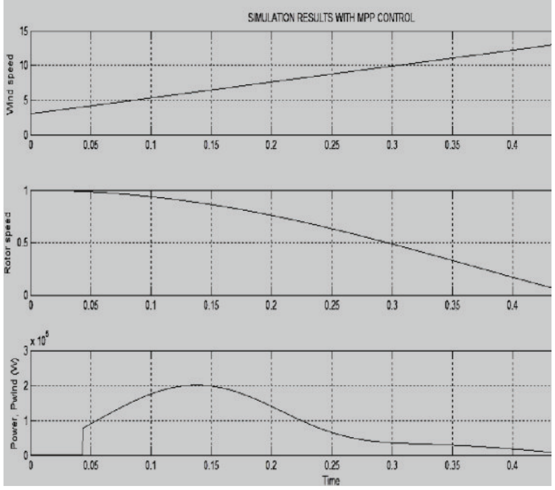

Figure 11: Simulation results with MPPT

The solar subsystem and wind subsystem with MPPT are combined and connected to the grid by proper means of control. The grid voltage and current obtained is shown in the Fig.12.

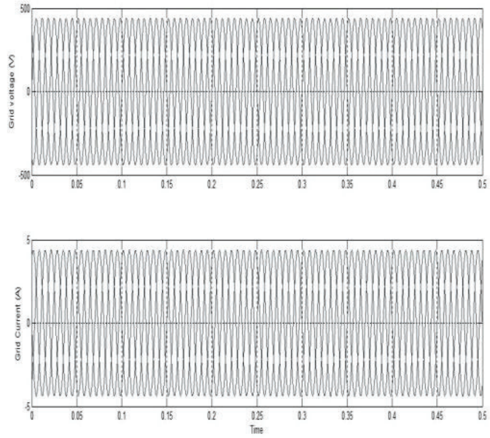

Figure 12: Grid voltage and current

VII.CONCLUSIONS

The Hybrid Energy Conversion System incorporating MPPT techniques is simulated in Matlab/Simulink and results were obtained. Grid connection of the system is also proposed in this work. A generalized PV model has been developed in Matlab/Simulink. Variable irradiance and constant temperature were considered due to the negligible temperature variations at one place. Adaptive P & O method was used in the system and inferred that there is a significant reduction in the oscillations compared to traditional method. PMSG is used in the WECS model because of its various advantages. A cost effective MPPT method namely TSR combined Hysteresis was used and obtained the required results. To maintain the grid voltage and inverter output voltage as same, grid side control using current controllers and powercontrollers was done.The zero reactive power obtained at the grid side, proves the accuracy of the current and power control methods adopted.

REFERENCES

[1] AryuantoSoetedjo, Abraham Lomi, Yusuf Ismail Nakhoda and AwanUjiKrismanto, "Modeling of Maximum Power Point Tracking Controller," TELKOMNIKA, Vol.10, No.3, July 2012.

[2] Ahmed K. Abdelsalam, Ahmed M. Massoud, Shehab Ahmed and Prasad N. Enjeti, "High-Performance Adaptive Perturb and Observe MPPT Technique forPhotovoltaic-Based Microgrids," IEEE Trans. PowerElectron., vol.26, no.4, Apr. 2011.

[3] Yuange Xia, KhaledH.Ahmed, and Barry W.Williams, "A new maximum power point tracking technique for permanent magnet synchronous generator based wind energy conversion system," IEEE Trans. Power Electron., vol.26, no.12, Dec.2011.

[4] Pritam Chowdary, Indrajit Koley, Sougata Sen, Dr. Pradip Kumar Saha and Dr. Gautam Kumar Panda, "Modelling, simulation and control of a grid connected nonconventional solar power generation system using matlab," IJAREEIE – Vol.2, issue 4, Apr. 2013.

[5] Yuvarajan, S and Kaderbhai, M., "Hybrid Renewable Energy System with Wind Turbine and PV Panels," IEEE Trans. Energy Convers.vol.21, no.2, Jun. 2010.

[6] Shun Yang, Lida Zhang, "Modeling and Control of the PMSG Wind Generation System with A Novel Controller," Third International Conference on Intelligent System Design and Engineering Applications, 978-0-7695-4923-1/12 $26.00 © 2012 IEEE DOI 10.1109/ISDEA.2012.226, 2013.

[7] Mirza MohdShadab, Abu Tariq, "Performance analysis of Permanent magnet synchronous generator connected with wind turbine," International Journal of Advanced Technology & Engineering Research(IJATER), Jun. 2009.

Dr Nafeesa K did her B.Tech in RIT Kottayam. She received her M.Tech and PhD from NIT Calicut. She is presently working as professor and head in the department of Electrical and Electronics Engineering department in MES College of Engineering.

Ms. Nesihath M K did B.Tech in Electrical and Electronics Engineering and M.Tech in Industrial drives and control from Mahatma Gandhi University, Kerala.

Sajina M K did B Tech in Electrical and Electronics Engineering from MG university and M Tech in power systems from NIT Calicut.

Anagha A. P got the B.Tech degree in Electrical and Electronics Engineering from MES College of Engineering, Kuttippuram, Kerala and M.Tech in High Voltage Engineering from National Institute of Technology, Calicut India.

MES JOURNAL OF TECHNOLOGY AND MANAGEMENT
Volume 4, No 1,61-71,2020

TECHNIQUE FOR ACTIVE COMPENSATION OF AN INTERFEROMETER FOR MEASURING SUBNANOMETER DISPLACEMENTS

Anil K Jacob
Department of Computer Science and Engg
MES College of Engg, Kuttipuram, Kerala
akanjama@gmail.com

ABSTRACT—*Small amplitude vibrations and their measurements are of importance in various scientific disciplines particularly in biological experiments such as the subnanometer movements in the inner ear of animals. A difficult aspect of such measurements is the interference caused by external disturbances of low frequency origin which in turn can jeopardize the accuracy of the results. Laser interferometers are commonly used to measure such microscopic movements. The external disturbances cause the operating point of the interferometer to drift around thereby producing non negligible errors. Therefore, it becomes imperative to stabilize the operating point of the interferometer at the point of maximum sensitivity. Control system techniques are used to stabilize the operating point of the interferometer. The results show that disturbances affecting the measurement are rejected by the control mechanism.*

Keywords: interferometer; compensation; controller; drift

1. INTRODUCTION

The interferometric method is a very accurate method that is used for the measurement of biological subangstrom displacements. Laser interferometry is used as an experimental technique for investigating cochlear mechanics [1]. Unlike interferometers using heterodyning methods, homodyning interferometers are less costly but suffer from problems arising from unstable interference conditions [1]. The problem of solving interferometer drift by stabilizing the operating point using direct current phase tracking is elaborated in [2]. In this proposed work, a closed loop control system is employed for stabilizing the drift in the operating point of the interferometer. Michelson's interferometer, where interference of light beams is brought about by division of amplitude, is used for implementing the technique.

The mirrors of the interferometer are adjusted so that fringes of sufficient thickness are formedthereby allowing a photodetector to follow the variation of the intensity of the interference pattern across it. The fringes are allowed to fall on a fast photodiode which in turn produces a current proportional to the intensity of light falling on it.If I_1 and I_2 are the intensities of the two beams of wavelength λ that interfere with one other and δ is the phase difference between them, the resultant intensity is given by [3].

$$I_0 = I_1 + I_2 + 2e\sqrt{I_1 I_2}\cos(\delta) \quad (1)$$

Where $\delta = 2k\Delta x$, $k = 2\pi/\lambda$, Δx is the path difference and 2 takes into account that the reflected light has travelled the distance twice.

The intensity of light falling on the photodetector when one of the reflectors is made to undergo sinusoidal vibration with amplitude a, angular frequency ω and phase φis given by

$$I_0 = I_1 + I_2 + 2e\sqrt{I_1 I_2}\cos(\Omega + 2ka\sin(\omega t + \phi)) \quad (2)$$

whereI_1 and I_2 are the intensities of individual beams and Ω is the static optical phase difference between the two beams.

A factor e, called the homodyning efficiency, is used in Eqn(2) to account for the finite diameter of the light source, lack of monochromacity of the light source and the slight misalignment of optics in the actual set up [4]. Simplifying Eqn(2)

$$I_0 = I_1 + I_2 + 2e\sqrt{I_1 I_2}cos\Omega\left\{J_0(2ka) + 2\sum_{n=1}^{\infty} J_{2n}(2ka)\cos(n(\omega t + \phi))\right\} - 2e\sqrt{I_1 I_2}sin\Omega\left\{2\sum_{n=0}^{\infty} J_{2n+1}(2ka)\sin((2n + 1)(\omega t + \phi))\right\} \quad (3)$$

whereJ_n is the n^th order Bessel function [5]. Eqn(3) can be approximated as

$$I_0 = I_1 + I_2 + 2e\sqrt{I_1 I_2}\{cos\Omega(1 + k^2 a^2 \cos(2\omega t + 2\phi)) - 2kasin\Omega\sin(\omega t + \phi)\} \quad (4)$$

Since the contribution by higher harmonics to the resultant current is negligible we consider only the second harmonic.The higher order terms have negligible contribution because the amplitude of vibration a is much less than the wavelength of light and therefore the higher order terms can be neglected in the Bessel function expansion.The mean phase difference Ω constantly changes due to thermal expansion, mechanical factors and external disturbances such as animal movement, movement of vehicles, machinery, objects, etc. This is reflected in Eqn(4) as the slowly varying term $2e\sqrt{I_1 I_2}cos\Omega$.

This shifting of the mean phase difference is manifested by a variation in the sensitivity, which will subsequently cause problems in the determination of the actual value of the amplitude of vibration. The constant drift of the operating point appears on the oscilloscope as an envelope around the expected sinusoidal intensity pattern from the vibration of one of the reflectors. From Figure 1, it can be clearly seen that the maximum sensitivity of measurements occurs when the operating point lies at the point of maximum slope (eg, pt A); i.e, the second derivative of intensity with respect to displacement is zero.

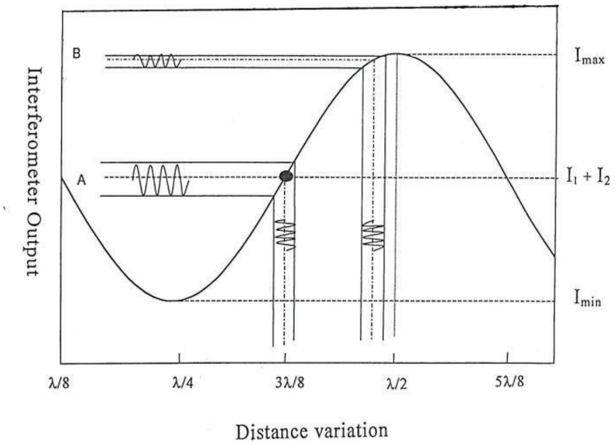

Figure 1: Interferometer Output vs Distance

If it is possible to bring the operating point to any one of the points of maximum sensitivity then displacement of amplitude less than λ/8 can be measured with considerable accuracy since in that region the curve can be considered linear. The interferometer can therefore be used to give an accurate value for the amplitude of vibration if the position of the fixed mirror is maintained such that the mean phasedifference$\Omega = (2n + 1)\pi/2$ $n = 0,1,2\ldots$. This ensures that the varying term $2e\sqrt{I_1 I_2}\, cos\Omega$ is always zero. When the interferometer is operating at the point of maximum sensitivity it is said to be in quadrature.

The interferometer is brought to quadrature and the fundamental component is picked out from Eqn(3) which is now a faithful reproduction of the input signal.The amplitude of the fundamental component which is $4e\sqrt{I_1 I_2}\, sin\Omega J_1(2ka)$ becomes $4e\sqrt{I_1 I_2}J_1(2ka)$ since $|sin\Omega| = 1$ at quadrature.The photodetector produces a voltage proportional to the fundamental component. The interferometer output voltage is given by

$$V = K_{pd}4e\sqrt{I_1 I_2}J_1(2ka) \quad (5)$$

where K_{pd} is a proportionality constant for the photodetector. $J_1(2ka) \approx ka$ for $2ka << 1$ [5]. Simplifying Eqn(5)

$$V = K_{pd} 4e\sqrt{I_1 I_2}ka \quad (6)$$

This expression shows that the interferometer output voltage is proportional to the amplitude of vibration.

2. TECHNIQUE FOR ACTIVE COMPENSATION

If the operating point drift is carefully observed, the disturbance signal can be largely approximated as a ramp signal with a slope of small magnitude. Such a disturbance can easily be rejected using a closed loop control system with an appropriate controller. The basis for the control system can be deduced from Eqn(4). The set point of the controller corresponds to the value required to keep the operating point at maximum sensitivity.From Figure 1 it can be seen that the set point value can be made equal to a value proportional tothe average value of I_{max} and I_{min}. The slowly varying signal of magnitude $2e\sqrt{I_1 I_2}\cos\,\Omega$ is the error signal produced by the drifting of the operating point and this signal can be used to control an actuator which produces sufficient displacement to keep the operating point at maximum sensitivity. The actuator that is used is a bimorph which is a piezoelectric device that undergoes deflection when a voltage is applied.The bimorph gets deflected until $|sin\Omega| = 1$ and $|cos\Omega| = 0$. As a result, the error becomes zero and the operating point rests on one of the points of maximum sensitivity.

A schematic arrangement of the closed loop system is given in Figure 2. The control loop consists of the interferometer, photodetector,filter, controller and the bimorph. There are two inputs to the closed control loop; namely, the disturbance input d(t) and the set point input r(t) as shown in Figure 3.

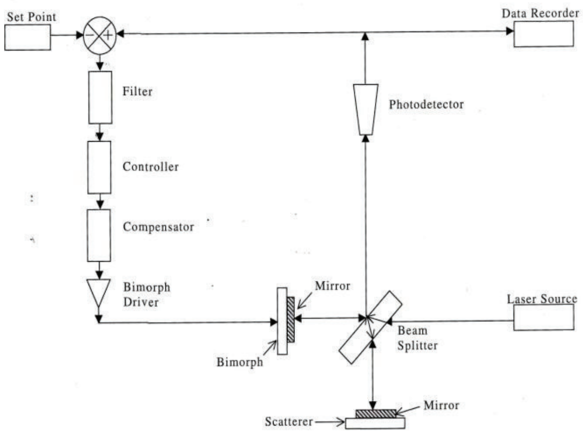

Figure 2: Schematic of the control loop

. Since the operating point is always supposed to remain at the point of maximum sensitivity, the set point can be considered constant. The load disturbance is always changing and has to be taken care of. The non-linear element represents the cosine characteristics of the fringes. The filter is used to remove those frequency components of the interferometer which we do not want to compensate for.

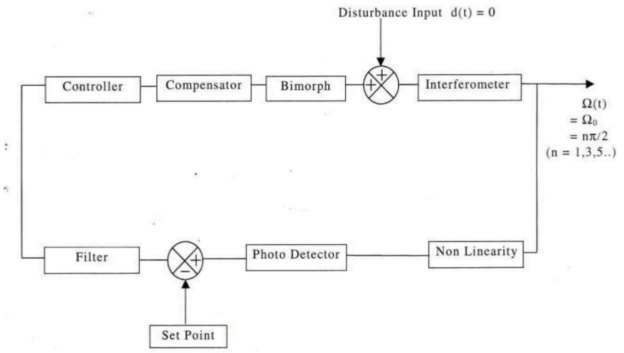

Figure 3: Control Loop during Steady State

The filter essentially determines the bandwidth of the system. If the curve is considered linear at $\Omega = 3\pi/2$ (or any other point of maximum positive slope), the gain at that point = $2e\sqrt{I_1 I_2}$ and the gain on the points of maximum negative slope = $-2e\sqrt{I_1 I_2}$.

2.1 Control Loop Components

The interferometer gain is given by $4\pi/\lambda$.

2.1.1 Photodiode Detector

The photodetector has a very fastresponse time and its time constant is in the order of microseconds. For our range of measurement, the spectral response of the photodetector is flat. The gain of the photodetector (K_{pd}) is assumed to be constant. Since it is difficult to find the gain of the photodetector alone, a method is used to find the product of the gains of the interferometer, photodetector and the nonlinear element. The product of the gain of the interferometer, non linear element which is considered to be linear at the operating point and the photodetector is given by G_{pd}.

$$G_{pd} = K_{pd}\left(\frac{4\pi}{\lambda}\right)\left(2e\sqrt{I_1 I_2}\right) \quad (7)$$

From Figure 1 it can be seen that

$$I_{max} - I_{min} = 4e\sqrt{I_1 I_2} \quad (8)$$

The photodetector produces a voltage proportional to the intensity of light falling on it. Hence from Eqn(7)

$$G_{pd} = \left(\frac{2\pi}{\lambda}\right)K_{pd}(I_{max} - I_{min}) \quad (9)$$

$\Delta V = K_{pd}(I_{max} - I_{min})$is the voltage produced bythe photodetector in volts. In order to measure Va large sinusoidal voltage is applied to the bimorph so that the varying path length produces the maximum and minimum values.

$$G_{pd} = \left(\frac{2\pi}{\lambda}\right)\Delta V \quad (10)$$

Using Eqn(6) the interferometer output voltage is obtained as $V = G_{pd}a$.

2.1.2 Bimorph

A bimorph is made up of twopolycrystalline piezoelectric ceramics bounded to a flexible, electrically conductive center strip [6]. When a voltage is applied across the bimorph, one ceramic expands and the other contracts and thereby a lateral flexion is produced.

TABLE 1

Bimorph Parameters

Manufacturer	Vernitron
Size	25x6.5x0.5mm
Depoling limit	300V/mm
Voltage limit at resonance	60V/mm
Capacitance	6nf/cm^2

The bimorph is used in a beam mounted mode. The two ends of the bimorph are glued to a metallic support using flexible silicon glue. The wires, which are very light and flexible, are attached to the bimorph near one of its ends where the motion is small.A gold plated mirror is glued to the center of the bimorph strip. The bimorph shows very good resonant behaviour. If the frequency of the driving voltage is near to the resonant frequency of the bimorph, the bimorph undergoes large deflection. The resonant frequency is given by the equation

$$f = \frac{1}{2\pi\sqrt{MC}} \quad (11)$$

whereM is the mass of the bimorph and C is the compliance. Since we are using the bimorph in a beam mounted mode, the effective mass is only half the real mass and the compliance is 1/16 of the actual value. Therefore, the resonant frequency in the experimental condition is $4\sqrt{2}$ times the unmounted value. However, since the bimorph is flexibly attached to the supports, the resonant frequency will have a lower value than the theoretical value for the mounted one. An optic lever is used to determine the resonant frequency. The frequency response shows a resonance peak of large amplitude at 1110 Hz. Since the effective bandwidth of the system is much less than1100Hz,the phase response is notmeasured. The mass of the mirror attached to the middle of the bimorph is negligible compared to the mass of the bimorph and will not cause an appreciable change in the resonant frequency.

2.1.3Bimorph driver

It is necessary to remove high frequency components from the driving signal. A simple RC filter can be used. Since the bimorph acts as a capacitor, only a resistor needs to be added in series with it. The time constant of the filter should be greater than the period of the resonant frequency i.e, RC >1/f_r.

2.1.4 Setpoint

The set point value, to a very good approximation, is proportional to the average of the upper and lower limits of the photocurrent. However, this is not entirely true since the homodyning efficiency is not entirely constant and the intensities of laser beams also vary because of the multimode aspect of the laser output [4]. For a particular set of measurements, the set point can be assumed to be constant by finding the average value of the maximum and minimum values of the photocurrent and by adjusting the supply voltage to the required value.

2.1.5 Controller

A block diagram of an unity feedback control system during transient condition is given in Figure 4. The output is given by [7].

$$y(s) = y_r(s)\frac{k'g(s)}{1+\ k'g(s)} + \ d(s)\frac{k_p g_p(s)}{1+\ k'g(s)} \qquad (12)$$

$y_r(s)$= reference input

$d(s)$= disturbance input

k_c= static gain of the controller

k_p=static gain of the process

$k' = k_c k_p$= dc loop gain

$g_c(s)$= normalized transfer function of the controller

$g_p(s)$= normalized transfer function of the process

$g(s) = g_c(s)g_p(s)$

The error is given by$e(s) = y_r(s) - y(s)$

$$= y_r(s)\frac{1}{1+\ k'g(s)} - \ d(s)\frac{k_p g_p(s)}{1+\ k'g(s)} \qquad (13)$$

If we consider the error due to the disturbance input only, then$y_r(s) = 0$.

$$\lim_{t\to\infty} e(t) = \lim_{s\to 0}\frac{sd(s)k_p g_p(s)}{1+k_p k_c g_p(s)g_c(s)} \qquad (14)$$

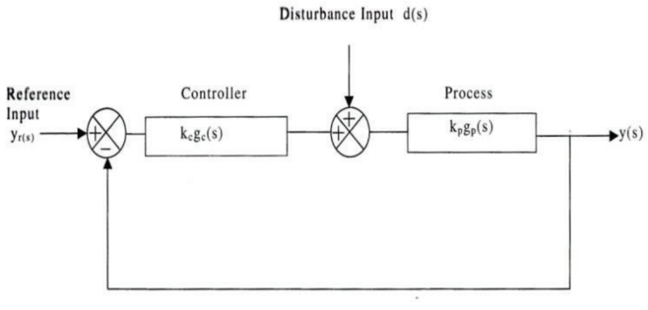

Figure 4: Unity Feedback Control System

The steady state error will obviously depend on the nature of the disturbance input. During normal conditions, the interferometer output undergoes a steady drift with time. Hence, it can be assumed that the input is of ramp type or

$d(s) = \frac{\beta}{s^2}$. Using Eqn(14) the steady state error is given by

$$\lim_{s\to 0} se(s) = \lim_{s\to 0} -\frac{\beta}{sk_c g_c(s)} \qquad (15)$$

if$\lim_{s\to 0}\frac{s}{g_p(s)} \to 0$

In our case the transfer function$g_p(s)$of the process, which consists of the interferometer and photodetector, has a constant gain and so Eqn(15) is valid. A minimum of 2 poles at the origin of the controller transfer function is necessary to bring steady state error to zero. However, a controller transfer function with only one pole will be used. This is because increasing the the number of integrators makes it more difficult to control the transient performance of the system. The steady state error produced as a result of using one integrator depends on the gain of the controller which can be varied according to our requirements. The error produced is too small to affect measurements substantially. Although sudden and large disturbances occur rarely, a derivative part is also added to$g_c(s)$to increase the overall stability of the system. Moreover, it causes an increase in proportional gain thereby increasing the speed of response. The disadvantage of using the derivative component is that it will amplify high frequency noise, but this noise can be reduced by proper circuit design. Since the entire system should behave as low pass filter in order to compensate for low frequency terms only, the role of the derivative component will be to produce phase lead to the overall system.

A circuit diagram of the PID controller is given in Figure 5. The transfer function of the PID controller is given by

$$g_c(s) = \frac{R}{R'}(1 + \frac{1}{R_I C_I s})(1 + R_D C_D s) \qquad (16)$$

where

$\frac{R}{R'} = K_p$ = variable proportional gain

$\frac{1}{R_I C_I}$ =variable integral gain

$R_D C_D = T_D$ = time constant of the derivative part

$R_I C_I = T_I$ =time constant of the integral part

The transfer function given in Eqn(16) can be rewritten as

$$g_c(s) = K_p \frac{(1 + T_I s)(1 + T_D s)}{T_I s} \qquad (17)$$

In typical applications$\frac{T_D}{T_I} \ll 1$

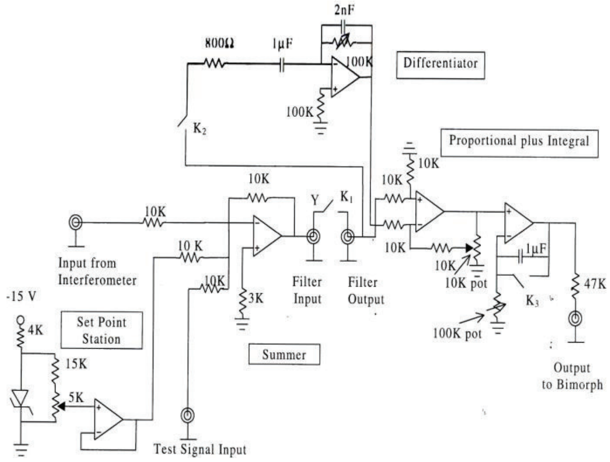

Figure 5: Circuit diagram of PID Controller

2.2Filter Design

The filter properties that merit consideration in our case are:

i) the roll off rate in the transition band, especially the attenuation rate at the corner frequency region.

ii) phase characteristics of the filter

iii) time domain performance which in turn depends on the delay time.

Since the complete system without the filter behaves as a low pass filter which does not have sufficient attenuation rate in the high frequency region, the use of a filter is justified only if it can produce the required roll off rate. A Chebyshev filter is considered due to the excellent roll off rate beginning from the corner frequency. Its transient performance is not as good as that of a Bessel filter with a large overshoot at the resonant frequency. How much this will affect the overall performance will be given by the closed loop response of the system. The order of the filter is another parameter that has to be investigated. If the order of the filter used increases, the phase lag becomes very severe and stability problems may arise. Another problem with increasing the order is that the accuracy of the values of the components used in making the filter becomes important.

A 4th order filter is initially considered. However,the system shows an inadequate gain in the low frequency region below the crossover frequency, poor settling time and high oscillatory response. Further, the bandwidth of the system becomes very low. An analysis using a lag compensator shows that it can provide only a marginal increase in the low frequency gain and which is insufficient for our requirements. Moreover, it adds another phase lag to the system and increases the settling time. A lead compensator produces a gain increase although not to the extent of a lag compensator in the low frequency region, increases the bandwidth of the system and a phase lead over the span of its corner frequencies. After taking all these factors into consideration a 2nd order filter is chosen, which can avoid the effect of the poorly damped poles of 4th order filter together with a lead compensator.

2.2.1 Design of the Filter

The parameters of the filter used are given in Figure 6. Passband frequency (f_p) = 5Hz

$f_s = 300$Hz

$A_1 = 1$dB ripple

A_2 to be determined

n = 2 (order of the filter)

The order of the filter satisfying these requirements is given by [8]

$$n = \frac{cosh^{-1}\left(\frac{10^{0.1A_2}-1}{10^{0.1A_1}-1}\right)^{\frac{1}{2}}}{cosh^{-1}\left(\frac{\omega_s}{\omega_p}\right)} \qquad (18)$$

Substituting all the parameters we get the value of A_2 as equal to 70dB. The transfer function of the filter is given by [8]

$$G(p) = \frac{1.1025}{p^2 + 1.0977p + 1.1025} \qquad (19)$$

wherep $= j(\omega/\omega_c)$

For a cutoff frequency of 5Hz, $\omega_c = 2\pi(5) = 31.4$ rad/sec.

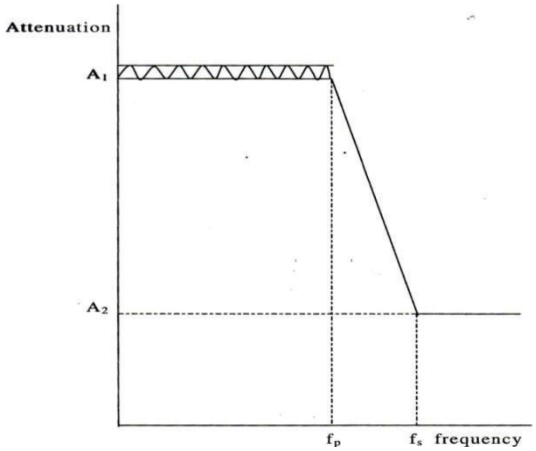

Figure 6: Filter Characteristics

2.1.2 Design of compensator

The transfer function of the lead compensator is given by [9]

$$-K_D\frac{T_1s+1}{\alpha T_1s+1} \qquad (20)$$

where
$K_D = \frac{R_F}{R_1+R_2} = 1$ if $R_F = R_1 + R_2$, $T_1 = R_1C$

$$\alpha = \frac{R_2}{R_1+R_2} \qquad (21)$$

By trial and error method we get

zero frequency = 5Hz

pole frequency = 167Hz

$K_D = 1$

$\alpha = 0.33$

$T_1 = 0.0318$

C is taken as 1μF. So R_1 = 32KΩ. To achieve this value a 100KΩ Potentiometer is used

From Eq(21) we get R_2 as 1KΩ. Therefore R_F = 33KΩ.

The circuit design of the filter and compensator is given in Figure 7. It is inserted into the system between points Filter Input and Filter Output in Figure 5.

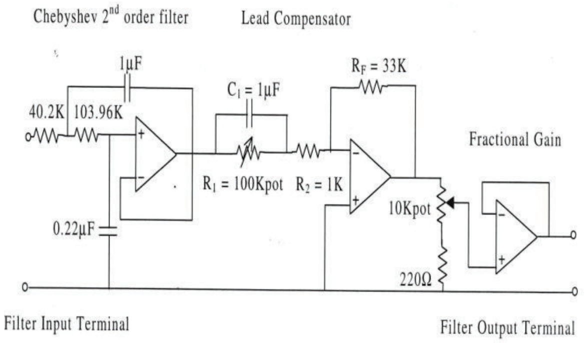

Figure 7: 2nd order Chebyshev filter and Lead Compensator

2.3 Open Loop Transfer Function of the System

The OLTF of the system is given by

$$K_0K_P\frac{(1+T_Is)(1+\ T_Ds)}{T_Is} * \frac{D(s)1.1025}{H(s)} \qquad (22)$$

where

$H(s) = \frac{s^2}{31.4^2} + \frac{1.0977s}{31.4} + 1.1025$ and $D(s)$ is the transfer function of the compensator.

The value of time constants of the integral and proportional part are

$T_1 = 0.0187$

$T_D = 0.00187$

$K_0$is the product of the static gains of 1) bimorph(K_b), 2) filter(K_f), 3) photodetector + nonlinear element + interferometer (G_{pd}) i.e.,

$$K_0 = K_bK_fG_{pd} \qquad (23)$$

The value of K_0 is fixed. Here K_b = 0.1 μm/V, K_f = 1.

$G_{pd} = (2\pi/\lambda)\Delta V = (2\pi/6400A^0)(122.5mV)$. Substituting these values in Eqn(23) we get K_0 = 0.12. The proportional gain K_p is obtained from the Bode plot shown in Figure 8. It is equal to 100.

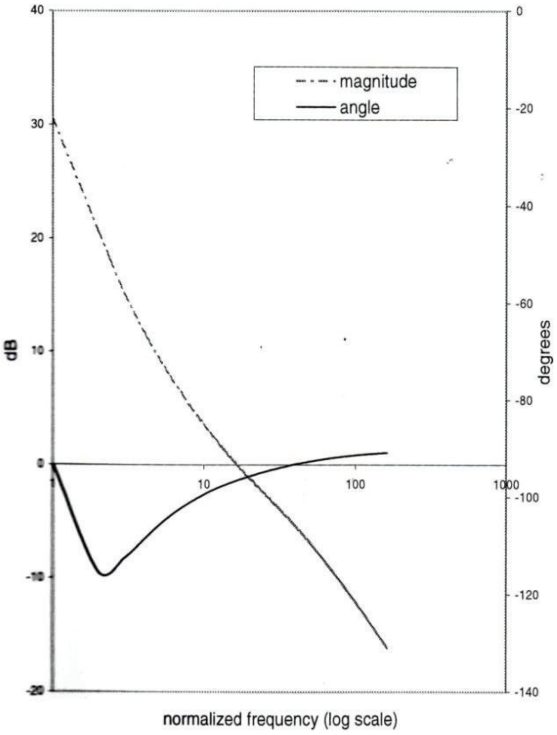

Figure 8: Bode plot of the system with filter and compensator

3. TESTING AND DISCUSSION OF RESULTS

The two important tests that are performed on the system are 1) step response to find the transient performance 2) the frequency response.

3.1 Step Response

The step response is performed by giving a step disturbance to the system, namely by giving a step input to one of the mirrors. However, in practical terms it is very difficult to give a step disturbance. This difficulty can be overcome by applying a step voltage to the summer and measuring the response from Y (See Figure 5) except for a proportionality constant or

$$\frac{X(s)}{D(s)} \propto \frac{Y(s)}{R(s)} \qquad (24)$$

The step response is given by

$$\frac{\Omega(s)}{D(s)} = \frac{\frac{4\pi}{\lambda}}{1+M(s)*\frac{(1+T_C s)}{(1+\alpha T_C s)}*\frac{1.1025}{H(s)}} \quad (25)$$

where

$$M(s) = K_0 K_P K_C \frac{(1+T_I s)(1+T_D s)}{T_I s}$$

T_C is the time constant of the compensator, and K_C is the static gain of the compensator.

The analytical solution of the step response is given in Figure9. The signal is generated and measured using the TDT dataacquisition system. A computer generates a step signal, theshape of which is shown in Figure 10. The parameters of thesignal applied are as given below

Step size = 0.01 V peak

Inter Stimulus Interval (2*step duration) = 200msec

Sampling period = 200μs

The experimental plot of the step response is given in Figure 11. It confirms the analytical plot of the step response. The response is smooth with a small overshoot and a low settling time of around 40msec.

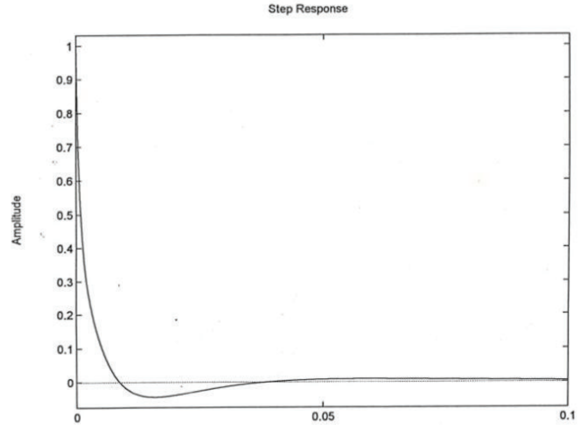

Figure 9: Step Response of the System with filter-analytical

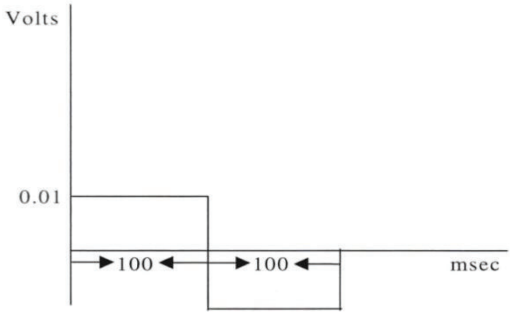

Figure 10: Step Signal used to find transient response

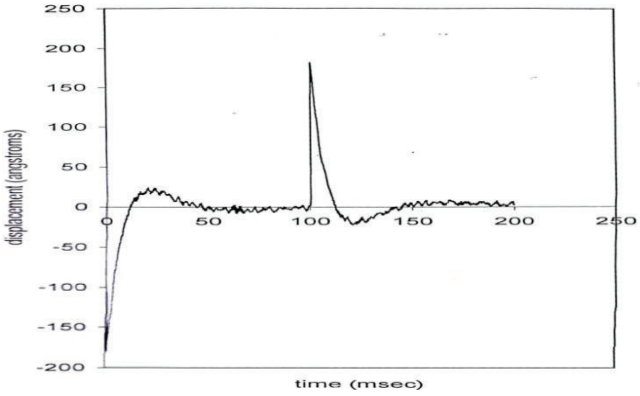

Figure 11: Actual Step Response of the system with filter

3.2 Frequency Response of the system

The frequency response is found by applying a voltage of 10mV at various frequencies. The frequency response plot is given in Figure 12. The response is flat up to around 20Hz. The closed loop bandwidth for the disturbance signal is around 10Hz.

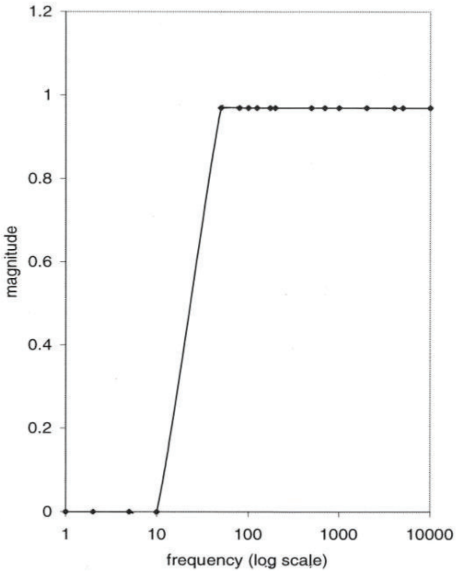

Figure 12: Magnitude plot of the system with filter

3.3 Discussion of Results

Figure 13 shows the graph obtained when the interferometer drifts without compensation. The graph has approximately a ramp shape with spikes superimposed on it due to sudden disturbances like the shutting of doors, starting of machinery etc. The graph also shows the interferometer operating point remaining steady at the point of maximum sensitivity even while disturbances are occurring.A sampling frequency of 0.5Hz has been used.Figure 14 shows the signal obtained from a 50 Hz vibration applied to the loudspeaker. The signal fed into the TDT system is sampled at 10kHz. Further, it is amplified 40dB by a dc amplifier. At very low frequencies the effect of noise will prevent the signal from taking a smooth shape.

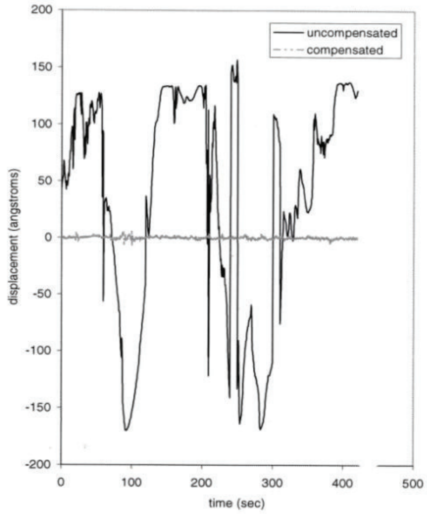

Figure 13: Drift of the interferometer with and without compensation

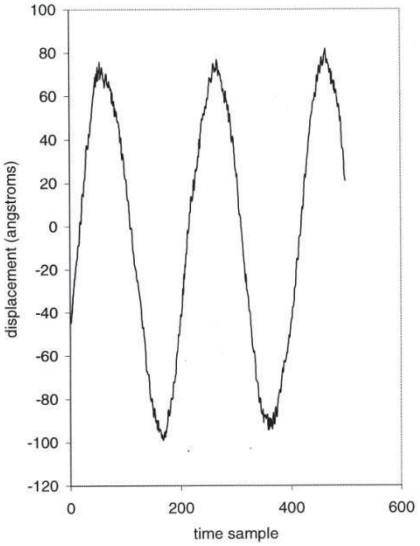

Figure 14: Interferometer output for a 50Hz vibration

4. CONCLUSION

It can be said without hesitation that this method is a very simple, convenient, accurate and easy method for stabilizing the operating point of the interferometer. Tuning of analog controllers is a laborious process. A computer controlled system would be much more easier, but it should be ensured that the time required for the correction of the signal does not stand in the way of stabilizing the operating point. It should be noted that although the value of Gpd is not fixed it can be assumed that it remains practically constant during the time of conducting the experiment.

ACKNOWLEDGMENTS

I would like to express my heartfelt gratitude to the HOD of Computer Science and Engineering Department,Dr Sasidharan Sreedharan, for encouraging me to write this paper. I would also like to express my sincere thanks to MrShiyas H and MrShamsudeen of Computer Science Engineering Department for helping me in the preparation of the paper. I am indebted to Dr.ShuwanXue who gave me guidance when this project was done.

REFERENCES

[1] F. Mammano and J. F. Ashmore, “Laser Interferometer for subnanometre displacements in the cochlea,” *Journal of Neuroscience Methods,* vol. 60, pp. 89-94, 1995.

[2] S. Chang, H. Zhu and P. Yang, “An Stabilization Technique of a Homodyne Interferometer Based on PTDC for High Frequency Hydrophone Calibration,” *Proc. of* 3rd *International Conference on Mechanical Engineeringand Intelligent Systems,* Yinchuan, China, Aug 15, 2015.

[3] M. Born and E. Wolf,“Principles of Optics,” Pergamon Press, New York, 1975.

[4] H. A. Deferrari, R. A. Darby and F. A. Andrews,“Vibrational Displacement and Mode-Shape Measurement by a Laser Interferometer,” *J.Acoustic.Am,* vol. 42, pp. 982-990, 1967.

[5] A. D. Drake and D. C. Leiner, “A Fiber Fizeau Interferometer for Measuring Minute Biological Displacements,”*IEEE Transactions on BioMedicalEngineering,* vol. 31, pp. 507-511,1984.

[6] D. P Corey and A. J. Hudspeth,“Mechanical stimulation with piezoelectric bimorph elements,” *Journal of Neuroscience Methods,* vol. 3, pp. 183-202, 1980.

[7] T. E. Fortmann and K. L. Hitz,“An Introduction to Linear Control Systems,” Marcel Dekker Inc, New York, 1977.

[8] C. Chen, “Active Filter Design,” Hayden Book Company Inc, New Jersey, 1982.

[9] G. F. Franklin, J. D. Powell and A. E. Naeimi, “Feedback Control of Dynamic Systems,” Addison-Wesley Publishing Company, New York, 1994.

Dr Anil K Jacob took his BTech degree in Electrical Engineering from College of Engineering, Trivandrum. He took MS in Bio Medical Engineering and another MS in Computer Science from New Mexico State University, USA. He received PhD from NIT Calicut in Wireless Body Area Networks. He is currently Professor in Department of Computer Science at MES College of Engineering, Kuttipuram.

MES JOURNAL OF TECHNOLOGY AND MANAGEMENT
Volume 4, No 1, 72-76,2020

Numerical Investigation of Split Injection on the Combustion Characteristics in DI Diesel Engine

S Gavudhama Karunanidhi
Department of Mechanical Engineering
MES College of Engineering
Kuttippuram
gavudham@gmail.com

G Subbarao
Geethanjali Institute of Science and Technology Nellore
gsubbrow@gmail.com

Rahumathunza I
Department of Mechanical Engineering
MES College of Engineering
Kuttippuram
rahumathunza@gmail.com

ABSTRACT

In this study, the effect of split injection on the combustion and emissions in DI diesel engine is investigated using CFD tool .One of the important problems in reducing pollutant emission from diesel engines is trade-off between soot and NOx. Split injection is one of the most powerful tools that decrease soot and NOx emissions simultaneously. Split injection is defined as splitting the main single injection profile in two or more injectionpulses with definite delay dwell between the injections. A four-stroke, single cylinder, diesel engine was taken into consideration at constant speed conditions . A model was developed for comprehensive predictions and assessments for variations in combustion phenomenon for DI diesel engines . By using the finite volume method the design and analysis of combustion chamber,emission characteristics were studied. The results of thesplit injection were compared with single injection and the optimum case of split injection was observed.

Keywords
SplitInjection,CFDtool,DIdieselengine,Emission,Optimumsplitinjection

I.INTRODUCTION

One of the important problems in reducing pollutant emission from diesel engines is trade-off between soot and NOx. Split injection is one of the most powerful tools that decrease soot and NOx emissions simultaneously. Stringent exhaust emission standards require the simultaneous reduction of soot and NOx. However it seems to be very difficult to reduce NOx emission without increasing soot emission.. The aim is to model and analyse the combustion and emission in an internal combustion engine using CFD tool (Fluent, ANSYS 14.5 package) .The split injection effect on the combustion process and emissions of a DI engine is investigated by the CFD Fluent tool..By using the finite volume method the design and analysis of combustion chamber, emission characteristic study is done for 6 different cases of split injection and comparing the results with the single injection case .

II. PROCEDURE IN COMPUTATION

The combustion simulation of compression ignition engine was developed using Fluent software (ANSYS 14.5 package) and the various equations of the multi-dimensional model were solved by the software automatically . The main inputs include engine speed, injection details of single injection, bore, stroke, connecting rod length, initial pressure and temperature[1]. Then the same procedure is repeated for 6 different split injection cases .The program concerning the simulation model predicts the cylinder pressure, cylinder temperature, emission etc. The results including graphs and various contours (NOx,Soot etc) were generated by Fluent software .

III DEFINITION OF MODEL

A 3D cylinder geometry with centrally located injector was considered .The mesh was created using ANSYS Workbench.The engine geometry details and specification details are given below. . A hexadominent mesh was created uniformly throughout the area and analysed using FLUENT, ANSYS 14.5 package. The complete meshed geometry contains 19722 faces and 48432 nodes.

Fig.1 Shows the meshed geometry of the cylinder. Connecting rod length :140 mm

Bore :80 mm

Crank radius :55 mm

Crank shaft speed :1500 rpm

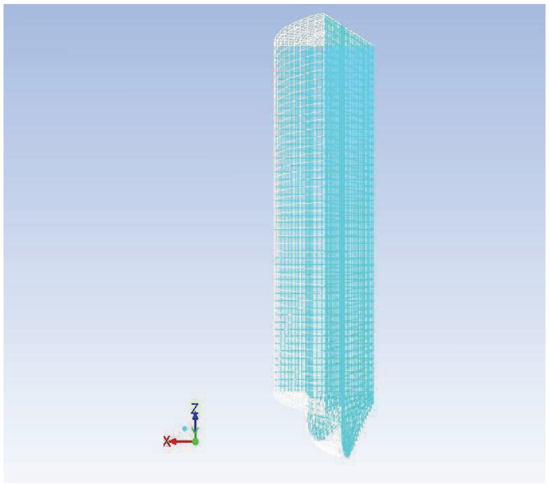

Fig.1 Meshed Geometry of the cylinder.

IV. MODELING TURBULENCE

Turbulent flows are characterized by fluctuating velocity fields. These fluctuations mix transported quantities such as momentum, energy, and species concentration, and cause the transported quantities to fluctuate as well. Since these fluctuations can be of small scale and high frequency, they are too computationally expensive to simulate directly in practical engineering calculations. Instead, the instantaneous (exact) governing equations can be time-averaged or otherwise manipulated to remove the small scales, resulting in a modified set of equations that are computationally less expensive to solve. However, the modified equations contain additional unknown variables, and turbulence models are needed to determine these variables in terms of known quantities. In this analysis standard k-ε model[1] is used.

V. BOUNDARY CONDITIONS

The boundary conditions should be given after modeling the geometry.In the analysis viscous standard k-e model is enabled for considering eddy dissipation,ie species transport model. The injection parameters and specifications are given below

X-position :0.50038 mm

Y- velocity :468 m/s

Diameter :0.287 mm

Temperature :341 K

Flow rate :0.001044 kg/S

Start crank angle :355 deg

Stop crank angle :377deg

Mainly 6 types of split injection cases are considered. They are 85%,5-15%,90%-5-10%,95%-5-5%,85%-10-15%,90%-10-105,95%-10-5%.In the 85%-5-15% split injection case ,85% of the total fuel is injected at first and remaining 15% of the fuel injected at a crank angle difference of 5 deg. All the other properties will be the same as in the single injection case.

VI. RESULTS AND DISCUSSIONS

1.**Combustion Characteristics** .

The combustion characteristics for the single injection and for all the 6 split injection cases were done.And the values of peak pressure and the temperature was approximately equal to the theoretical values.

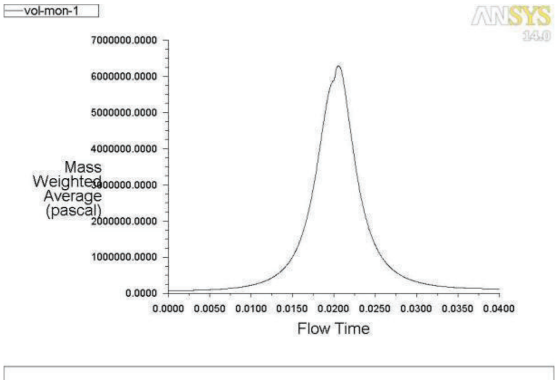

Fig. 2. Pressure v/s Flow time

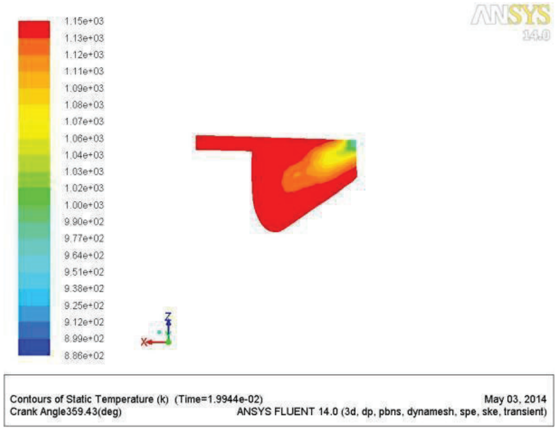

Fig. 3. Temperature contour

2.EMMISION CHARACTERISTICS

NOx and soot emission characteristics were obtained for the split injection cases .The obtained results were compared with the single injection case.The NOx and soot emission for the single injection contours are shown in the Fig.4.

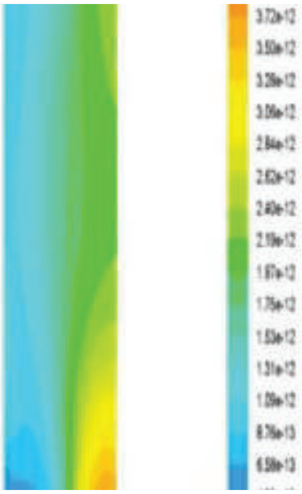

Fig. 4. NOx and soot contour-single injection

The reduction in NOx and soot emission was found less in the 85%-5-15% and in 90%-10-10% respectively. Fig 5 shows the contours of both the cases. The NOx and soot emission were plotted against the Crank angle and compared it with the single injection which is shown in the Fig.6..Then the optimum split injection case,ie the highest average reduction is calculated from all the split injection cases which is tabulated in the Fig .6.

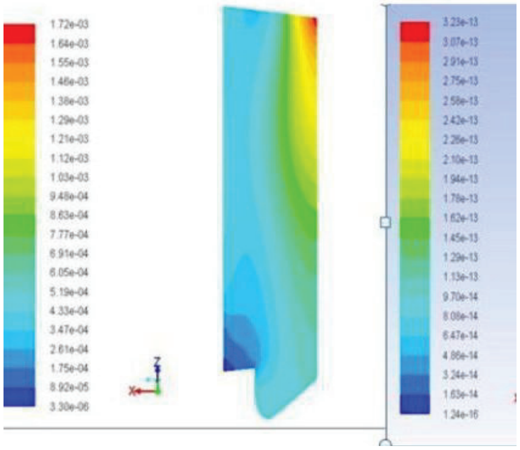

Fig. 5. NOx (85%-5-15%) Soot(90%-10 10%)contour

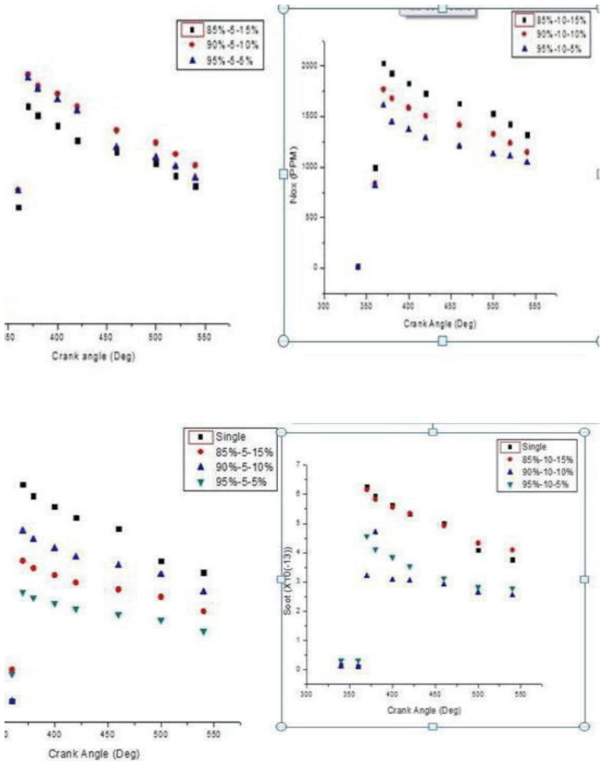

Fig. 6. Comparison of emission characteristics

VII.CONCLUSION

At the present work, the effect of the split injection on combustion and pollution of DI diesel engines was studied by the CFD tool. The target was to obtain the optimum split injection cases for these engine in which the total exhaust NOx and soot concentrations are the lowest .Three different split injection schemes, in which 5, 10 and 15% of total fuel injected in the second pulse, was considered. The delay dwell between injections pulses is varied from 5°CA to 10° Crank angle. Use of CFD tool has shown reliable results by saving cost, time and material.

The results are as follows.

The calculated combustion and performance parameters, exhaust NOx and soot emissions for the single injection case showed a good agreement with the corresponding theoretical value.

The lowest NOx and Soot emissions are related to the 85%-5-15% and 90%-10-10%cases respectively. Finally, optimum case was 90%- 10-10% regarding the highest average of Nox and soot reduction

VIII .REFERENCE

[1] Lakshminarayanan, P. A. et. Al, Modellingdiesel combustion (Springer,2009)

[2] Abdullah N, Tsolakis A, Rounce P, Wyszinsky M, Xu H, Mamat R et al.,.“Effect of injection pressure with split injection in a V6 diesel engine,” SAE Paper NO. 2009-24-0049; 2009.

[3] Bianchi GM, Peloni P, Corcione FE, Lupino F et al., “analysis of passenger car HSDI diesel engines with the 2nd generation of common rail injection systems: The effect of multiple injections on emissions”,SAE Paper NO. 2001-01-1068; 2001

[4] Chryssakis CA, Assanis DN, Kook S, Bae C et al.,. “ Effect of multiple injections on fuel-air mixing and soot formation in diesel combustion using direct flame visualization and CFD techniques”, Spring Technical Conference, ASME NO. ICES2005-1016; 2005

[5] Ehleskog R et al.,. “ Experimental and numerical investigation of split injections at low load in an HDDI diesel engine equipped with a piezo injector”, SAE Paper NO. 2006-01-3433; 2006.

[6] F. Payri , J. Benajes, X. Margot , A. Gil et al., “CFD modeling of the in-cylinder flow in direct-injection Diesel engines” ,Computers & Fluids 33 (2004) 995–1021

[7] Franz X. Tanner et al “CFD-based optimization of fuel injection strategies in a diesel engine using an adaptive gradient method”. Applied Mathematical Modelling 33 (2009) 1366–1385 .

[8] Gomaa M, Alimin AJ, Kamarudin KA et al.,”Trade-off between NOx, soot and EGR rates for an IDI diesel engine fuelled with JB5”,WorldAcademyofScience,450 .

[9] J. Blazek,"Computational Fluid Dynamics:Principles and Applications", Elsevier Science Ltd,2001,1-39.

[10] Jafarmadar S, Zehni A. et al., " Multi-dimensional modeling of the effects of split injection scheme on combustion and emissions of direct-injection diesel engines at full load state" IJE, 2009; Vol. 22, No. 4

S Gavudhama Karunanidhi received his M.Tech degree in Mechanical Engineering from IIT Madras and currently he is the faculty in Mechanical Engineering in MES College of Engineering.

G Subba Rao received his PhD from SCSVMV Deemed University Kancheepuram. Currently he is the Principal in Geethanjali Institute of Science and Technology

Rahumathunza received her PhD in Kerala University. Currently she is Professor and Head in the department of Mechanical Engineering in MES College of Engineering.

CALL FOR PAPERS

The objective of the journal is to capture innovations and challenges in technical and management areas and their fine exhibition in current researches. In line with the objectives of the journal, the editors seek articles, review papers and research papers for publication. All articles and papers are referred for independent review by peer experts. Authors are requested to submit their papers to mesjtm@mesce.ac.in

This national journal seeks articles related to technology and management, not limited to the following topics:

- Material science, Computers and Information technology.
- Electrical, Electronics, Communication and Instrumentation Engineering.
- Engineering production, Mechanical, Automobile and Textile Engineering.
- Structural design, Civil and Architectural Engineering.
- Mechatronics, Nanotechnology and Robotics.
- Business Innovations and Management Practices.